2018

Somatotopic Organization Of The Mammalian Pain System And Developmental Mechanisms

William Paul Olson
University of Pennsylvania, wio@pennmedicine.upenn.edu

Somatotopic Organization Of The Mammalian Pain System And Developmental Mechanisms

Abstract
Commonly, different regions of sensory maps are used to meet separate functional requirements. For the somatosensory system (which mediates sensation from the skin including touch, pain, and related modalities), the distal limbs have special behavioral importance for exploration and object manipulation. Accordingly, the hands and fingertips show heightened sensitivity for both touch and pain sensation in human subjects. In contrast to the touch system, the neural mechanisms for region-specific pain sensation are poorly understood. Despite over a century of research into the neural basis of pain, past work has not clearly defined the functional organization of the pain system across the body (somatotopic) map. In Chapter 2, we use a novel genetic mouse line to map the organization of one major class of mammalian pain-sensory neurons (the Mrgprd+ non-peptidergic nociceptors) across the body map. While we find no obvious peripheral mechanisms for high sensitivity in the distal limbs (mouse plantar paw skin has a low density of Mrgprd+ terminals, and single-cell arbor areas are comparable between paw and trunk skin), we reveal a novel region-specific organization in the spinal cord terminal arbors of these neurons. Specifically, paw and trunk neurons grow 'round' and 'long' arbor morphologies, respectively, such that paw neurons have a wider mediolateral spread in the spinal cord. We show that this region-specific morphology closely correlates with increased signal transmission for paw pain circuits. We conclude that region-specific organization of Mrgprd+ spinal cord terminals provides a possible mechanism for the high pain sensitivity of the distal limbs. In Chapter 3, we investigate potential developmental mechanisms for region-specific arbor morphologies. Disruption of peripheral target innervation does not alter their central arbor morphologies, suggesting that this central somatotopic difference develops independent of cues/processes from the periphery. However, this difference is present from very early developmental stages, suggesting that pre-programming mechanisms might govern this somatotopic pattern. Collectively, this work reveals that region-specific organization is a fundamental principle for the pain system with clear implications for our understanding of pain in both normal and pathological conditions.

Degree Type
Dissertation

Degree Name
Doctor of Philosophy (PhD)

Graduate Group
Neuroscience

First Advisor
Wenqin Luo

Keywords
pain, region-specific organization, somatosensation, somatotopy

SOMATOTOPIC ORGANIZATION OF THE MAMMALIAN PAIN SYSTEM AND DEVELOPMENTAL MECHANISMS

William P. Olson

A DISSERTATION

in

Neuroscience

Presented to the Faculties of the University of Pennsylvania

in

Partial Fulfillment of the Requirements for the
Degree of Doctor of Philosophy

2018

Supervisor of Dissertation

_____

Wenqin Luo, MD, PhD
Assistant Professor Neuroscience

Graduate Group Chairperson

_____

Joshua I Gold, PhD
Professor of Neuroscience

Dissertation Committee:

Steven S. Scherer, MD, PhD, Professor of Neurology
Minghong Ma, PhD, Professor of Neuroscience
Diego Contreras, MD, PhD, Professor of Neuroscience
Xinzhong Dong, PhD, Professor of Neuroscience, Johns Hopkins University

DEDICATION

This thesis is dedicated to my parents David and Diane, my sister Anna, and my partner Jun. I would not have been able to do this without them.

ACKNOWLEDGEMENT

I want to first express my sincere gratitude for my mentor, Dr. Wenqin Luo, for all her guidance and support during my PhD training. She has been an amazing mentor and role model, and her knowledge, intelligence, and insight were instrumental for all of the research in this thesis.

I also want to thank my thesis committee, Drs. Steven Scherer, Minghong Ma, Diego Contreras, and Xinzhong Dong. Their questions, comments, and suggestions played a major role in this thesis, and I sincerely appreciate their time serving on my committee.

I want to thank all the past and present members of the Luo Lab: Dr. Ishmail Abdus-Saboor, Katherine Beattie, Dr. Lian Cui, Dr. Peter Dong, Dr. Michael Fleming, Dr. Nathan Fried, Omar Johnson, Kim Kridsada, Suna Li, Dr. Jingwen Niu, Dr. Paclink Thaweerattanasinp, and Anna Vysochan. Working with such a talented, fun group of people has been motivating and inspiring, and I will truly miss working with all of them.

I want to thank all of my family: my parents David and Diane, my sister Anna, my aunts Mary and Karen, my uncles Dennis, Beau, and Jim, all of my cousins, and my grandparents Paul, Dorothy, Ewald, and Doris. Their intelligence and unending support are the reason I have been able to reach this point, and I cannot thank them enough.

Lastly, I want to thank my partner Jun Kang. His patience, kindness and love have meant everything to me during these last years of my thesis.

ABSTRACT

SOMATOTOTPIC ORGANIZATION OF THE MAMMALIAN PAIN SYSTEM AND DEVELOPMENTAL MECHANISMS

William P. Olson

Wenqin Luo

Commonly, different regions of sensory maps are used to meet separate functional requirements. For the somatosensory system (which mediates sensation from the skin including touch, pain, and related modalities), the distal limbs have special behavioral importance for exploration and object manipulation. Accordingly, the hands and fingertips show heightened sensitivity for both touch and pain sensation in human subjects. In contrast to the touch system, the neural mechanisms for region-specific pain sensation are poorly understood. Despite over a century of research into the neural basis of pain, past work has not clearly defined the functional organization of the pain system across the body (somatotopic) map. In Chapter 2, we use a novel genetic mouse line to map the organization of one major class of mammalian pain-sensory neurons (the Mrgprd+ non-peptidergic nociceptors) across the body map. While we find no obvious peripheral mechanisms for high sensitivity in the distal limbs (mouse plantar paw skin has a low density of Mrgprd+ terminals, and single-cell arbor areas are comparable between paw and trunk skin), we reveal a novel region-specific organization in the spinal cord terminal arbors of these neurons. Specifically, paw and trunk neurons grow 'round'

and ‘long’ arbor morphologies, respectively, such that paw neurons have a wider mediolateral spread in the spinal cord. We show that this region-specific morphology closely correlates with increased signal transmission for paw pain circuits. We conclude that region-specific organization of Mrgprd+ spinal cord terminals provides a possible mechanism for the high pain sensitivity of the distal limbs. In Chapter 3, we investigate potential developmental mechanisms for region-specific arbor morphologies. Disruption of peripheral target innervation does not alter their central arbor morphologies, suggesting that this central somatotopic difference develops independent of cues/processes from the periphery. However, this difference is present from very early developmental stages, suggesting that pre-programming mechanisms might govern this somatotopic pattern. Collectively, this work reveals that region-specific organization is a fundamental principle for the pain system with clear implications for our understanding of pain in both normal and pathological conditions.

TABLE OF CONTENTS

LIST OF TABLES

LIST OF ILLUSTRATIONS

CHAPTER 1

Introduction

This chapter was written by William P. Olson. Portions of this chapter have been adapted from:

Olson W, Dong P, Fleming M, Luo W (2016) The specification and wiring of mammalian cutaneous low-threshold mechanoreceptors. Wiley Interdiscip Rev Dev Biol 5:389-404.

Region-specific organization in sensory and motor systems

We interact with the world through our sensory and motor systems, and the organization of these neural systems reflects what we require from them for this interaction. One common theme is that *separate regions of sensory/motor maps are often subject to distinct functional requirements.* For example, while the center of our visual field is adept at processing fine-detail stimuli to aid in object identification (i.e. reading a highway sign), the surrounding peripheral visual field has a much lower resolution for detail. Similarly, while motor circuits controlling our distal limbs carry out fine motor commands, the circuits controlling axial muscles are dedicated to gross movements and postural control.

Since distinct information processing can be required from separate regions of sensory and motor maps, it is not surprising that they commonly feature **region-specific circuit organization** to meet these distinct requirements. While the details of this region-specific organization vary greatly between systems, they commonly feature regional specialization of peripheral units (either primary sensory receptors or lower motor neurons) and/or regional specialization of central representations. Classic work has defined many examples of these general principles.

In the visual system, the center of the primate retina (known as the 'fovea') mediates vision from the central visual field, while the peripheral retina mediates vision from the peripheral visual field. The foveal retina features a different cell-type composition (e.g. a high concentration of cone rather than rod photoreceptors along with a different composition of bipolar and ganglion cells)(Ahnelt, 1998; Masland, 2001) and circuit

structure (a lower overall photoreceptor-to-ganglion cell convergence rate)(Kolb, 1994) compared to the periphery. Additionally, in the primary visual cortex, the central visual field is greatly over-represented (i.e. occupies more physical space per unit area of the visual field) than the periphery (Daniel and Whitteridge, 1961). Both the retinal organization and the **central magnification** of the fovea is thought to facilitate the detection of color stimuli and high spatial detail (Daniel and Whitteridge, 1961; Kolb, 1994). The ability to detect fine spatial detail of stimuli is known as **spatial acuity**, and regions of high acuity are known as **sensory fovea** across sensory systems. In contrast to the visual fovea, the organization of the peripheral visual circuits facilitate vision in low light situations, especially for moving stimuli (Kolb, 1995).

An analogous form of region-specific organization is found in the auditory systems of echolocating bats and owls. These animals feature an 'auditory fovea' that mediates sensitive detection of the frequency used for echolocation. The amount of space dedicated to this frequency in the peripheral (the cochlea) and central circuits is expanded compared to other frequencies (Pollak and Bodenhamer, 1981; Kössl and Vater, 1985; Vater et al., 1985; Köppl et al., 1993). Strikingly, individual bats use characteristic frequencies to differentiate self from non-self signals, and the fovea of their auditory cortex is exquisitely matched to their 'personalized' frequency (Suga et al., 1987).

Further, recent work has identified region-specific organization in the olfactory system. In this organization, the primary olfactory sensory neurons (OSNs) display distinct ciliary structure between regions of the olfactory epithelium (Challis et al., 2015). Specifically,

region-specific cilia length governs regional differences in OSN sensitivity, with the longest cilia lengths and highest sensitivity seen in the dorsal recess of the epithelium. This is possibly related to the differential absorption of various odorants across the olfactory epithelium and could therefore facilitate detection and differentiation of odorants with diverse chemical properties.

Lastly, the motor system shows multiple levels of region-specific organization. In the peripheral motor system, the lower motor neurons of the ventral spinal cord are grouped into separate 'motor pools' that innervate either distal limb or proximal muscle groups (Goetz et al., 2015). The fine motor commands executed by the distal limbs are thought to be facilitated by a cortical magnification of these regions in the primary motor cortex (Penfield, 1937) as well as by a specialized ipsilateral connectivity with resident spinal cord neurons (Goetz et al., 2015) compared to proximal motor circuits.

Region-specific organization of the tactile somatosensory system

As the largest sensory organ of our body, the skin mediates our sensation of physical contact with objects in our environment. Sensation in the skin is mediated through the **somatosensory system** (which also mediates our sense of body part position in space). As animals move through and interact with the environment, certain somatotopic regions (i.e. the hands and feet for humans, the distal limbs and face for quadrupedal mammals) are positioned to be likely sites of initial contact with these stimuli. Therefore, the somatosensory system requires highly sensitive discriminatory abilities in these regions.

Indeed, one of first identified examples of region-specific differences in sensation relates to regional differences in the spatial acuity of the light touch system. As was first reported by EH Weber in 1834 (Weber, 1834), and further studied by Weinstein in 1968 (Weinstein, 1968), certain regions of the body (notably the fingertips, tongue and lips) show a much higher tactile acuity compared with the rest of the body. This has classically been quantified using the **two-point discrimination threshold** (2PD) method, in which two small point stimuli are repeatedly placed on the skin of a subject with the distance varied to find the minimal distance at which the subject can distinguish them as separate points. Based on various reports, the fingertips have a ~4-12X lower 2PD threshold for tactile stimuli compared to the upper back, indicating much higher tactile spatial acuity (Weber, 1834; Weinstein, 1968; Mancini et al., 2014). While cats, rodents and other whiskered mammals rely heavily on the whisker system for object localization and navigation, reports indicate that cats and mice also likely show high tactile acuity in the distal limbs (Brown et al., 2004; Orefice et al., 2016; Abraira et al., 2017).

Light touch (tactile) stimuli are detected by low threshold mechanoreceptors

The primary sensory neurons that detect light touch stimuli are known as low threshold mechanoreceptors (LTMRs). All primary somatosensory neurons, including LTMRs, have cell bodies in the dorsal root ganglia (DRG) along the spinal column or in the trigeminal ganglia (TG) at the base of the skull. They grow a single axon that bifurcates in the ganglion into two branches: one enters the spinal nerve (or trigeminal nerve for TG afferents) to innervate the periphery (skin and other tissues) while the other enters the dorsal route to enter the spinal cord/central nervous system (CNS). DRG neurons can be

classified based on their axon diameter, myelination level, and conduction velocity (CV). LTMRs are either **Aß** (large diameter, myelinated, fast CV), **Aδ** (intermediate diameter, myelinated, intermediate CV) or **C** (small diameter, unmyelinated, slow CV) fibers. They are often further classified into rapidly adapting (**RA**), slowly adapting (**SA**) or intermediate adapting (**IA**) groups based on their response properties to 'ramp-and-hold' stimulation. The various classes of LTMRs associate with characteristic end organs in the skin (Fleming and Luo, 2013; Olson et al., 2016).

Mammals have two skin types: hairy and glabrous (non-hairy). Glabrous skin is located on the plantar paws (hands/feet in humans) and lips. Hairy skin covers the rest of the body, including the face. Glabrous and hairy skin are innervated by different classes of LTMRs, representing one level of regional specialization among peripheral somatosensory circuits (Li et al., 2011; Fleming and Luo, 2013; Olson et al., 2016). Glabrous skin is innervated by: (1) Meissner's corpuscle-associated (RA type I, RAI) Aß and (2) Merkel cell-associated (SA type I, SAI) Aß units, along with (3) Pacinian corpuscle-associated (RA type II, RAII) Aß fibers. The hairy skin is innervated by (1) Merkel cell-associated SAI fibers along with multiple fiber types innervating hair follicles including (2) Aß lanceolate ending (RA) fibers, (3) Aß circumferential ending (RA) fibers, (4) Aδ lanceolate ending (RA) fibers, and (5) C lanceolate ending (IA) fibers.

Centrally, LTMRs enter the spinal cord through the dorsal root and bifurcate in the dorsal funiculus (i.e. dorsal column, a white matter tract at the dorsomedial edge of the spinal cord), to grow a longitudinal projection that ascends to the brainstem, synapsing

on the dorsal column relay nuclei. LTMRs extend '3rd order' projections out of this ascending longitudinal projection to innervate the spinal dorsal horn (DH) grey matter at multiple spinal levels. While the dorsal column projections are the major pathway for tactile signal transmission to the brain, these local 3rd order projections into the dorsal horn grey matter contribute to local cross-talk with multiple sensory modalities.

The **somatotopic map** is the topographic representation of the body in the somatosensory pathways. In the spinal cord, this map has been determined with gross anatomy, retrograde tracing, and *in vivo* physiological recording experiments (Brown and Fuchs, 1975b; Brown and Koerber, 1978; Koerber and Brown, 1982; Cervero and Connell, 1984; Swett and Woolf, 1985; Woolf and Fitzgerald, 1986; Shortland et al., 1989; Brown et al., 1991; Millecchia et al., 1991; Takahashi et al., 2002). In the spinal cord, segments are defined by the bilateral sets of dorsal and ventral roots exiting each segment to form the spinal nerves. Each bilateral set of spinal nerves innervates a strip of skin surrounding the body circumference called a **dermatome**. The *rostrocaudal body plan is therefore represented in the DH by the segmental arrangement*: cervical segments represent the neck, upper body, and forelimbs; thoracic segments represent the trunk; lumbar segments represent the lower body and hind limbs; sacral segments represent anogenital (and tail for tailed mammals) skin. Cervical and lumbar segments contain the cervical (C4-C7 in mice)/lumbar (L3-L5 in mice) enlargements, which are wide segments innervating the limbs. In the cervical/lumbar enlargements, *proximodistal location along the limb is represented based on mediolateral position in the DH*. Importantly, *the proximodistal map is 'flipped' in the DH,* with the most distal limb regions (digits and plantar paws/hands

and feet) represented in the most medial DH. In thoracic segments, mediolateral position corresponds to dorsoventral location in the periphery, with the medial DH representing ventral-most skin.

Defined region-specific mechanisms could explain the 'tactile fovea'

Given that the 'tactile foveae' of the distal limbs and face have long been appreciated, several underlying neural mechanisms have been defined. In the peripheral tactile system, two such mechanisms have been identified. The skin of the fingertips and the plantar distal limbs has a greatly *increased density* of two unit types, Meissner's corpuscle-associated RAI and Merkel cell complex-associated SAI units (Johansson and Vallbo, 1979; Vallbo and Johansson, 1984). These two units are likely utilized for fine detail discrimination because they have small, well-defined **receptive fields** (RFs, the area of skin in which stimuli will excite a single unit)(Fleming and Luo, 2013; Olson et al., 2016). Furthermore, as a population, LTMRs have a *smaller RF size* in the distal compared to the proximal limb (Brown and Koerber, 1978; Brown et al., 2004). In the spinal cord, the distal limb representation is magnified in the DH touch circuits, which in this system has been estimated using a variable called 'map scale' (the unit of DH space dedicated to a unit area of space in the periphery) (Millecchia et al., 1991; Wang et al., 1997; Brown et al., 2004). Moreover, in the brain, the magnification of distal limb and face regions was revealed by Wilder Penfield and colleagues, who used focal stimulation of the cortex of human subjects to map the function of cortical regions, including primary somatosensory cortex (S1) (Penfield, 1937). They called these maps 'homunculi' for 'little humans', and they demonstrated the distal limbs and face occupy greatly expanded portions of the S1

map. It should be noted that the functional importance of distal limb magnification in the DH is unclear given that the major pathway for tactile signal transmission to the brain is through the dorsal column pathway.

The increased density of LTMRs in the distal limbs, along with the central magnification of these regions, has been predicted to sharpen spatial representations in the CNS based on computational modeling (Brown et al., 2004). The magnification of distal limbs in the CNS has commonly been thought to follow from the increased density of LTMRs in the periphery (Wang et al., 1997; Brown et al., 2004). However, in addition to peripheral receptor density, mechanisms in downstream circuits can also differentially magnify sensory map regions. In one example, the extremely high spatial acuity exhibited by one of the facial tactile appendages ('rays') of the star-nosed mole does not result from an increased density of peripheral receptors (Catania and Kaas, 1997; Catania et al., 2011). Instead, individual tactile afferents from this ray expand their representation within the CNS, a mechanism known as **afferent magnification**.

What is the region-specific organization of the pain somatosensory system?

Nociception, which is the detection of harmful mechanical, thermal, or chemical stimuli, is mediated through separate peripheral and central neural pathways than light touch. Until recently, it has been unclear whether pain shows analogous regional differences in sensation like the touch system. This partly because stimuli the intense mechanical stimuli commonly used to activate the pain system (like a pinprick) also activate LTMRs,

precluding the use of standard 2PD testing paradigms to study pain circuits. Recent work, however, has demonstrated that *the fingertips are a 'fovea' for pain stimuli in human subjects* (Mancini et al., 2013; Mancini et al., 2014). This work used focal laser stimuli that specifically activate Aδ thermal nociceptors, and then mapped pain 2PD thresholds across the body. While overall spatial acuity is higher for touch compared to pain stimuli, pain shows regional variation in 2PD thresholds with the lowest values in the fingertips, hands, feet, and face.

This result was surprising, since it was known that human skin biopsy staining for nociceptive nerve terminals (stained by antibodies against PGP9.5, see below) showed that fingertip skin has a lower neurite density compared to skin from the dorsal hand surface (Mancini et al., 2013). This indicates that pain likely does not use one of the major mechanisms used for the tactile fovea: the increased density of peripheral receptors. Moreover, *this suggests that unrecognized region-specific organization may exist in the pain system*, possibly in CNS circuits, to facilitate sensitive sensation in the 'pain fovea'.

Physiological, Anatomical, Molecular Genetic, and Functional Descriptions of the Mammalian Pain System

Past work has provided detailed characterization of the pain system at both the population and the single-cell level. This includes analysis of both cutaneous and non-cutaneous (muscle, viscera, etc) pain pathways in both 'normal' and pathological conditions. However, in contrast to the touch system, *past work has not systematically characterized somatotopic differences within the pain system.* Based on this, much remains

unclear regarding the region-specific processing of pain. The following overview covers past descriptions of cutaneous nociceptors under non-pathological conditions, and will highlight the limitations in this work for dissecting somatotopic differences in this system.

Physiological characterizations of nociceptors

Pain stimuli are detected by nociceptors

Based on the discovery in the late 19th century of discrete spots in human skin sensitive to painful stimulation, Maximilion von Frey proposed that pain was a distinct sensory modality mediated by specialized nerve fibers (Norrsell et al., 1999). Charles Sherrington, in 1906, proposed the existence of single primary sensory neurons dedicated to the detection of noxious (i.e. extreme mechanical, thermal, or chemical) stimuli, which he termed **nociceptors** (Sherrington, 1906). The first clear identification of single neurons that could code for noxious stimuli came from *in vivo* cutaneous nerve recordings in the 1950s and 60s, notably the work of Edward Perl along with Paul Richards Burgess and Paul Bessou (Iggo, 1959; Iggo, 1960; Burgess and Perl, 1967; Perl, 1968; Bessou and Perl, 1969). In cutaneous nerve recordings from the cat and monkey, they found single units that did not respond to stimuli reported as non-painful by human subjects (low intensity thermal or mechanical stimuli), but did fire in response to stimuli reported to be painful by humans (punctate mechanical stimuli applied with >1 g, or 10 mN, of force, and thermal stimuli >46°C). These units conducted in either the A-fiber (~5-40 m/s) or C-fiber (<2 m/s) range. Subsequent work from many labs have further characterized these

units across multiple species, and these recordings confirm that dedicated cutaneous populations code for stimuli with the potential to cause tissue damage.

In nerve recording studies, nociceptors are classified into A- and C-fiber groups and then sub-classified based on the stimulus/stimuli to which they respond. A-fiber nociceptors are commonly classified as Aδ fibers, although the conduction velocities of these fibers can extend into the low Aß range (Burgess and Perl, 1967; Georgopoulos, 1976; Treede et al., 1998). Aδ nociceptors are thought to mediate the sharp 'fast pain' that is immediately felt after the onset of a noxious stimulus, while C nociceptors are thought to mediate the dull 'slow pain' that occurs 1-2 seconds later (Price, 1972; Torebjörk and Hallin, 1973; Price et al., 1977).

Nociceptors often have polymodal response properties

Importantly, many Aδ and C nociceptors have 'polymodal' response properties, meaning they respond to noxious stimuli of several modalities (mechanical, thermal, and/or chemical). Polymodal nociceptors have been identified in rodent (Lynn and Carpenter, 1982; Fleischer et al., 1983; Kirchhoff et al., 1990; Liu et al., 2012), rabbit (Fitzgerald and Lynn, 1977), cat (Iggo, 1959; Burgess and Perl, 1967; Bessou and Perl, 1969), monkey (Croze et al., 1976; Georgopoulos, 1976; Georgopoulos, 1977), and human (Van Hees and Gybels, 1972; Torebjörk, 1974; Van Hees and Gybels, 1981; Schmidt et al., 1995) nerve recordings, and their physiological properties are consistent across species. These neurons have little to no background activity at ambient temperatures but fire in response to noxious heat (>45-46°), high-intensity mechanical, and often noxious chemical stimuli

(such as mustard oil, paint remover, or inflammatory agents). They are therefore termed AMH (A-mechanoheat) or CMH (C-mechanoheat) units. AMH and CMH units also respond to extreme cold temperatures (with cold thresholds below 12°C), but cold responses have been less systemically tested (Georgopoulos, 1976; Simone and Kajander, 1996; Simone and Kajander, 1997). CMH units are by far the most prevalent among the C nociceptors (representing 50-80% of C units sampled in various studies), while AMH units may account for roughly half of Aδ units (Georgopoulos, 1976; Schmidt et al., 1995). AMH and CMH units exhibit slow adaptation responses to ramp-and-hold stimuli, and show monotonic increases in firing rate with increased stimulus intensity (up to a saturation intensity) (Garell et al., 1996).

In addition to polymodal nociceptors, some nociceptors respond to noxious mechanical but not thermal stimuli and are termed AM or CM units (Burgess and Perl, 1967; Bessou and Perl, 1969; Georgopoulos, 1976; Fitzgerald and Lynn, 1977; Leem et al., 1993; Schmidt et al., 1995). Further, more recent studies that used electrical rather than mechanical search stimuli identified so-called mechanically insensitive afferents (A-MIAs or C-MIAs), sometimes called 'silent nociceptors' (Meyer et al., 1991; Treede et al., 1998; Schmidt et al., 2000). Many A-MIAs and C-MIAs respond to noxious heat and/or chemical stimuli. They may be involved in coding intense pain caused by prolonged mechanical forces stronger than the saturation stimuli for AMH/CMH units (Garell et al., 1996; Schmidt et al., 2000). Additionally, some change their response properties after application of chemicals and may therefore play a role in inflammatory or chronic pain (Meyer et al., 1991; Schmidt et al., 1995).

Importantly, nociceptor response properties are dramatically affected by stimulus history and by tissue damage/skin inflammation (Fitzgerald and Lynn, 1977; Campbell and Meyer, 1983; Kirchhoff et al., 1990; White et al., 1990). A large body of work has compared physiological response properties of units in uninjured vs. injured skin to understand possible mechanisms for heightened pain during injury conditions (Treede et al., 1992).

Physiological receptive field maps provide limited information regarding nociceptor peripheral structure

Single-unit nerve recordings have revealed the spatial structure of nociceptor receptive fields (RF, area of skin in which stimulation will excite a single neuron). Most of this analysis has come from mapping the RF using focal mechanical stimuli, though use of heat lasers allows for estimations of thermal RFs (Treede et al., 1990). The best studied are the CMH units. CMH RFs are described as small circular or elliptical areas. RF areas were estimated to be < 2 mm in diameter in the dorsal hind paw of the rat and cat (Bessou and Perl, 1969; Lynn and Carpenter, 1982) and somewhat larger in monkeys and humans (<3 mm diam. in monkey hands or limbs (Croze et al., 1976; Georgopoulos, 1976), and 10 mm diam. on average in the human dorsal foot (Schmidt et al., 1997)). A minority of CMH units have complex RFs, which contain 2 nearby but non-contiguous areas (Van Hees and Gybels, 1972; Torebjörk, 1974; Beitel and Dubner, 1976; Croze et al., 1976). Recordings in monkeys and humans have found 2-10 'hot-spots' in CMH RFs, which are small points of heightened sensitivity within the RF (Torebjörk, 1974; Beitel and Dubner,

1976; Croze et al., 1976; Georgopoulos, 1976). While such hot-spots may be present in rat and cat CMH units, they may be difficult to detect due to their small size.

While informative, physiological RF mapping has a few limitations: (1) While detailed maps of nociceptor RFs from large RFs in monkeys and humans have been reported (Beitel and Dubner, 1976; Schmidt et al., 1997), in general these physiological RF maps have low spatial resolution. (2) It is evident from these studies that the RF map is highly dependent on stimulus intensity and/or experimental methodology (e.g.(Treede et al., 1990)). The best analyses of RF structure likely come from use of electrical mapping stimuli, though these 'eRFs' also have limited resolution and could change based on the physiological properties of the nociceptor (Meyer et al., 1991; Schmidt et al., 1997). (3) For methodological reasons, these past descriptions have focused on the upper and lower limbs and, in some cases, the face. It is therefore difficult systematically compare nociceptor structure across the body.

Regarding point (3), these recording studies have made some observations regarding regional differences in nociceptor RFs. One study of human C-fiber mechanosensitive afferents reports significantly larger RFs in the proximal compared to distal leg (with leg RFs ~5 times larger than RFs in the toes)(Schmidt et al., 1997). This study included both nociceptive and non-nociceptive (C-fiber LTMR) units. Similarly, there are some reports of A-fiber nociceptive units showing smaller overall RFs in distal vs. proximal limb (Perl, 1968; Lynn and Carpenter, 1982). It remains to be determined whether these reported differences are caused by regional variation in the anatomical area of units, in single-unit

physiological properties, or in the composition of unit types present in various skin regions.

Anatomical and molecular characterizations of nociceptors

Von Frey linked pain sensation to 'free nerve terminals' in the skin, in contrast to other cutaneous nerve fibers associated with various end organs which he linked to light touch sensation (Norrsell et al., 1999). This proposal was supported by physiological studies establishing that nociception was mediated by medium diameter, thinly-myelinated Aδ and small diameter, unmyelinated C fibers, which innervate the skin as free nerve terminals. However, this connection is complicated by the fact that other cutaneous neuronal populations conduct in the C-fiber range including efferent sympathetic neurons, warm- and cool-sensing thermoceptors, and some low threshold mechanoreceptor afferents. This issue has been clarified by studies combining physiological and/or molecular identification of nociceptors with anatomical studies, as described below. A combination of electron microscopy, light microscopy, and molecular genetic tracing have characterized the peripheral and central anatomy of nociceptive afferents.

Molecular and genetic analysis identified two major mammalian nociceptor populations

Nociceptor cell bodies, like all primary somatosensory neurons, lie in the DRGs/TGs. Immunostaining studies identified various molecular markers expressed by small and medium diameter (i.e. C and Aδ (Hoheisel and Mense, 1987)) DRG neurons in rodents. This work identified two classes of nociceptors based on molecular marker expression: (1)

'**peptidergic nociceptors**', which express the neuropeptides substance P and calcitonin gene-related peptide (CGRP), but do not express fluoride resistant acid-phosphatase (FRAP), and (2) '**non-peptidergic nociceptors**', which have FRAP activity and bind the plant isolectin B4 (IB4) (Nagy and Hunt, 1982; Kruger et al., 1989; Silverman and Kruger, 1990). Transgenic mouse lines later allowed for the genetic targeting of these classes. The most useful/specific of these use the *Calca* locus (coding for CGRP) to target peptidergic nociceptors(McCoy et al., 2012; McCoy et al., 2013) and the *Mrgprd* locus (coding for Mas-related gene product receptor) to target the majority (~75%) of IB4+ non-peptidergic nociceptors(Zylka et al., 2005). Mrgprd is one of a large class of mouse G-protein coupled receptors (GPCRs) specifically expressed in the DRG/TG of mice(Dong et al., 2001) (see below for information regarding Mrgprd function).

Nociceptors predominantly innervate the skin as free nerve terminals

Nociceptor peripheral branches leave the DRG to enter the spinal nerves (or the TG to enter the trigeminal nerve) and travel to their peripheral target (skin or deeper tissues). Immunostaining and genetic tracing have revealed the skin innervation of peptidergic and non-peptidergic nociceptor populations. Peptidergic fibers are visualized with CGRP immunostaining (Kruger et al., 1989; Zylka et al., 2005) and with $Calca^{GFP}$ (McCoy et al., 2012) knock in mice, while non-peptidergic fibers are visualized with staining for the pan-neuronal marker PGP9.5 (Kennedy, 2004) or with or $Mrgprd^{EGFPf}$ knock-in mice (Zylka et al., 2005). Both fiber types form a horizontal plexus in the dermis. Peptidergic fibers associate with blood vessels, sebaceous glands, and form some free nerve endings in the dermis. Isolated peptidergic/non-peptidergic axons leave the dermal plexus to branch,

enter the epidermis, and terminate as intraepidermal free nerve endings. While peptidergic fibers form thick intraepidermal knobs terminating in the stratum spinosum, non-peptidergic fibers form twisted free terminals that terminate more superficially in the stratum granulosum. CGRP+ and Mrgprd+ endings sometimes intertwine in the epidermis, and Mrgprd+ fibers are the most prevalent ending type in the epidermis (comprising ~60% of PGP9.5+ free nerve endings).

Nociceptors predominantly form free nerve endings in the skin, however recent work has a cutaneous nociceptor population that expresses CGRP, conducts in the A∂ range, and innervates hair follicles. These 'Circ-HTMR' fibers (Circumferential High Threshold Mechanoreceptor) form circumferential-type endings encircling the deep hair follicle and respond to noxious pulling of the hair follicle (Ghitani et al., 2017). Stainings from *Mrgprd*^{EGFPf} knock-in mice indicate that non-peptidergic fibers also form endings around hair follicles, though these endings have not been carefully characterized (Zylka et al., 2005).

The ultrastructure of nociceptor peripheral innervation has been described by electron microscopic (EM) studies. EM of DRGs identified a class of small-diameter neurons (termed 'type B' DRG neurons) with unmyelinated or thinly myelinated axons and that had a dark, dense Nissl staining appearance (Sommer et al., 1985). Peripherally, unmyelinated C-fibers and myelinated A∂ nociceptor travel in the nerve in bundled fascicles enclosed by collagen and a Schwan cell sheath (Cauna, 1973; Kruger et al., 1981;

Cauna, 2008). While Aϑ fibers loose their myelin in the upper dermis, individual C and Aϑ terminals retain their Schwann cell sheath as they penetrate the epidermal basal membrane and form intraepidermal endings. These endings loose this Schwann cell sheath in isolated spots to directly contact epidermal keratinocytes. While the axoplasm of nociceptor terminals in general shows few organelles, both small clear and dense core vesicles are seen, likely related to signaling molecules released by nociceptor terminals in various conditions (Mense, 2009).

These studies have described the peripheral innervation patterns of nociceptor populations, but there are limitations in this work regarding the somatotopic organization of these populations. While immunostaining studies have noted differences between glabrous and hairy skin innervation (Kruger et al., 1989; Zylka et al., 2005), they cannot resolve the anatomy of single nociceptors and therefore cannot compare single nociceptors between regions. Further, EM studies have described of single nociceptor terminals, but often not in the context of entire terminal arbors, and they are not suited to systematic comparisons between body regions.

Nociceptor central projections synapse on spinal cord circuits for integration and relay of pain signals

The spinal cord grey matter is commonly categorized based on the laminar organization system developed by Bror Rexed in the early 1950s (Rexed, 1952, 1954). Rexed identified 10 lamina (I-X, from dorsal to ventral) based on characteristic cytoarchitecture. Notably, layer II in the superficial dorsal horn corresponds to the 'substantia gelatinosa of

Rolando' which was first characterized by the Italian physician Luigi Rolando in 1824 (Rexed, 1952). Rolando named this region based on its gelatinous appearance under light microscopy, which is due to a lack of myelinated fibers primary afferent fibers. Subsequent work showed that the substantia gelatinosa (SG) is a critical locus for the intake and processing of pain information in the central nervous system.

Nociceptor fibers enter the spinal cord through the dorsal root, travel rostrocadually in Lisseur's tract at the dorsolateral margin of the spinal cord, and then dive ventrally to innervate the DH. The clearest early descriptions regarding the laminar innervation of DRG neurons came from single-cell tracing experiments (Scheibel and Scheibel, 1968; Light and Perl, 1979; Sugiura et al., 1986; Sugiura et al., 1989). This was later combined with immunostaining (for CGRP, FRAP, IB4 and other markers) and genetic tracing experiments (Nagy and Hunt, 1982; Zylka et al., 2005). Nociceptors innervate either the superficial (layer I and II) or deep (layer V) DH. Dissection of circuits in the SG has divided this layer into 'outer' and 'inner' segments (layer II_o and II_i). Peptidergic fibers (both thinly myelinated Aϑ and unmyelinated C fibers) innervate layer I/II_o and layer V. Non-peptidergic fibers only innervate layer II ventral to peptidergic fibers, and *Mrgrd*^{EGFPf} fibers were found to innervate a boundary between II_o and II_i (identified as II_m in this study (Zylka et al., 2005)).

The first descriptions of nociceptor single-cell morphology in the CNS came from Golgi stainings (Szentagothai, 1964; Scheibel and Scheibel, 1968; Scheibel and Schiebel, 1969; Rethelyi, 1977). Later work combined *in vivo* intracellular recording of DRG cell bodies

with axon filling techniques (using horseradish peroxidase for Aδ nociceptors and plant lectins for C nociceptors) (Light and Perl, 1979; Sugiura et al., 1986; Sugiura et al., 1989). Based on these studies, Aδ and C nociceptors send thin axons into the DH that elaborate terminal axonal arbors in their appropriate layer(s). While C nociceptors will grow a single arbor in either layer I or layer II, Aδ nociceptors can grow arbors in both layer I and layer V (although some neurons will innervate only one layer). Axons in these arbors have *en passant* swellings thought to represent sites of synaptic contact (see below). In general, these studies proposed a model in which nociceptor arbors are flattened in the mediolateral axis and stretched in the rostrocaudal (sagittal) axis, so that the primary afferent neuropil comprises a series of 'sagittal sheets' contacting the DH neurons.

EM studies have described the synaptic contacts of nociceptors with DH neurons (Gobel, 1974, 1976; Duncan and Morales, 1978; Ribeiro-da-Silva and Coimbra, 1982; Ribeiro-da-Silva, 1995). These contacts are commonly organized in an arrangement known as a 'synaptic glomerulus'. These glomeruli feature (1) a central terminal (C), which is the nociceptor primary afferent terminal, in contact with (2) dendrites and (3) axonal terminals. Glomeruli are separated from the surrounding neuropil by glial processes. The diameter of these glomeruli closely matches the diameters of *en passant* axonal swellings, supporting that these swellings are synaptic contacts. The vast majority of nociceptor synaptic contacts are 'typical' axo-dendritic synapses of C terminals onto post-synaptic dendritic shafts (Duncan and Morales, 1978). However, within synaptic glomeruli, dendro-axonic (dendritic shafts signaling to C terminals or other axons) and dendro-dendritic (dendritic shafts signaling to each other) are seen. Moreover, axo-axonic

synapses (from DH interneuron or descending projections from the brainstem) provide pre-synaptic inhibitory control of transmitter release from C terminals. This has been shown to provide critical 'gain control' of pain signaling in various behavioral states (Todd, 1996; Mason, 2012). Overall, the synaptic organization of these terminals reflects the complex signaling that controls pain transmission.

Taken together, while informative, these studies have not provided a somatotopic model for nociceptor primary afferent innervation of the spinal cord. Due to the technical difficulty of staining small diameter afferents with dye backfilling (especially for C fibers), only a relatively small number of nociceptor central arbors have been characterized from isolated somatotopic regions. Additionally, it is difficult to detangle in these studies whether morphological differences are related to differences between subtypes or to somatotopic location. EM studies provide detailed information about synaptic organization, but somatotopic differences have not been carefully addressed in this work.

Functional and Behavioral characterizations of nociceptors

Following from the identification of molecularly-defined nociceptor populations, recent work has tested the necessity of these populations for expression of mouse pain behaviors. One surprising result from these studies is that, while most nociceptors are polymodal in their physiological responses, ablation of certain populations shows selective behavioral deficits regarding pain modalities. This remains an intriguing question in the field.

Peptidergic nociceptors play a predominant role in mouse thermal pain behavior

Peptidergic nociceptors highly co-express the thermal pain receptors Transient receptor potential cation channel (Trp) subfamily V1 (*Trpv1*), Trp subfamily A1 *(Trpa1*) and Trp subfamily M3 (*Trpm3*) (Vriens et al., 2011; McCoy et al., 2012; Usoskin et al., 2014; Vandewauw et al., 2018). Consistent with this expression, genetically labeled CGRP+ neurons show robust noxious thermal heat responses, and both pharmacological (high-dose treatment with the TRPV1 agonist capsaicin) or genetic ablation of this population causes severe reduction in thermal pain responses (Stucky and Lewin, 1999; Cavanaugh et al., 2009; McCoy et al., 2012; McCoy et al., 2013). Interestingly, although many peptidergic neurons are polymodal in their physiological responses (Ghitani et al., 2017), these ablation studies did not report obvious changes in mechanical pain behavior, though cold pain responses were heightened. This supports that peptidergic nociceptors are the major mediators of thermal pain. These are likely to be the subset of CGRP+ neurons ending in free nerve terminals rather than follicle-innervating Circ-HTMRs, as the latter do not show noxious heat responses (Ghitani et al., 2017).

Mrgprd+ non-peptidergic nociceptors play a role in mechanical pain and beta-alanine induced itch

Studies defining the functional role of non-peptidergic fibers have used the *Mrgprd* locus to target this population in mice. Physiological characterization (using loose-patch *in vivo* recordings in *Mrgprd*^{EGFPf} mice) showed that Mrgprd+ neurons are both CMH (mechanical and heat polymodal) and CM (mechano-only) units (Rau et al., 2009). Genetic ablation of these neurons results in a reduction in mechanosensitivity (up to 1.4

g/14 mN of force) but does not cause thermal pain deficits (Cavanaugh et al., 2009). However, ablation of these fibers *after ablation of peptidergic fibers* does reveal a minor role for this population in thermal pain (Pogorzala et al., 2013). These findings support that Mrgprd+ fibers play a role in mechanical pain behavior, though it should be noted that the mechanosensitivity of Mrgprd-ablated animals was tested up to a relatively low mechanical force (1.4 g) (Cavanaugh et al., 2009).

In addition to mechanical pain, Mrgprd+ fibers respond robustly to beat-alanine (B-AL), a naturally occurring amino acid that induces itch (Liu et al., 2012). Mrgprd is the receptor for B-AL, and Mrgprd knockout mice show no B-AL induced itch. Interestingly, despite the expression of Mrgprd across this population, only ~50% of these neurons respond to B-AL *in vitro*, suggesting lack of some downstream signaling molecular in half this population. It remains unknown how this population can differentially encode itch and pain sensation. *In vivo* recordings from *Mrgprd* knockouts also showed decreased sensitivity to all stimuli, suggesting that natural ligands for Mrgprd may set baseline sensitivity of these fibers (Crozier et al., 2007). Notably, *Mrgprd* has a human homologue (*Mrgprd*), human subjects respond to the Mrgprd ligand B-AL, and units with similar properties to mouse non-peptidergic nociceptors have been identified in primates(Liu et al., 2012; Wooten et al., 2014).

Overall, knockout and neuronal ablation studies show that peptidergic fibers are the likely major mediators of thermal pain while non-peptidergic fibers are likely major mediators of mechanical pain. In general, these studies tested the *necessity* but not the *sufficiency* of these fiber populations for pain behavior. Molecular genetic expression of

optogenetic tools (as described in Chapter 2) will allow for a more complete understanding of the functional role of these populations.

Downstream central partners/pathways of nociceptors

The spinal cord DH contains (1) interneurons, involved in local signal processing, (2) ascending projection neurons, whose axons enter ascending white matter tracts to relay information to supraspinal sites, and (3) so-called 'propriospinal' projection neurons that send axonal projections to other rostral or caudal spinal cord segments (Brown, 1982). The cell bodies of ascending projection neurons for the pain pathway are located in layer I and layers III-VI (but are absent from the SG/layer II) (Brown, 1982). They are revealed by antidromic stimulation or retrograde labeling from supraspinal sites, and they predominantly express the Substance P receptor TACR1 (NK1R) (Lima and Coimbra, 1988; Marshall et al., 1996). Ascending projection neurons are a minority of the neurons in these layers (Yu et al., 2005). The axons of these neurons grow ventrally, cross the midline, and enter a group of (contralateral) white matter tracts on the anterolateral edge of the spinal cord. They terminate in multiple locations including the thalamus (spinothalamic tract), parabrachial nucleus (spinoparabrachial tract), and periacquaductal grey (spinomesencephalic tract). Further, through multisynaptic pathways, they signal to sites throughout the brain including the cortex, amygdala, hypothalamus, and others (Lima and Coimbra, 1988; Spike et al., 2003; Braz et al., 2005).

Cell types of the superficial DH were classically defined using dendritic arbor morphology as revealed by Golgi staining or cell filling (including work from Ramon y

Cajal(Ramón y Cajal, 1909)) (Scheibel and Scheibel, 1968; Grudt and Perl, 2002; Lu and Perl, 2003, 2005; Yu et al., 2005). While classification schemes differ between studies, layer I neurons are commonly divided into 'fusiform', 'multipolar' and 'pyramidal' morphological groups, and projection neurons seem to be evenly distributed between these types (Yu et al., 2005). Layer II neurons are commonly divided into four groups: 'islet', 'central', 'radial', and 'vertical' (Grudt and Perl, 2002; Lu and Perl, 2003, 2005). More recent work has used gene expression to identify DH neuron populations and identified a number of molecular classes (Koch et al., 2018). For example, somatostatin (SOM) marks excitatory interneurons in layers II_o-III that are necessary for signal transmission of mechanical pain (Duan et al., 2014). In general, however, much remains unclear regarding DH cell identities. Morphological schemes leave some neurons 'unclassified', and clear correlations between morphology and circuit function have been difficult to define (Grudt and Perl, 2002). Furthermore, genetic populations are often heterogeneous with regards to morphology, physiology, and/or connectivity. While much has been learned, the further dissection of DH circuits is an important subject for future work.

Like primary afferents, DH neurons have modality response properties and peripheral RFs that can be determined by *in vivo* recording (Light et al., 1992). The majority (~60-70% in various studies) of layer I/II_o neurons respond to nociceptive stimuli (either mechanical only, thermal only, or mechanical and thermal polymodal responses). Some will respond to innocuous mechanical or thermal stimuli, including neurons that respond to both innocuous and noxious stimuli (sometimes called Wide-Dynamic-Range, WDR,

neurons). Interestingly, ablation of peptidergic vs. non-peptidergic primary afferents was reported to cause modality-specific deficits in DH neuron nociceptive responses (peptidergic ablation causing mainly thermal deficits and non-peptidergic ablation causing mainly mechanical deficits) (Zhang et al., 2013). While DH neuron RFs are in general larger than primary afferent RFs (suggesting convergence of primary afferent inputs), the somatotopic map revealed by DH neuron recordings corresponds to the primary afferent maps.

The dendritic and axonal geometry of layer I and layer II interneurons reveals a predominantly horizontal (intra-layer) connectivity, however dorsoventral projections from certain cell types provides pathways for inter-layer connectivity (Scheibel and Scheibel, 1968; Brown, 1982; Kosugi et al., 2013). Since peptidergic fibers project to layers I and V, they synapse onto both projection and non-projection neurons. Layer II-projecting non-peptidergic fibers synapse onto interneurons but not projection neurons. One study that drove the light activated cation channel Channelrhopsin-2 (ChR2) in Mrgprd+ non-peptidergic fibers found that they provide monosynaptic input to all identified layer II cell types (except for inhibitory islet cells) (Wang and Zylka, 2009). Non-peptidergic nociceptors relay pain information by signaling to projection neurons in layers I or V through polysynaptic pathways (Braz et al., 2005; Lu and Perl, 2005).

In addition to feeding into ascending systems, the DH interneurons perform complex signal integration and processing. Among these, local inhibitory neurons allow for both cross-modality (i.e. inhibition of pain signaling by touch input) and within-modality

inhibition (Lu and Perl, 2003; Kardon et al., 2014; Bourane et al., 2015; Cui et al., 2016; Sun et al., 2017). The latter case is the mechanism for **surround inhibition** in CNS pain circuits (Hillman and Wall, 1969; Kato et al., 2011). In surround inhibition, a CNS neuron will have both an excitatory RF (peripheral area in which pain stimuli will excite the neuron) surrounded by a much wider inhibitory RF (peripheral area in which pain stimuli will inhibit the neuron). This surround inhibition mechanism is thought to play a major role for spatial localization of stimuli by sharpening CNS spatial representations.

Despite the progress gained from previous studies, *the region-specific organization of DH pain circuitry has received comparatively little attention.* Much, though not all, of the past research into the cell types and circuits of the DH has focused on the lumbar enlargement. It therefore remains unknown whether cell type compositions, morphologies, and/or circuits may change systematically between body regions. Interestingly, superficial DH neuron RF areas have been reported to vary between body locations, with much smaller RFs in the distal limbs compared to proximal parts of the body (Light et al., 1992). This could play a major role in increasing pain acuity for the distal limbs. The organization mechanisms underlying this difference (DH neuron morphology, primary afferent convergence, surround inhibitory mechanisms, etc.) are unknown.

Development of the mammalian pain system

The mature mammalian pain system is a product of complex developmental processes controlling the specification and wiring of nociceptors. These processes are controlled by

the interplay of trophic factor signals with transcription factors, in addition to other mechanisms. Despite past progress, much remains unclear. In particular, the mechanisms controlling the somatotopically appropriate wiring of pain circuits are largely unknown. The following overview summarizes what is known regarding the development of mammalian pain circuits.

Nociceptor neurogenesis and specification

DRG neurons are derived from neural crest progenitors that exit the cell cycle in two successive waves between E10.5 and E13.5 (in mice) (Lawson and Biscoe, 1979). The first of these neurogenic waves is controlled by expression of the transcription factor *Neurog2* and produces large diameter (mechanoreceptor and limb-position-sensing proprioceptor) DRG neurons. The second wave is controlled by expression of *Neurog1* and produces some large diameter and all small diameter DRG neurons (including nociceptors) (Ma et al., 1999). *Neurog1/2* promote expression of other transcription factors (including *Neurod1*, *Neurod4*, *Pou4f1*, and *Isl1*), which in turn promote the expression of diverse sensory neuron genes (Fedtsova and Turner, 1995; Fode et al., 1998; Montelius et al., 2007; Sun et al., 2008; Lanier et al., 2009). Among these are the genes for the neurotrophic factor receptors NTRK1, NTRK2, and NTRK3 (also known as TRKA, TRKB, and TRKC). These receptors define three lineages producing separate populations of somatosensory neurons (Olson et al., 2016).

Peptidergic and non-peptidergic nociceptors are part of the NTRK1^{+} lineage. NTRK1 is the receptor for NGF, and NGF-NTRK1 signaling is necessary for survival and

specification of nociceptors (White et al., 1996; Patel et al., 2000; Luo et al., 2007). The transcription factor *Runx1* segregates the NTRK1 lineage; while it is initially expressed in almost all NTRK1$^+$ neurons (in a NTRK1-dependent manner (Luo et al., 2007)), by E17.5 ~50% of NTRK1$^+$ neurons have downregulated *Runx1*. Neurons that downregulate *Runx1* will maintain NTRK1 into adulthood, express *Calca,* and become peptidergic nociceptors. Those that maintain *Runx1* will downregulate NTRK1, express the neurotrophic factor receptor RET and its co-receptors, and will become non-peptidergic nociceptors (along with related minor populations)(Chen et al., 2006). Within the RET+ subset, *Runx1* promotes expression of *Mrgprd* and the closely related *Mrgpra*/*b*/*c* genes between E16.5 and P2. While these *Mrgpr* genes are initially highly co-expressed, they are segregated into separate 'Mrgprd' and 'MrgprA/B/C' neuronal compartments postnatally. This segregation is also controlled by *Runx1*; postnatally, the MrgprA/B/C compartment downregulates *Runx1*, while maintained *Runx1* in the MrgprD compartment represses *Mrgpra/b/c* genes (Liu et al., 2008). While *Ret* is not required for survival of the non-peptidergic lineage, it is required for expression of *Mrgpr* genes (Luo et al., 2007).

Wiring of nociceptor connectivity

The initial outgrowth/wiring of DRG neuron projections occurs concomitant with the differentiation of various DRG populations. Beginning around E12-13, DRG neurons develop pseudounipolar axon morphology that extend into the periphery and the spinal cord (Smith, 1983; Reynolds et al., 1991; Mirnics and Koerber, 1995b). Just as large diameter DRG neurons are born before small diameter neurons, outgrowth and wiring of small diameter (including nociceptor) fibers follows the large diameter myelinated

afferents. Centrally, outgrowing large-diameter axons (immunostained using NEFH) reach the dorsal margin of the spinal cord, pause for ~1-2 days, and begin to innervate the DH grey matter from the medial edge ~E16.5. They are followed by the small diameter fibers (immunostained using NTRK1), which begin to innervate the DH just before birth (Reynolds et al., 1991; Mirnics and Koerber, 1995a; Jackman and Fitzgerald, 2000). Peripherally, large-diameter myelinated afferents begin to the proximal hindlimb ~E14. Skin innervation proceeds distally, reaching the distal foot and toe epidermis by E17-E18. Innervation by small diameter fibers (immunostained using TRKA) follows shortly after, penetrating the proximal hindlimb epidermis ~E15 and reaching the distal hindpaw epidermis around the time of birth (Mirnics and Koerber, 1995b; Jackman and Fitzgerald, 2000).

The peripheral wiring of nociceptors is dependent on trophic factor signaling. Mutant mice lacking *Ntrk1* or *Ngf* (which also lack the pro-apoptotic gene *Bax* to bypass cell death) lack epidermal innervation of both peptidergic and non-peptidergic fibers (Patel et al., 2000). Similarly, deletion of *Ret* expression prevents epidermal innervation by non-peptidergic fibers (Luo et al., 2007). However, central innervation is maintained in all these cases, suggesting that separate developmental mechanisms control the central and peripheral development of nociceptors.

Topographic wiring of the somatosensory system

Much is known regarding the developmental mechanisms for the topographic specification and wiring of the lower motor neurons of the ventral spinal cord (Dasen et

al., 2005; De Marco Garcia and Jessell, 2008; Dasen and Jessell, 2009). In this system, transcription factor codes specify pools of motor neurons based on their muscle target, and these codes direct motor neuron wiring by driving expression of guidance factors. By comparison, very little is understood regarding the developmental mechanisms directing somatotopically-appropriate wiring of somatosensory neurons. Nerve tracing experiments have shown that cutaneous sensory topographic innervation patterns (in both the periphery and the spinal cord) traced in late embryonic/early postnatal chicks and rodents are similar to the mature pattern, suggesting that DRG afferents form topographically 'correct' maps in their initial innervation (Smith, 1983; Mendelson et al., 1992). Sensory neurons also innervate the correct laminar position during their initial growth into the DH (Ozaki and Snider, 1997). Interestingly, somatosensory cell bodies appear to be somatotopically segregated in embryonic DRGs (Mirnics and Koerber, 1995b), although this segregation is less clear in adults.

Based on the rough coincidence of peripheral and central target innervation, and based on the proximal-to-distal progression of hind limb epidermal innervation, it was proposed that peripheral innervation could direct topographic innervation of the spinal cord (Reynolds et al., 1991). However, multiple lines of evidence have since suggested that peripheral and central topographic innervation patterns develop independently of one another. First, in contrast to the proximal-to-distal progression of skin innervation, proximal and distal hind limb afferents innervate the DH simultaneously (Mirnics and Koerber, 1995a). Further, cultured spinal segments with attached DRGs taken from chick embryos have shown that cutaneous afferents can innervate the DH in the absence of any

peripheral targets (Sharma et al., 1994). Lastly, Wang and Scott (Wang and Scott, 2002) found that inducing DRGs to innervate a novel cutaneous target does not change the location of their central innervation patterns. In these experiments, shifting chick limb buds rostrally before DRG outgrowth results in a comparatively normal topographic innervation map in the new rostral location. While this work has shown that peripheral and central innervation patterns are likely established through independent mechanisms, they have not identified how these maps are directed during development. This is an important question for future work.

CHAPTER 2:

Sparse-genetic tracing reveals region-specific organization of the mammalian pain system

This chapter is adapted from:

Olson W, Abdus-Saboor I, Cui L, Burdge J, Raabe T, Ma M, Luo W (2017) Sparse genetic tracing reveals regionally specific functional organization of mammalian nociceptors. Elife 6.

Abstract

The human distal limbs have a high spatial acuity for noxious stimuli but a low density of pain-sensing neurites. To elucidate mechanisms underlying regional differences in processing nociception, we sparsely traced non-peptidergic nociceptors across the body using a newly generated *Mrgprd*^{CreERT2} mouse line. We found that mouse plantar paw skin also innervated by a low density of Mrgprd+ nociceptors, while individual arbors in different locations are comparable in size. Surprisingly, the central arbors of plantar paw and trunk innervating nociceptors have distinct morphologies in the spinal cord. This regional difference is well correlated with a heightened signal transmission for plantar paw circuits, as revealed by both spinal cord slice recordings and behavior assays. Taken together, our results reveal a novel somatotopic functional organization of the mammalian pain system and suggest that regional central arbor structure could facilitate the "enlarged representation" of plantar paw regions in the CNS.

Introduction

The skin mediates physical contact with environmental mechanical, thermal, and chemical stimuli. As an animal moves through the world, certain parts of the skin are likely sites of "first contact" with these stimuli (the distal limbs, face/whiskers, and tail for quadrupedal mammals like mice). Therefore, these somatosensory regions require heightened sensitivity to fulfil behaviorally relevant functions, such as environment exploration.

Touch and pain are the two most important somatosensory modalities for this functional purpose: touch allows for feature detection while pain prevents tissue damage. Indeed, classic work has defined important regional specialization of the nervous system for tactile sensation in these areas. Two mechanisms in the peripheral organization of the discriminative touch system facilitate high spatial acuity sensation in the primate distal limbs and mouse whisker pad. These are the *high innervation density* and *smaller receptive field sizes* of the primary light touch neurons, the Aβ mechanoreceptors, in these regions (Weinstein, 1968; Brown and Koerber, 1978; Johansson and Vallbo, 1979, 1980; Rice et al., 1993; Pare et al., 2002; Brown et al., 2004). In contrast, the question of whether regional specialization exists in the mammalian pain system has remained elusive until recently. Upon stimulation using nociceptive-specific laser beams, human subjects show a heightened spatial acuity in the distal limbs (especially the fingertips) for pain stimuli, much like they do for touch stimuli (Mancini et al., 2012; Mancini et al., 2013; Mancini et al., 2014). This suggests that this region is also a "pain fovea" for humans. However, human fingertip skin has a relatively *low density of pain-sensing neurites*(Mancini et al.,

2013). While this suggests that region-specific organization likely exists in pain circuits downstream of the periphery (i.e. central nervous system), currently the exact underlying neural mechanisms are unclear.

Though previous work has mapped the peripheral receptive fields or traced the central terminals of mammalian nociceptors (Szentagothai, 1964; Bessou and Perl, 1969; Rethelyi, 1977; Lynn and Carpenter, 1982; Sugiura et al., 1986; Lynn and Shakhanbeh, 1988; Sugiura et al., 1989; Treede et al., 1990; Schmidt et al., 1997; Schmidt et al., 2002), these studies have not established a model for the somatotopic functional organization of the mammalian pain system due to the limited number of neurons traced from restricted skin regions. Recently, the single-cell structure of defined somatosensory neurons has been successfully revealed using sparse genetic tracing, a technique in which genetically targeted neurons are labeled at low density to resolve single neuron morphology (Liu et al., 2007; Li et al., 2011; Wu et al., 2012).

To reveal the region-specific organization of mammalian nociceptors across the entire body, we sought to perform sparse genetic tracing of Mrgprd+ non-peptidergic neurons. We chose this population because they are the most abundant type of cutaneous nociceptor and they likely correspond to the main type of free nerve terminals stained with anti-PGP9.5 antibody in previous human skin biopsy data (Zylka et al., 2005; Mancini et al., 2013). We generated a novel *Mrgprd*^{CreERT2} mouse line and utilized this line to characterize the somatotopic organization of this populations.. Indeed, like the human skin biopsy results, we found that Mrgprd+ neurites have a comparatively low neurite

density in plantar paw compared to trunk skin. Retrograde tracing experiments further show that the number of Mrgprd+ neurons innervating plantar paw glabrous skin is lower compared to those innervating upper hind limb hairy skin. In addition, and in contrast to the Aß mechanoreceptors, sparse genetic tracing revealed that the arbor field sizes of individual nociceptors are comparable between different skin regions. Strikingly, plantar paw and trunk innervating nociceptors display distinct morphologies in their central terminals. Moreover, using *Mrgprd*^{CreERT2}; *Rosa*$^{ChR2\text{-}EYFP}$ mice, we specifically activated these nociceptors using blue laser light during *in vitro* spinal cord slice recordings and during behavior assays. We found that, while almost all layer II DH neurons in all locations receive direct Mrgprd+ afferent input, the optical threshold required to induce postsynaptic responses is much lower in plantar paw regions. This was paralleled by a decrease in the light intensity threshold required to elicit a withdrawal response in paw, compared to upper thigh, skin stimulation. Collectively, we have identified a previously unappreciated somatotopic difference in the central terminals of mammalian nociceptors. Our anatomical, physiological, and behavior data suggest that region-specific central arbor structure could be one important mechanism to magnify the representation of plantar paw nociceptors in the DH to facilitate region-specific pain processing.

Generation and specificity of *Mrgprd*^{CreERT2} mice

Given that previous descriptions of nociceptor structure have not allowed for systematic comparisons between body regions, we sought to use sparse genetic labeling to trace

single nociceptor morphologies across the entire somatotopic map. We generated a mouse line in which a tamoxifen-inducible Cre (CreERT2) cassette is knocked into the coding region of Mas-related gene product receptor D (*Mrgprd*) (Figure 1, Figure 2A). Consistent with the previous finding that *Mrgprd* is expressed more broadly in early development than in adulthood(Liu et al., 2008), early embryonic (E16.5-E17.5) tamoxifen treatment of $Mrgprd^{CreERT2}$ mice labels *Mrgprd* expressing neurons along with non-peptidergic neurons expressing other *Mrgpr* genes, such as *Mrgpra3* and *Mrgprb4* (Figure 3). In contrast, when we crossed $Mrgprd^{CreERT2}$ mice with a Cre-dependent $Rosa^{ChR2\text{-}EYFP}$ line and provided postnatal (P10-P17) tamoxifen treatment (Figure 2B), Mrgprd+ non-peptidergic nociceptors were specifically labeled. We examined these treated mice at 4 postnatal weeks or older (>4pw), a time point at which Mrgprd+ non-peptidergic nociceptors have completely segregated from other $Mrgpr^{+}$ DRG neurons (Liu et al., 2008). We found that ChR2-$EYFP^{+}$ DRG neurons bind IB4 (a marker for non-peptidergic DRG neurons) but do not express CGRP (a marker for peptidergic DRG neurons) (Zylka et al., 2005) (Figure 2C), and ChR2-$EYFP^{+}$ DH terminals similarly overlap with IB4 but not CGRP (Figure 2G). Double *in situ* hybridization demonstrated that this strategy efficiently labels DRG neurons expressing *Mrgprd* (88.1 ± 1% of ChR2-$EYFP^{+}$ neurons, $n = 3$ animals) but not those expressing *Mrgpra3* (1.4 ± 0.1%) or *Mrgprb4* (0.4 ± 0.3%) (Figure 2D-F). Almost all *Mrgprd* expressing neurons were labeled with ChR2-EYFP (92.9 ± 4.6% of *Mrgprd*+ neurons) by this treatment. Therefore, this newly generated inducible $Mrgprd^{CreERT2}$ line allows for the specific and efficient targeting of adult Mrgprd+ nociceptors.

We then sought to trace individual Mrgprd+ non-peptidergic nociceptors using sparse genetic labeling. When crossed with a Cre-dependent alkaline phosphatase reporter line (*Rosa*^{iAP}), we found that sparse recombination occurs in the absence of tamoxifen treatment (Figure 4A&B). This background recombination labels 3-11 neurons/DRG (5.2 ± 1.6 neurons/DRG, n = 47 DRGs from 3 animals) in 3-4 pw animals (Figure 4C), which represents <1% of the total Mrgprd+ nociceptor population (Molliver et al., 1997; Wright et al., 1997; Zylka et al., 2005). The sparsely labeled DRG neurons co-express non-peptidergic nociceptor markers peripherin, PAP (Zylka et al., 2008), and RET (Figure 4D, F, H), but do not express NF200 or CGRP (Figure 4E, G). To further determine the specificity of this sparse recombination, we used an *Mrgprd*^{EGFPf} knock-in line(Zylka et al., 2005), in which expression of EGFP mimics the dynamic expression of endogenous *Mrgprd*. We generated *Mrgprd*$^{CreERT2/EGFPf}$; *Rosa*^{iAP} triple mice and found that almost all AP^{+} neurons co-express *Mrgprd*^{EGFPf} (93. 7 ± 2.3%, n = 126 AP^{+} neurons from 3 animals) (Figure 4I) in 3 to 4pw mice. This result indicates that, although *Mrgprd* is broadly expressed during early development, this background recombination occurred preferentially in adult Mrgprd+ nociceptors.

Genetic tracing of Mrgprd+ skin terminals reveals a relatively comparable somatotopic organization in the periphery

Mrgprd+ neurons innervate both hairy and glabrous skin and are the most abundant class of cutaneous free nerve arbors (Zylka et al., 2005). To systematically compare the peripheral single-cell structure of mammalian pain neurons across the somatotopic map,

we performed whole mount colorimetric AP staining using untreated 3-4 pw *Mrgprd*^{CreERT2}; *Rosa*^{iAP} skin.

We found that 98.4% (130/132 arbors, n = 4 animals) of single-cell arbors have a "bushy ending" morphology (Figure 5A&B, D&E, Figure 6A) (Wu et al., 2012), featuring thickened terminal structures in the epidermis. The distal ends of arbors in glabrous plantar paw skin have single, un-branched thickened neurites (Figure 5A&B), while arbors in the hairy skin feature both un-branched neurites as well as dense neurite clusters (Figure 5D&E). These dense clusters form circumferential like endings that innervate the necks of hair follicles (red arrowheads in Figure 5E&F, Figure 6) (Zylka et al., 2005). Whole mount immunostaining of *Mrgprd*^{EGFPf} skin shows that all three types of hair follicles in mouse hairy skin (guard, awl/auchenne, and zigzag(Li et al., 2011)) are innervated by *Mrgprd*^{EGFPf} fibers (Figure 6D-H). A very small minority (1.6%) of arbors in the hairy skin have "free endings" (Wu et al., 2012) lacking these thickened structures (Figure 6A-C).

Mrgprd+ non-peptidergic nociceptive field sizes range from 0.08 to 0.9 mm^2, with the smallest average field size found in the head skin between the ears and in the proximal limbs (Figure 5G, Table 1). Interestingly, non-peptidergic nociceptors innervating the distal limbs (plantar and dorsal paw skin) have average arbor sizes close the middle of this range, and distal limb and trunk arbors are comparable in size (Figure 5G&H, Table 1). In addition, consistent with human skin (Mancini et al., 2012), whole-population labeling of Mrgprd+ fibers using tamoxifen (0.5 mg at P11) reveals that the overall neurite density is

similar or slightly lower in the paw glabrous skin compared to trunk hairy skin (Figure 5C&F). We further performed a retrograde DiI labeling experiment using *Mrgprd*^{EGFPf} mice to compare the Mrgprd+ neuron innervation densities (i.e. number of neurons innervating a unit area of skin) between paw and upper hind limb regions (Figure 7, Table 2). Consistent with the overall neurite density, we found that the neuron density is higher in the proximal hind limb compared to plantar paw (cells/mm^2 of skin: proximal hind limb = 97.6 ± 33.4, plantar hind paw = 21.0 ± 3.0, n = 7 injections for each, p = 0.04, Student's t test) (Figure 5I). In short, in contrast to mammalian Aβ mechanoreceptors, plantar paw innervating mouse non-peptidergic nociceptors do not display higher density or smaller receptive field sizes compared to other regions.

Mrgprd+ nociceptors show regionally distinct organization in their central arbors

Since the peripheral organization of Mrgprd+ non-peptidergic nociceptors does not exhibit an obvious mechanism to facilitate heightened sensitivity in the plantar paw, we next used whole mount AP staining of untreated 3-4 pw *Mrgprd*^{CreERT2}; *Rosa*^{iAP} spinal cords to compare their central arbors between regions. Non-peptidergic nociceptor central branches enter the spinal cord through the dorsal root, travel rostrally or caudally for 0 to 3 segments, and then dive ventrally to establish arbors in layer II of the DH (Table 3)(Zylka et al., 2005). Most Mrgprd+ central branches do not bifurcate (65.8%, n = 234 neurons from 3 animals), and most also terminate within the segment of entry (72.6%) (Table 3). However, some (34.2%) bifurcate one or more times in the spinal cord, and some (27.3%) travel up to 3 segments from the point of entry (Table 3). For the central

branches that bifurcate, most of their secondary/tertiary branches join other branches from the same neuron to co-form one axonal arbor, while some end with a second arbor or terminate in the spinal cord without growing an arbor (Table 3, Figure 9). The majority (91.9%) of labeled nociceptors have only one arbor, but a few have 2 (6.8%), or 3 (0.9%) central arbors, and for a small number of Mrgprd+ nociceptors (0.4%), we could not identify any arbor (Table 3).

Strikingly, Mrgprd+ non-peptidergic nociceptor central arbors display two different morphologies that can be distinguished by the ratio of their mediolateral width to their rostrocaudal height (W/H ratio) (Figure 8H). We defined arbors with W/H ratios >0.2 as "round" (Figure 8A-C, H, and Table 4) and arbors with W/H ratios <0.2 as "long and thin" (Figure 8B-F, H, and Table 4). Further, these morphological types are regionally segregated. Round arbors are found in DH regions known to represent the distal limbs (medial cervical and lumbar enlargements) as well as tail, anogenital (sacral DH), and head/face (descending trigeminal terminals in the upper cervical DH and medulla) skin (Figure 8B&C, H, J, and Figure 9) (Koerber and Brown, 1982; Molander and Grant, 1985). Long arbors are instead located in regions corresponding to the proximal limbs (lateral cervical and lumbar enlargements) and trunk skin (thoracic DH) (Figure 8B-F, H, J) (Koerber and Brown, 1982; Cervero and Connell, 1984; Molander and Grant, 1985). While round and long arbors differ in morphology, they do not differ in area (Figure 8G).

In the cervical and lumbar enlargements (C3-C6, L3-L6), the medial DH contains a curved zone of round arbors that is encircled by laterally located long arbors (Figure 8C).

Somatotopic mapping of the cat and rat DH indicates that this medial curved zone in the lumbar enlargement matches the representation of the plantar paw and digits, with the dorsal paw and proximal limb representations lying more laterally (Brown and Fuchs, 1975b; Koerber and Brown, 1982; Molander and Grant, 1985; Swett and Woolf, 1985; Woolf and Fitzgerald, 1986; Brown et al., 1991; Takahashi et al., 2002; Takahashi et al., 2007). We compared the number of labeled peripheral arbors in the toe and plantar paw skin with the number of round DH terminals in the corresponding half of the lumbar enlargement. This showed a very close correlation (Figure 8I), supporting that the round central arbors of the lumbar enlargement correspond to plantar paw and digit Mrgprd+ nociceptors, while nociceptors from other regions of the hindlimb (including dorsal hindpaw and proximal hindlimb) grow long central arbors located more laterally.

In our sparse *Mrgprd*^{CreERT2}; *Rosa*^{iAP} mice, <1% of Mrgprd+ neurons are traced. It therefore remains possible that this round-vs.-long central arbor regional distinction we identified may be an artifact of sparse labeling. For example, if both types were found throughout the DH but were differentially enriched between regions, sparse labeling might only trace the most prevalent type in each location. Using increasing dosages of tamoxifen, we found that these arbor types occupy mutually exclusive zones of the DH (Figure 10). The maintained segregation of long and round arbors in the DH despite the increased number of AP^{+} DRG neurons indicates that these arbor morphologies represent a true somatotopic distinction among Mrgprd+ non-peptidergic nociceptors.

Given the clear difference in paw and trunk Mrgprd+ central arbors, we next asked whether the population-level density of non-peptidergic innervation of the DH also shows regional differences. In *Mrgprd*^{CreERT2}; *Rosa*$^{ChR2\text{-}EYFP}$ mice (P10-P17 tamoxifen, Figure 2), we saw comparable expression of ChR2-EYFP, as measured by native fluorescence intensity, in the cell bodies of thoracic (T9-T12) and hind limb-level (L3-L5) DRGs (Figure 11A, C, E). However, in the DH, medial lumbar enlargement (plantar paw) regions show a significant increase in EYFP fluorescence compared to lateral lumber or thoracic regions (Figure 11B, D, F). The same is true for membrane-bound EGFPf fluorescence in *Mrgprd*^{EGFPf} mice (Figure 11G-L), indicating that this is not due to differential trafficking of a given protein. These findings suggest an overall increase in the amount of Mrgprd+ afferent membrane in the spinal cord region representing the plantar paw compared to trunk regions.

Neighboring non-peptidergic nociceptors highly overlap in the skin and spinal cord

The axonal arbors of some somatosensory neurons have a non-overlapping arrangement between neighbors ("tiling") in the body wall of the fly and zebrafish (Grueber et al., 2002; Sagasti et al., 2005). To determine if mammalian non-peptidergic nociceptive arbors tile in the skin, we generated double knock-in *Mrgprd*$^{CreERT2/EGFPf}$; *Rosa*^{tdTomato} mice. After low-dose tamoxifen treatment, sparsely labeled Mrgprd+ neurons in these mice express tdT while the entire population expresses EGFP. The arbor fields of individual double tdT^{+}/EGFP^{+} neurons are always co-innervated by EGFP^{-}only^{+} fibers in both hairy and glabrous skin (Figure 12A-D), indicating that peripheral arbors of neighboring non-

peptidergic nociceptors do not tile but instead overlap extensively. In hairy skin, sparse labeled tdT$^+$ neurites co-innervated hair follicles with EGFP-only$^+$ fibers, indicating that multiple Mrgprd+ neurons can innervate a single hair follicle. This sparse labeling reveals that a single hairy-skin Mrgprd+ arbor can innervate both hair follicles and form free nerve endings in the epidermis (Figure 12A-C). This single-cell arrangement has not previously been demonstrated for any nociceptor population. In the DH, both round and long DH arbors of non-peptidergic nociceptors highly overlap with their neighbors, similar to the periphery (Figure 12E&F).

Heightened signal transmission in the paw DH circuitry of Mrgprd+ neurons

Next, given the striking somatotopic differences in the central arbor organization of Mrgprd+ nociceptors, we asked whether we could find regional (plantar paw vs. trunk) differences in the transmission of sensory information at the dorsal horn. We generated *Mrgprd*^{CreERT2}; *Rosa*$^{ChR2\text{-}EYFP}$ mice, which were treated with postnatal tamoxifen (>P10, Figure 2), to compare the synaptic transmission of these neurons between somatotopic regions in spinal cord slice recordings. We first used *Mrgprd*$^{CreERT2/+}$; *Rosa*$^{ChR2\text{-}EYFP/ChR2\text{-}EYFP}$ mice (mice homozygous for the *Rosa*$^{ChR2\text{-}EYFP}$ allele) to perform *in vitro* whole-cell patch-clamp recordings of layer II interneurons located in the territory innervated by ChR2-EYFP$^+$ fibers in transverse spinal cord sections (Fig. 13A). Light-evoked excitatory postsynaptic currents ($EPSC_L$s) in these neurons could be differentiated into monosynaptic or polysynaptic responses based on latency, jitter, and response failure rate during 0.2 Hz blue light stimulation (Figure 13B&C) (Cui et al., 2016). Almost all

recorded neurons in both medial and lateral lumbar DH showed $EPSC_L$s (Figure 13D, Table 5), with most cells (14/17 = 82.4% in medial lumbar, 14/16 = 86.5% in lateral lumbar) showing monosynaptic $EPSC_L$s in both locations. This indicates that the majority of DH neurons in this innervation territory receive direct Mrgprd+ input, and that the incidence receiving direct input is equivalent for medial lumbar and lateral lumbar DH.

Given the very high level of ChR2 expression in these mice, any potential difference between the medial and lateral lumbar spinal cord may be masked by a "ceiling" effect. We therefore halved the genetic dosage of $Rosa^{ChR2\text{-}EYFP}$ by taking slices from $Mrgprd^{CreERT2;}$ $Rosa^{ChR2\text{-}EYFP/+}$ mice (heterozygous for the $Rosa^{ChR2\text{-}EYFP}$ allele). $Rosa^{ChR2\text{-}EYFP}$ hetereozygous DRGs have a ~40% reduction in ChR2-EYFP protein compared to $Rosa^{ChR2\text{-}EYFP}$ homozygous DRGs based on Western blotting (Figure 14D&E). Interestingly, we saw a dramatic difference when comparing the medial and lateral lumbar DH of double heterozygous mice. Medial lumbar DH neurons showed a much higher incidence of light responses than lateral lumbar neurons, with a ~9-fold higher (15/17 = 88.2% vs. 2/19 = 10.5%) incidence of monosynaptic $EPSC_L$s over lateral lumbar neurons (Figure 13E, Table 5). Similar to the lateral lumbar DH, the incidence of monosynaptic $EPSC_L$s of layer II neurons in the medial and lateral thoracic region are also very low (1/11 = 9.1%) (Figure 13E, Table 5). Moreover, even among responsive neurons, the pulse duration threshold required to elicit $EPSC_L$s was much longer in lateral lumbar and thoracic DH neurons compared to medial lumbar neurons (Figure 13F). These results showed a lower threshold for light-trigged excitatory currents in medial lumbar compared to lateral lumbar and thoracic DH neurons, suggesting a heightened signal transmission in plantar

paw circuits. We repeated these recordings in sagittal spinal cord slices and similarly found a higher $EPSC_L$ incidence in medial lumbar compared to lateral lumbar or thoracic DH (Table 5). This confirms that these differences are not caused by the different orientation of nociceptors in round vs. long arbor regions. Lastly, we also looked for Mrgprd-driven inhibitory currents by changing the holding potential of DH neurons during the recording in *Mrgprd*$^{CreERT2;}$ *Rosa*$^{ChR2\text{-}EYFP/+}$ heterozygotes. Neurons showing monosynaptic $EPSC_L$ also showed IPSCs triggered by Mrgrd activation ($IPSC_L$s), and these were blocked by bath application of bicuculline and strychnine (blockers for $GABA_A$ and glycine receptors, respectively) (Figure 15A). The incidence of these $IPSC_L$s showed similar regional differences to excitatory currents, with most medial lumbar (13/17 = 76.5%) neurons showing $IPSC_L$s and most lateral lumbar (16/19 = 84.2%) and thoracic (8/11 = 72.7%) neurons showing no $IPSC_L$s (Figure 15B, Table 5).

Taken together, our results show that, while most DH neurons in the Mrgprd+ innervation territory receive direct Mrgprd+ input, the overall signal transmission is heightened in plantar paw compared to trunk nociceptive circuits. This heightened transmission was seen specifically at the level of nociceptor-to-DH neuron connections, and it correlates closely with the region-specific organization of Mrgprd+ central arbors. Further, we found that this heightened connectivity also translates into stronger Mrgprd+ driven inhibitory currents, though this result will need to be complemented with recording from *Mrgprd*$^{CreERT2;}$ *Rosa*$^{ChR2\text{-}EYFP/ChR2\text{-}EYFP}$ homozygotes. This result is interesting as it could provide a mechanism for strengthened surround inhibition in Mrgprd+ circuits.

Plantar paw Mrgprd+ nociceptors have a lower stimulation threshold to induce avoidance behaviors

Finally, we asked whether the anatomical and physiological region-specific differences we identified are correlated with functional differences in a freely behaving animal. To activate ChR2 in skin-innervating nociceptors of behaving mice, we stimulated *Mrgprd*^{CreERT2}; *Rosa*$^{ChR2\text{-}EYFP/ChR2\text{-}EYFP}$ (M) and *Rosa*$^{ChR2\text{-}EYFP/ChR2\text{-}EYFP}$ (C) mice (P10-17 tamoxifen treatment) at both the paw and upper-thigh leg skin (Figure 16B&E) with either 473nm blue light or 532nm green light as a negative control. We only used ChR2 homozygous mice in these behavior assays because ChR2 heterozygous mice do not show any obvious response to peripheral optogenetic stimulation (data not shown). High levels of ChR2-EYFP were expressed in peripheral neurites in both plantar paw and upper leg skin (Figure 16A&D). Consistent with the AP labeling (Figure 5), upper leg skin shows a much higher density of EYFP^{+} neurites than the paw glabrous skin (Figure 17A-C). In addition, ChR2-EYFP^{+} neurites in paw glabrous skin terminate much farther from the surface than leg hairy skin neurites (Figure 17A, B, D) due to the thicker outer *stratum corneum* layer in glabrous skin.

We first stimulated the paw skin of both groups of mice with green light (5mW, 10 Hz, sine wave) and observed no avoidance behavior such as paw withdrawal (Figure 16C). When we stimulated both groups of mice with 1mW of blue light (10 Hz, sine wave), control mice did not respond, while 12.5% of *Mrgprd*^{CreERT2}; *Rosa*$^{ChR2\text{-}EYFP}$ mice displayed light-induced paw withdrawal (Figure 16B&C). When stimulated with 5mW blue light

(10 Hz, sine wave), 100% of *Mrgprd*^{CreERT2}; *Rosa*$^{ChR2\text{-}EYFP}$ mice displayed clear light-induced paw withdrawal. Control mice still did not respond (Figure 16B&C, Figure 17F).

Strikingly, when we activated Mrgprd+ neurites in the shaved upper-thigh skin, neither control nor *Mrgprd*^{CreERT2}; *Rosa*$^{ChR2\text{-}EYFP}$ mice responded to 5mW blue light (Figure 16E&F, Figure 17F). Rather, to observe a fully penetrant avoidance behavior response in the upper-thigh of *Mrgprd*^{CreERT2}; *Rosa*$^{ChR2\text{-}EYFP}$mice, the blue light power intensity had to be increased to 10 or 20 mW (2-4 times higher than the requirement in the paw) (Figure 16E-G). When taking the temporal delay of avoidance responses (Figure 16H) into consideration, 20mW intensity blue light is required at the leg to trigger responses comparable to 5mW intensity stimulation of the paw. In short, the light intensity threshold required to trigger an avoidance response is significantly lower in the paw compared to the upper-limb of *Mrgprd*^{CreERT2}; *Rosa*$^{ChR2\text{-}EYFP}$mice.

Discussion

Here, we identified a novel somatotopic organization in the central arbors of mammalian Mrgprd+ nociceptors, which is very well correlated with a regional increase in the sensitivity of paw nociceptive circuits to external stimuli. Our results suggest a model (Fig. 17), in which the wider mediolateral spread of plantar paw nociceptor central arbors could facilitate "afferent magnification" (Catania and Kaas, 1997; Catania et al., 2011) in downstream CNS circuits and facilitate heightened pain sensitivity of the plantar paw. Remarkably, two features of mouse non-peptidergic nociceptors revealed by our study, the peripheral neurite density distribution and the heightened sensitivity of pain processing in the distal limb, are consistent with findings in humans (Mancini et al., 2012; Mancini et al., 2013; Mancini et al., 2014). Therefore, the organizational mechanisms we discovered in mice are likely to be conserved in humans, which provides a possible explanation for the human "pain fovea".

Mrgprd^{CreERT2} allows for specific targeting of adult Mrgprd+ nociceptors

Adult mice have two functionally distinct DRG neuronal populations expressing Mas-related gene product receptor (*Mrgpr*) genes. One expresses *Mrgpra, Mrgprb,* and *Mrgprc* genes and the other only expresses *Mrgprd* (Dong et al., 2001; Zylka et al., 2003; Liu et al., 2007; Liu et al., 2008; Liu et al., 2009; Liu et al., 2012; Han et al., 2013). Mrgpra/b/c^{+} neurons also transiently express *Mrgprd* during early development (Liu et al., 2008). To specifically target Mrgprd+ neurons, we generated a new inducible *Mrgprd*^{CreERT2} mouse line that allows for temporally controlled recombination. We demonstrated that postnatal

(P10 or later) tamoxifen treatment of *Mrgprd*^{CreERT2} mice specifically targets Mrgprd+ but not Mrgpra/b/c^{+} neurons (Figure 2, 3).

To our advantage, we also found that sparse recombination in untreated *Mrgprd*^{CreERT2}; *Rosa*^{iAP} mice is very specific for Mrgprd+ neurons (~94% AP+ neurons are Mrgprd+, Figure 2I). We noticed that most of this random recombination likely occurs postnatally, as untreated *Mrgprd*^{CreERT2}; *Rosa*^{iAP} tissue at P7 or younger shows no AP+ neurons (data not shown). This temporal delay of recombination, along with the fact that there are many more Mrgprd+ than Mrgpra/b/c+ neurons (Dong et al., 2001; Liu et al., 2007; Liu et al., 2008; Liu et al., 2009), likely contributes to the specificity of sparse AP labeling in these mice.

In this chapter, data is presented using prenatal tamoxifen treatment of *Mrgprd*^{CreERT2} mice for two experiments: increasing density labeling (Figure 10) and *Mrgprd*$^{CreERT2/EGFPf}$; *Rosa*^{tdTomato} labeling to show nociceptor overlap (Figure 12). In these experiments, both Mrgprd+ and Mrgpra/b/c+ neurons could be targeted. For the overlap experiment, neurites were chosen that had both red (*Mrgprd*^{CreERT2} ; *Rosa*^{tdTomato}) and green (*Mrgprd*^{EGFPf}) fluorescence at 3pw, indicating these were Mrgprd+ neurites. For the increased density labeling experiment, even with high dosage (population-level) prenatal tamoxifen treatment of this line, Mrgpra/b/c+ neurons make up <20% of the total cells labeled (Figure 3). Given the nature of this experiment, we believe that our interpretation is not confounded by this issue.

Peripheral features of Mrgprd+ nociceptors show no obvious mechanism for heightened pain sensitivity in the paw.

Though previous studies have traced various cutaneous somatosensory neurons, no systematic characterization of nociceptor morphology across the somatotopic map has been performed. In the periphery, sparse tracing of *Pou4f1* expressing somatosensory neurons (which includes almost all somatosensory DRG neuron classes (Badea et al., 2012)) in the back hairy revealed a "bushy ending" morphological type (Wu et al., 2012). The authors suggested these terminals might correspond to C-fiber nociceptors or thermoceptors. In addition, Mrgprb4+ and TH+ C fibers , which mainly mediate light touch but not pain, and innervate hairy skin only, have been genetically traced and analyzed (Liu et al., 2007; Li et al., 2011). Mrgprb4+ neurons innervate the skin in large patches of free terminals (Liu et al., 2007), while TH+ neurons form lanceolate endings around hair follicles (Li et al., 2011). To our knowledge, single-cell tracing has not previously been performed for any C-fiber nociceptors innervating the glabrous skin.

Mrgprd+ nociceptors innervate both hairy and glabrous skin but not deep tissues (Zylka et al., 2005), making this population ideal for analysis of somatotopic differences. Our *Mrgprd*^{CreERT2} tracing reveals that Mrgprd+ nociceptors display a bushy-ending morphology in hairy skin and thickened endings in the epidermis in the glabrous skin (the plantar paw and finger tips) (Figure 5). Interestingly, individual Mrgprd+ afferents in hairy skin innervate both the hair follicle and the interfollicular skin (Figure 5, Figure 6, Figure 12). Recently, a separate population of afferents that express CGRP and form

circumferential endings around the deep hair follicle (deeper than Mrgprd+ endings) were identified as mediators of pain upon hair pulling (Ghitani et al., 2017). Our single-cell tracing suggests that a single Mrgprd+ afferent may signal both hair pulling as well as mechanical noxious stimuli applied to the skin surface. Further analysis would be required to test this possibility. Very rarely, we found "free ending" terminals that lack thickened epidermal ending (Figure 6). These match the morphology and size of Mrgprb4+ light touch neurons (Liu et al., 2007), possibly indicating very rare labeling of this subset. The fact that <2% of hairy skin terminals displayed this morphology further supports the specificity of *Mrgprd*^{CreERT2} sparse recombination.

We found that (1) the density of Mrgprd+ C fiber nociceptive neurites is similar or slightly lower in paw (including digit tips) compared to trunk skin, (2) Mrgprd+ neuron density is lower in the plantar paw compared to the upper hind limb skin, and (3) paw and trunk individual terminals are comparable in the innervation area (Figure 5). This last result contrasts with the work of Schmidt et al (Schmidt et al., 1997), in which single-fiber recordings of human mechanically responsive C-fiber units showed smaller receptive fields in the distal leg. This discrepancy could be caused by differences between species, techniques (physiological vs. direct anatomic tracing), or the composition of neurons that were analyzed (the previous study presumably recorded from multiple molecular classes). In short, in our analysis of mouse Mrgprd+ nociceptors, we did not find any obvious peripheral mechanism that might readily explain the heightened pain acuity of the distal limbs seen in human subjects or the increased sensitivity of the mouse plantar paw to optogenetic skin stimulation (Figure 16).

Mrgprd+ nociceptors display region-specific organization of central arbors

Classic studies have characterized the single-cell central arbors of C-fiber afferents using Golgi staining or backfill techniques and described them as longitudinally-oriented "thin sheets" that are short in the mediolateral axis and extended in the rostrocadual axis (Scheibel and Scheibel, 1968; Sugiura et al., 1986; Sugiura et al., 1989). This description corresponds well to the "long arbors" we found in DH zones representing proximal limb and trunk regions (Figure 4). The central terminals of Mrgprb4^{+} and TH^{+} C-fiber light touch neurons also match this long terminal morphology, consistent with the fact that these classes only innervate hairy skin (Liu et al., 2007; Li et al., 2011). Nevertheless, a systematic comparison of nociceptive central terminals across the entire somatotopic map has not been conducted.

Here, we found regionally distinctive central arbor organization among Mrgprd+ nociceptors; those innervating the distal limbs, tail, anogenital skin, and the head/face display round central terminals, while those innervating the trunk hairy skin display long and thin central arbors (Figure 8). Given that neurons in the medulla and sacral spinal cord display round arbors (Figure 8 and Figure 9), this morphological difference does not correlate with hairy vs. glabrous skin regions but instead seems to correlate with regions located at the extremities. In addition, upon optogenetic activation of Mrgprd+ central terminals, we saw a close correlation between region-specific central arbor type (round vs. long) and signal transmission strength. In *Mrgprd*^{CreERT2};*Rosa*$^{ChR2\text{-}EYFP}$ heterozygous

mice, lateral lumbar and thoracic circuits showed similar post-synaptic response incidences/stimulus duration thresholds, whereas medial lumbar circuits had a much higher response incidence and a lower stimulus duration threshold (Figure 13). While we cannot rule out a role for regional differences in the single-cell physiology of Mrgprd+ neurons (such activation threshold, transmitter release, etc.), this correlation suggests that region-specific central arbor structure could be a key contributor to the increased pain signal transmission of paw circuits. Taken together, we have uncovered a novel form of region-specific functional organization for mammalian nociceptors.

Previous psychophysical studies that defined the 'pain fovea' in humans used heat nociceptive stimuli. Thermal pain in mice is primarily mediated through a separate population of afferents (CGRP+ peptidergic nociceptors) from the Mrgprd+ fibers that we studied (Cavanaugh et al., 2009; McCoy et al., 2012). This suggests that region-specific organization could exist in peptidergic fibers as well. However, whether they also display somatotopic central arbor differences like Mrgprd+ non-peptidergic nociceptors remains to be determined. In addition, some previous studies suggest that the third-order DH collaterals of Aβ mechanoreceptors are also wider (in the mediolateral axis) in the medial lumbar enlargement compared to other DH regions (Shortland et al., 1989; Brown et al., 1991; Millecchia et al., 1991). However, the primary signal transmission for discriminative information occurs in the dorsal column nuclei but not the dorsal spinal cord. Thus, it is currently less clear whether this central arbor morphological difference contributes to differential touch sensitivity.

Interneurons in DH layer II are morphologically and physiologically heterogeneous, and several interneuron subtypes have been defined (Grudt and Perl, 2002; Lu and Perl, 2003, 2005). Mrgprd+ fibers synapse on most identified classes of layer II interneurons (Wang and Zylka, 2009) and signal to pain pathway projection neurons located outside of layer II through polysynaptic pathways (Lu and Perl, 2005). However, past work on these circuits oftentimes focused on lumbar enlargement spinal cord. It is therefore unclear if there are systematic somatotopic differences in the subtypes or organization of DH interneuron circuits, and whether the different morphological central arbor types identified by our study may contact the same or different downstream pathways.

Increased sensitivity of mouse paw pain circuits to external input

Finally, we determined the stimulus threshold (laser power) required to trigger avoidance behaviors of freely behaving *Mrgprd*^{CreERT2}; *Rosa*$^{ChR2\text{-}EYFP}$ mice upon paw or upper leg skin light stimulation. Our experiments show a clear heightened sensitivity of plantar-paw-innervating Mrgprd+ nociceptors to stimulation (Figure 16, Figure 17). Interestingly, our use of peripheral optogenetic stimulation likely bypasses the effects of some peripheral parameters, such as the mechanical or thermal conduction properties of the skin or the expression of molecular receptors, on the sensation of natural stimuli. Further, given that Mrgprd+ neurites terminate farther from the skin surface (Figure 17), it is unlikely that the laser stimulus has more ready access to Mrgprd+ terminals in plantar paw skin. Nevertheless, we cannot rule out the contribution of other regional differences among the peripheral terminals of these neurons that we did not measure.

Collectively, our results suggest that region-specific Mrgprd+ central arbor organization could magnify the representation of the plantar paw within pain circuits to contribute to heightened pain sensitivity (Millecchia et al., 1991) (Figure 18). This central organization mechanism could allow for the sensitive detection of harmful stimuli in these areas, despite a lower density in the periphery. This finding is relevant for pain research using rodent models, which has historically relied heavily on pain assays in plantar paw/medial lumbar circuits (Le Bars et al., 2001). Given our findings, it would be interesting to examine whether region-specific differences exist in the molecular and physiological pathways of acute and/or chronic pain models. Such work could be informative for the translation of preclinical models to clinical treatment.

Materials and Methods

Mouse strains:

Mice were raised in a barrier facility in Hill Pavilion, University of Pennsylvania. All procedures were conducted according to animal protocols approved by Institutional Animal Care and Use Committee (IACUC) of the University of Pennsylvania and National Institutes of Health guidelines. *Rosa*^{tdTomato} (RRID:IMSR_JAX:007909), *Rosa*^{iAP} (RRID:IMSR_JAX:009253), *Rosa*$^{ChR2\text{-}EYFP}$ (RRID:IMSR_JAX:012569), and *Mrgprd*^{EGFPf} (RRID:IMSR_TAC:tf0437) lines have been described previously(Zylka et al., 2005; Badea et al., 2009; Madisen et al., 2010; Madisen et al., 2012).

Generation of *Mrgprd*^{CreERT2} mice:

Targeting construct arms were subcloned from a C57BL/6J BAC clone (RP24-316N16) using BAC recombineering, and the CreERT2 coding sequence followed by a FRT-flanked neomycin-resistance selection cassette was engineered in-frame following the *Mrgprd* starting codon by the same approach (Figure 1A). The targeting construct was electroporated into a C57/129 hybrid (V6.5, RRID: CVCL_C865) mouse embryonic stem cell line by the Penn Gene Targeting Core. V6.5 cells were provided directly from the group that developed the line(Eggan et al., 2001) at passage 12 and then expanded in the Penn targeting vector core to passage 15, which was used for *Mrgprd*^{CreERT2} targeting. Cells were analyzed for correct morphology and chromosome number and were confirmed to be mycoplasma negative. ES clones were screened by PCR using primers flanking the 3' insertion site (Figure 1C). Positive clones were further screened using Southern blot with

both internal and external probes (Figure 1B). The Penn Transgenic Core assisted in *Mrgprd*^{CreERT2} ES clone blastocyst injection and in the generation of chimeric mice, which were mated to a *Rosa*^{Flippase} line (RRID:MMRRC_007844-UCD) to excise the Neo cassette. Neo cassette-negative progeny (verified via PCR of genomic DNA) were mated to C57 (RRID:IMSR_JAX:000664 or CD1 (RRID:IMSR_CRL:22) mice to establish the line.

Genetic labeling of Mrgprd+ nociceptors:

To label Mrgprd+ nociceptors, *Mrgprd*^{CreERT2} mice carrying the relevant reporter allele were treated with tamoxifen (Sigma, T5648) pre- or postnatally. For prenatal treatment, pregnant females were given tamoxifen along with estradiol (Sigma, E8875, at a 1:1000 mass estradiol: mass tamoxifen ratio) and progesterone (Sigma, P3972, at a 1:2 mass progesterone: mass tamoxifen ratio) in sunflower seed oil via oral gavage at E16.5-E17.5, when *Mrgprd* is highly expressed in mouse non-peptidergic nociceptors (Chen et al., 2006). For postnatal treatment, 0.5mg tamoxifen extracted in sunflower seed oil was given via i.p. injection once per day from P10-P17 (or P14-P21 for spinal cord slice recording experiments, Figure 13). At least one week was given to drive recombination and reporter gene expression.

Tissue preparation and histology:

Procedures were conducted as previously described(Fleming et al., 2012). Briefly, mice used for immunostaining or AP staining were euthanized with CO2 and transcardially perfused with 4% PFA/PBS, and dissected tissue (either skin or spinal cord and DRGs) was post-fixed for 2 hr in 4% PFA/PBS at 4° C. Tissue used for immunostaining was cryo-

protected in 30% sucrose/PBS (4% overnight) before freezing. Mice used for in situ hybridization were euthanized and unfixed dissected tissue was frozen. Frozen glabrous skin and DRG/spinal cord sections (20-30 μm) were cut on a Leica CM1950 cryostat. Immunostaining of sectioned DRG, spinal cord, and glabrous skin tissue, whole mount skin immunostaining, and double fluorescence in situ hybridization was performed as described previously (Fleming et al., 2012; Niu et al., 2013). The following antibodies and dyes were used: rabbit anti-CGRP (ImmunoStar Cat# 24112, RRID:AB_572217), rat anti-CK8 (DSHB Cat# TROMA-I, RRID:AB_531826), chicken anti-GFP (Aves Labs Cat# GFP-1020, RRID:AB_10000240), rabbit anti-GFP (Thermo Fisher Scientific Cat# A-11122 also A11122, RRID:AB_221569), conjugated IB4-Alex488 (Molecular Probes Cat# I21411 also I21411, RRID:AB_2314662), rabbit anti-NF200 (Sigma-Aldrich Cat# N4142, RRID:AB_477272), chicken anti-PAP (Aves Labs PAP, RRID:AB_2313557), chicken anti-peripherin (Aves Labs Cat# ABIN361364, RRID:AB_10785694), mouse anti-PKCγ (Innovative Research Cat# 13-3800, RRID:AB_86589), rabbit anti-RET (Immuno-Biological Laboratories Cat# 18121, RRID:AB_2301042), rabbit anti-RFP (Clontech Laboratories, Inc. Cat# 632496, RRID:AB_10013483). Mrgprd, Mrgpra3, and Mrgprb4 in situ probes were previously described (Luo et al., 2007).

Tissue (skin or spinal cord with attached DRGs) for whole mount AP colorimetric staining with BCIP/NBT substrate (Roche, 1138221001 and 11383213001) and for fluorescent staining with HNPP/FastRed substrate (Roche, 11758888001) was treated as previously described(Niu et al., 2013). Following AP colorimetric labeling, tissue was

either cleared in BABB for imaging or sectioned using a VT1200S vibratome (Leica Microsystems, Nussloch, Germany) (200 μm), followed by BABB clearing for imaging. Fluorescent labeled DRGs co-stained using antibodies were cleared in glycerol and for imaging.

Retrograde DiI labeling

DiI (1 μL, 0.2 mg/mL dissolved in DMSO then diluted 1:5 with PBS) was subcutaneously injected in the plantar hind paw or shaved ventral proximal hind limb of 4pw *Mrgprd*^{EGFPf} mice (each mouse received DiI at both locations on opposite sides, and side-location combinations were alternated between mice). 7 days after injection, mice were perfused and skin and L3-L5 DRGs were dissected. Skin was post-fixed and mounted in PBS for imaging. DRGs were post-fixed, cryoprotected and then serially cryosectioned through the whole ganglion, and sections were mounted and imaged for quantification.

Electrophysiology

Spinal cord slices recordings were conducted as previously described (Cui et al., 2011). Basically, 4-6pw MrgprdCreERT2; RosaChR2-EYFP/ChR2-EYFP or MrgprdCreERT2 ; RosaChR2-EYFP/+ mice were anesthetized with a ketamine/xylazine/acepromazine cocktail. Laminectomy was performed, and the spinal cord lumbar segments were removed and placed in ice-cold incubation solution consisting of (in mM) 95 NaCl, 1.8 KCl, 1.2 KH2PO4, 0.5 CaCl2, 7 MgSO4, 26 NaHCO3, 15 glucose, and 50 sucrose, oxygenated with 95% O2 and 5% CO2, at a pH of 7.35–7.45 and an osmolality of 310–320 mosM. Sagittal or transverse spinal cord slices (300-500 m thick) were prepared using a

VT1200S vibratome (Leica Microsystems, Nussloch, Germany) and incubated in 34°C incubation solution for 30 min.

The slice was transferred to the recording chamber and continuously perfused with recording solution at a rate of 3–4 ml/min. The recording solution consisted of (in mM) 127 NaCl, 1.8 KCl, 1.2 KH2PO4, 2.4 CaCl2, 1.3 MgSO4, 26 NaHCO3, and 15 glucose, oxygenated with 95% O2 and 5% CO2, at a pH of 7.35–7.45 and an osmolality of 300–310 mosM. Recordings were performed at RT. Spinal cord slices were visualized with an Olympus BX 61WI microscope (Olympus Optical, Tokyo, Japan), and the substantia gelatinosa (lamina II), which is a translucent band across the dorsal horn, was used as a landmark. Fluorescently labeled ChR2-EYFP terminals in the DH were identified by epifluorescence, and neurons in this innervation territory were recorded in the whole cell patch-clamp configuration. Glass pipettes (3–5 MΩ) were filled with internal solution consisting of (in mM) 120 K-gluconate, 10 KCl, 2 MgATP, 0.5 NaGTP, 20 HEPES, 0.5 EGTA, and 10 phosphocreatine di(tris) salt at a pH of 7.29 and an osmolality of 300 mosM. All data were acquired using an EPC-9 patch-clamp amplifier and Pulse software (HEKA, Freiburg, Germany). Liquid junction potentials were not corrected. The series resistance was between 10 and 25 MΩ.

Light induced EPSCs (EPSCLs) were elicited at a frequency of 2/min by 473nm laser illumination (10 mW, 0.1-5ms, Blue Sky Research, Milpitas, USA). Blue light was delivered through a 40X water-immersion microscope objective. Mono- or polysynaptic EPSCLs were differentiated by 0.2 Hz light stimulation. We classified a connection as

monosynaptic if the EPSC jitter (average standard deviation of the light-induced EPSCs latency from stimulation) < 1.6 ms(Doyle and Andresen, 2001; Wang and Zylka, 2009).

Western blotting

Western blotting was performed as previously described (Fleming et al., 2015). Briefly, L3-L5 DRG protein lysates were prepared in 600 uL RIPA buffer (50 mM Tris, 150 mM NaCl, 1% NP-40, 0.5% sodium deoxycholate, 0.1% sodium dodecyl sulfate, pH = 8.0) with added protease inhibitors (Sigma, P8340), and mixed with equal parts 2X Sample buffer (0.125 M Tris, 20% glycerol, 4% SDS, 0.16% bromophenol blue, 10% 2-mercapatoethanol) before denaturing (100°C, 10 min). 10 uL of lysate samples were run on duplicate 4-15% mini-Protean TGX gels (Biorad, 456-1086), and both gels were transferred to nitrocellulose membranes. Membranes were blotted with either rabbit anti-GFP (1:2000) or rabbit anti-NF200 (1:2000), followed by AP-conjugated goat anti-rabbit secondary (1:5000, Thermo Fisher Scientific Cat# T2191, RRID:AB_11180336). AP was detected using CDP-Star (Thermo Scientific, T2218) and imaged with a Chemi-Blot System (BioRad).

Optogenetic stimulation of Mrgprd+ nociceptors in paw and leg skin

To induce light-evoked behavior in freely moving animals, we used P10-P17 tamoxifen treated *Mrgprd*^{CreERT2}*; Rosa*$^{ChR2\text{-}EYFP/ChR2\text{-}EYFP}$ mice and control littermates (*Rosa*$^{ChR2\text{-}EYFP/ChR2\text{-}EYFP}$) who were also tamoxifen treated, but lacked the Cre-driver. All tested animals were between 2-6 months old. An additional control was to shine 532nm green laser light

(Shanghai Laser and Optics Century, GL532T8-1000FC/ADR-800A) to the paw skin of both experimental groups. To induce light-evoked aversive behavior in Mrgprd+ neurites in the paw skin, 1 or 5mW of 473nm blue light laser (Shanghai Laser and Optics Century, BL473T8-150FC/ADR-800A) was shined directly to the paw skin through a mesh bottom floor, with a cutoff time of 10 seconds. We tested different light waveforms and found that 10Hz sine waveform pulsing gave the best behavior responses. Thus, we used this waveform for all our behavior tests.

To induce light-evoked aversive behavior in Mrgprd+ neurites in the leg skin, first, all hair was removed from the leg with Nair hair remover under light 3% isoflourane anesthesia, and animals were given two days before being tested again. For leg stimulation, 1, 5, 10, or 20mW of 473nm blue light laser, with 10Hz sine waveform pulsing, was shined directly to the leg skin. The cutoff time for this behavior assay is 10 seconds. For habituation to either paw or leg skin light stimulation, on the first two days, animals were habituated to the testing paradigm by being placed in the plexiglass testing chamber (11.5×11.5×16 cm) for 30 minutes each day. On the third testing day, animals were placed in the plexiglass testing chamber for 15 minutes prior to light stimulation. Green and blue light testing were performed on different days, but two weeks separated the paw and leg skin light stimulation. For all stimulation, the laser light was delivered via an FC/PC Optogenetic Patch Cable with a 200micrometer core opening (ThorLabs) and there was approximately 1cm of space between the cable terminal and the targeted skin area. Light power intensity for each experiment was measured with a Digital Power Meter with a 9.5mm aperture (ThorLabs). For leg skin stimulation, power intensity was only

slightly impeded by the thin wall (0.02cm) of the plexiglass holding chamber, as measured by the Digital Power Meter (Figure 17E).

To gain precise spatial and temporal resolution of behavior responses, we recorded behaving animals at 500 frames/second with a high-speed camera (FASTCAM UX100 800K-M-4GB - Monochrome 800K with 4GB memory) and attached lens (Nikon Zoom Wide Angle Telephoto 24-85mm f2.8). With a tripod with geared head for Photron UX100, the camera was placed at a ~45degree angle at ~1-2 feet away from the plexiglass holding chambers where mice performed behaviors. The camera was maximally activated with far-red shifted 10mW LED light that did not disturb animal behavior. All data were collected and annotated on a Dell laptop computer with Fastcam NI DAQ software that is designed to synchronize Photron slow motion cameras with the M series integrated BNC Data Acquisition (DAQ) units from National Instruments.

Image acquisition and data analysis:

Images were acquired either on a Leica DM5000B microscope (bright field with a Leica DFC 295 camera and fluorescent with a Leica 345 FX camera), on a Lecia SP5II confocal microscope (fluorescent), or on a Leica M205 C stereoscope with a Leica DFC 450 C camera (bright field). Image manipulation and figure generation were performed in Fiji (RRID:SCR_002285), Adobe Photoshop (RRID:SCR_014199) and Adobe Illustrator (RRID:SCR_014198). Cell number counting, nociceptor arbor measurements, and fluorescence measurements were performed in Fiji. For section histology experiments, *n* = 3-6 sections per animal from 3 animals. Central arbor height/width measurements were

taken to be the relevant axes of fitted ellipses. Column graphs, pie charts and scatter plots were generated in GraphPad Prism5. Column graphs show mean ± SEM. Statistical significance was analyzed using unpaired, two-tailed Student's *t*-tests, one-way ANOVA with Tukey's multiple comparisons, linear regression, Spearman's rank correlation test, or Chi-square tests in GraphPad Prism5 (RRID:SCR_002798). For area measurements of DiI skin labeling, fluorescence intensity thresholds were set at 10 standard deviations above mean background fluorescence, and area was measured from pixel counts above threshold in Fiji. Densitometry quantification of Western blot bands was performed using Image Lab (RRID:SCR_014210). For DRG fluorescence intensity measurements, the average fluorescence of outlined cells was normalized to mean background fluorescence (Figure 11). For DH fluorescence intensity measurements, the width of the DH was divided into thirds, and the average intensity of the outlined medial third of the terminal layer was compared to the lateral-most third (Figure 11).

Figures

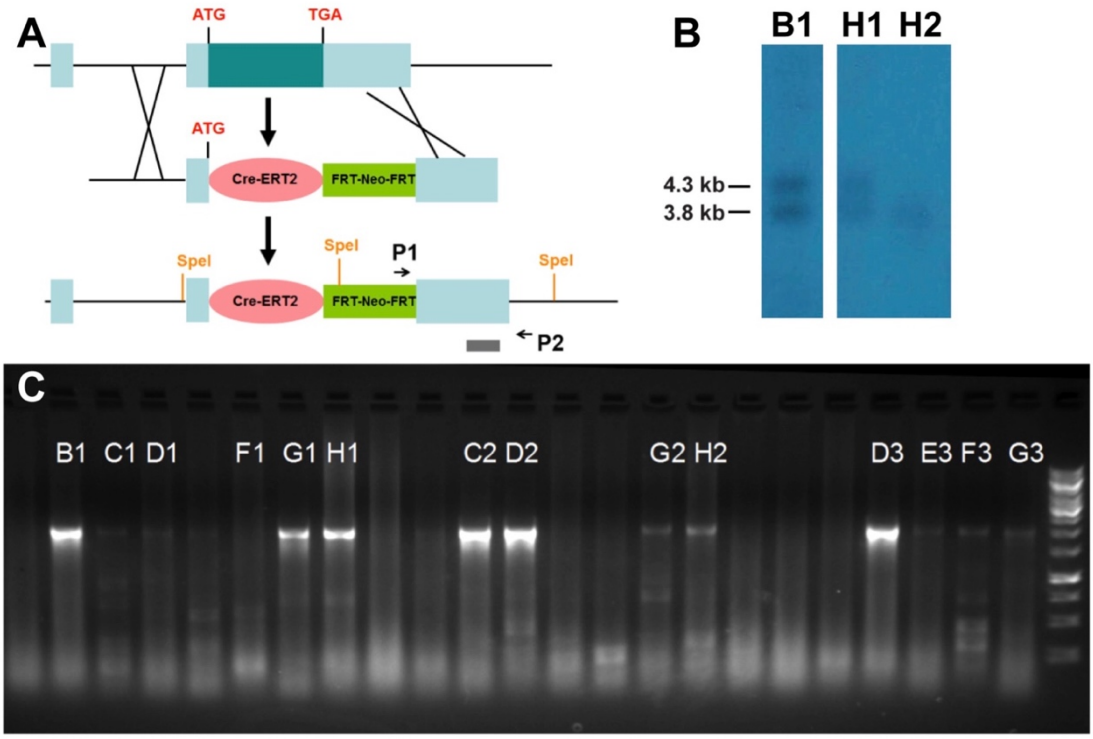

Figure 1. Generation of *Mrgprd*^{CreERT2} knock-in mouse line. (A) Illustration showing the knock-in targeting strategy. Grey bar, 3' UTR Southern blot probe site. P1, P2, primers for PCR screening. (B) Southern blot of SpeI-digested ES genomic DNA, using a probe against *Mrgprd* 3' UTR (grey bar in A). 4.3 kb, *Mrgprd*^{CreERT2} knock-in allele. 3.8 kb, *Mrgprd* wild-type allele. (C) PCR screen of electroporated ES clones, using P1, P2 primers. The positive PCR product is about 2 kb.

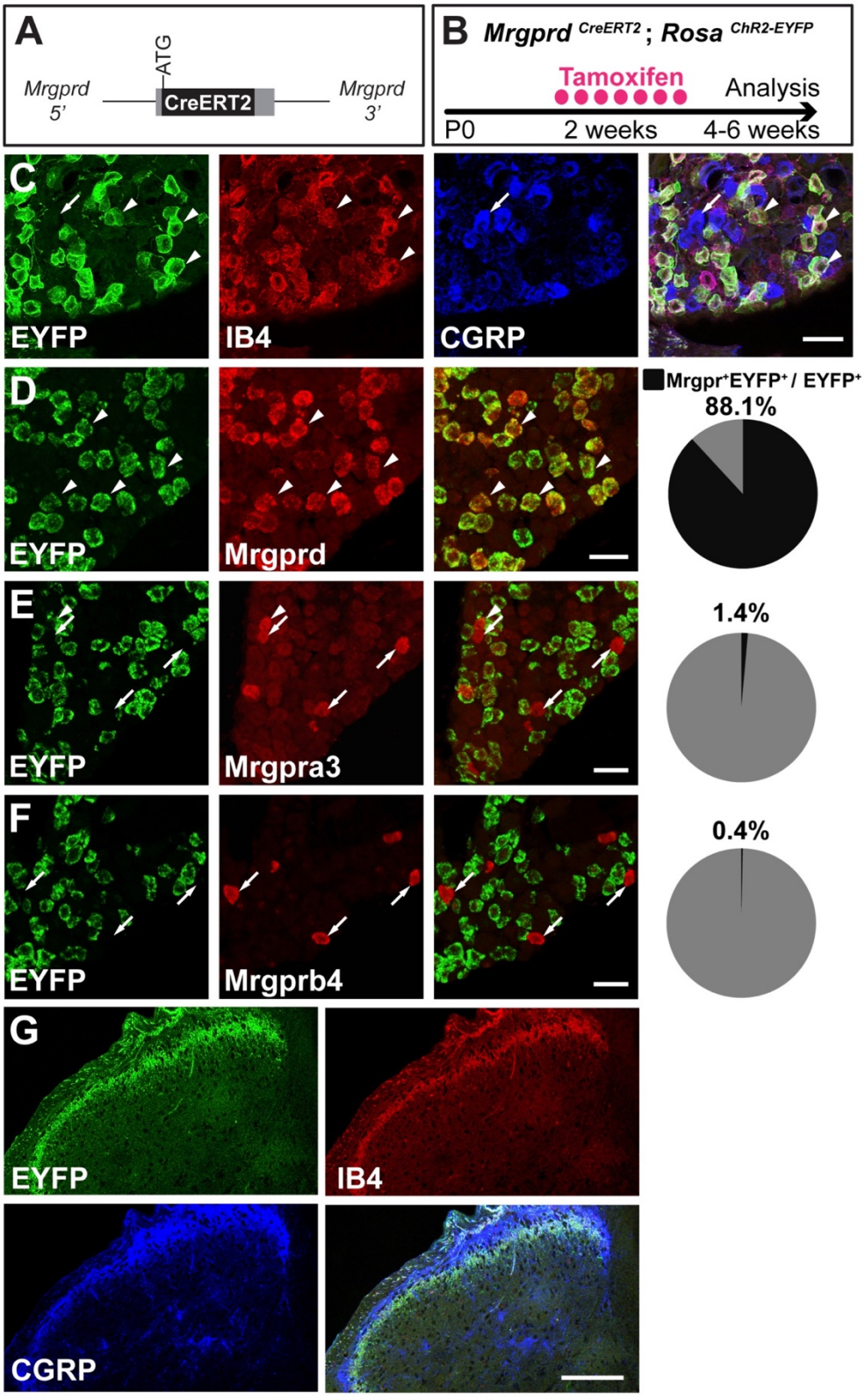
A
ATG
Mrgprd 5'
CreERT2
Mrgprd 3'
B Mrgprd CreERT2; Rosa ChR2-EYFP
Tamoxifen
Analysis
P0
2 weeks
4-6 weeks
C
EYFP
IB4
CGRP
D
EYFP
Mrgprd
E
EYFP
Mrgpra3
F
EYFP
Mrgprb4
Mrgpr+EYFP+ / EYFP+
88.1%
1.4%
0.4%
G
EYFP
IB4
CGRP

Figure 2. *Mrgprd*^{CreERT2} mice can mediate recombination specifically in adult Mrgprd+ non-peptidergic nociceptors. (A) Knock-in *Mrgprd*^{CreERT2} allele. (B) Illustration showing tamoxifen treatment scheme, 0.5 mg tamoxifen / day, P10-P17 treatment of *Mrgprd*^{CreERT2}; *Rosa*$^{ChR2\text{-}EYFP}$ mice. (C) Triple staining of DRG section showing EYFP overlaps with IB4 but not CGRP. (D-F) Double fluorescent *in situ* DRG sections showing EYFP in *Mrgprd* (D) but not *Mrgpra3* (E) or *Mrgprb4* (F) cells. Pie charts show overlap quantification (% of EYFP$^+$ cells that co-express Mrgpr, n = 3 animals). (G) DH section showing EYFP$^+$ terminal overlap with IB4 but not CGRP. Arrowheads show overlapping cells, arrows show non-overlapping cells. Scale bars = 50μm (C-F), 100μm (G).

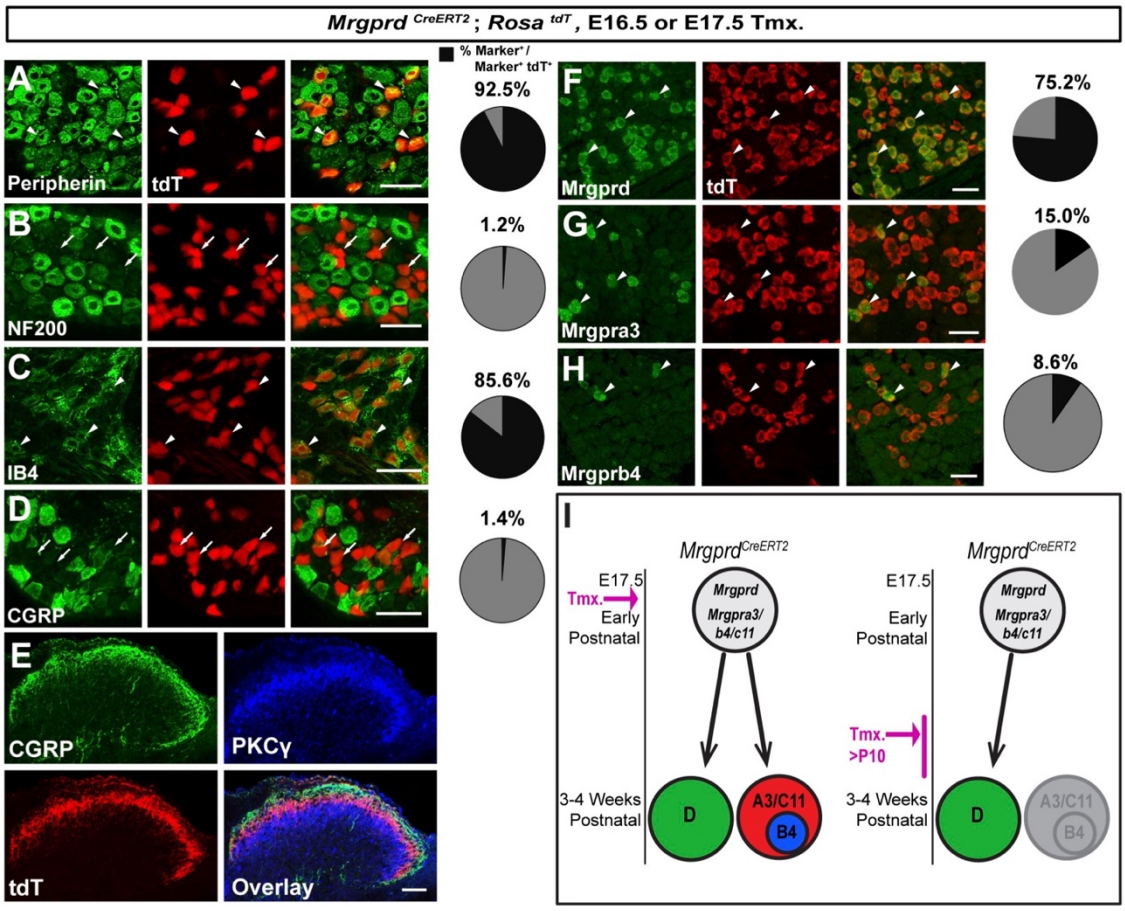

Figure 3. Prenatal tamoxifen treatment labels Mrgprd+ along with Mrgpra3/b4⁺ non-peptidergic DRG neurons. (A-D) Representative DRG sections of 3pw *Mrgprd*^{CreERT2}; *Rosa*^{tdTomato} mice (2.5-5 mg tamoxifen at E16.5) immunostained with the indicated markers. tdT⁺ neurons are positive for non-peptidergic neuron markers peripherin (92.5 ± 4.0%) (A) and IB4 (85.6 ± 1.2%) (C), but do not express NF200 (1.2 ± 0.01%) (B) or CGRP (1.4 ± 0.00%) (D). (E) Representative immunostained DH section showing tdT⁺ fibers innervating layer II, ventral to CGRP+ fibers but dorsal to PKCγ interneurons. (F-H) Double fluorescent *in situ* shows expression of *Mrgprd* (75.2 ± 0.8%) (F), *Mrgpra3* (15.0 ± 0.2%) (G) and *Mrgprb4* (8.6 ± 0.1%) (H) in *Tdtomato* expressing neurons from prenatally treated *Mrgprd*^{CreERT2}; *Rosa*^{tdTomato} mice (5 mg tamoxifen at E17.5). (I) Model

showing *Mrgprd*^{CreERT2} specificity based on time of tamoxifen dosage. *Mrgprd*^{CreERT2} recombination is consistent with expression of *Mrgprd* across development. Arrowheads indicate marker overlap with tdT, arrows indicate tdT^{+} cells that do not express indicated marker. Scale bars, 50μm (A-D, F-H), 100μm (E).

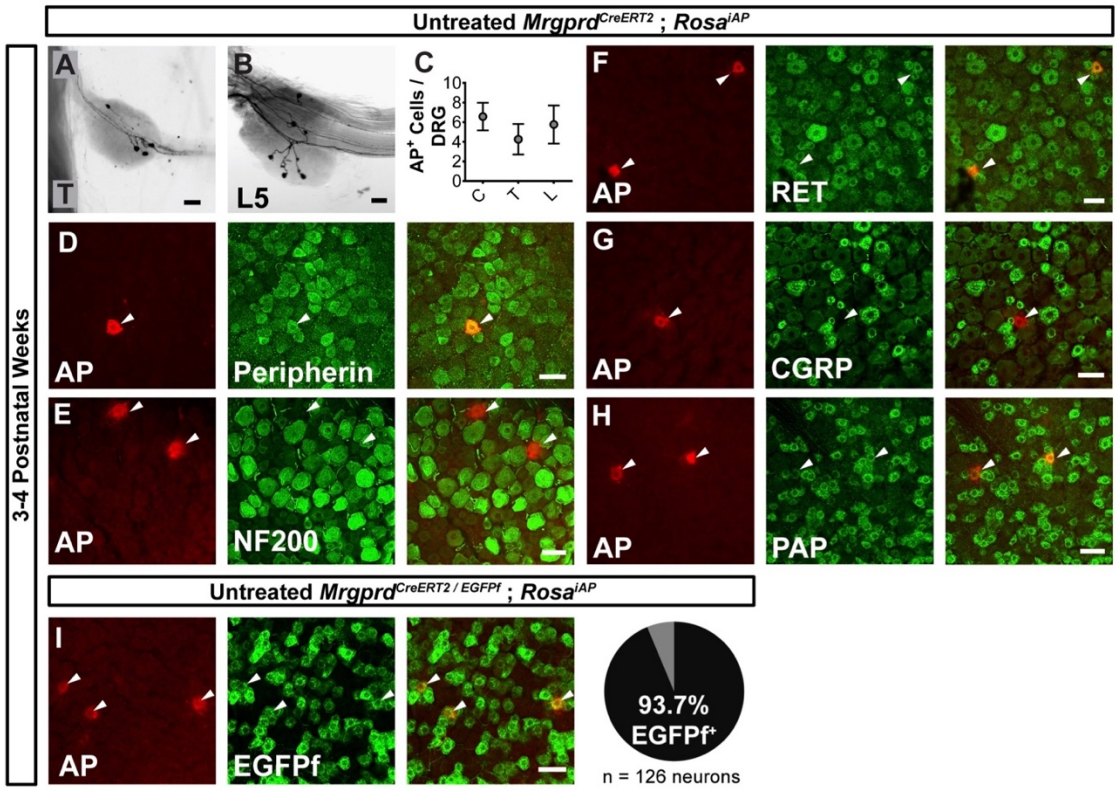

Figure 4. Sparse Mrgprd+ nociceptor labeling in untreated 3-4 pw *Mrgprd*^{CreERT2}; *Rosa*^{iAP} mice. (A&B) Whole mount AP DRG staining of thoracic (A) and L5 (B) DRGs. (C) AP$^+$ cells / DRG for cervical (C), thoracic (T), and lumbar (L) DRGs, *n* = 47 DRGs from 3 animals. (D-H) Whole mount DRG immunostaining plus AP fluorescent staining. Sparse AP$^+$ cells express non-peptidergic nociceptor markers peripherin (D), RET (F) and PAP (H) but not large diameter neuron maker NF200 (E) or peptidergic marker CGRP (G). (I) Whole mount EGFPf immunostaining plus AP fluorescence staining of untreated *Mrgprd*$^{CreERT2/EGFPf}$; *Rosa*^{iAP} DRGs. AP$^+$ neurons are Mrgprd+ nociceptors. Quantification of overlap (% of AP$^+$ cells that co-express *Mrgprd*^{EGFPf}, *n* = 126 neurons from 3 animals). Scale bars = 50μm.

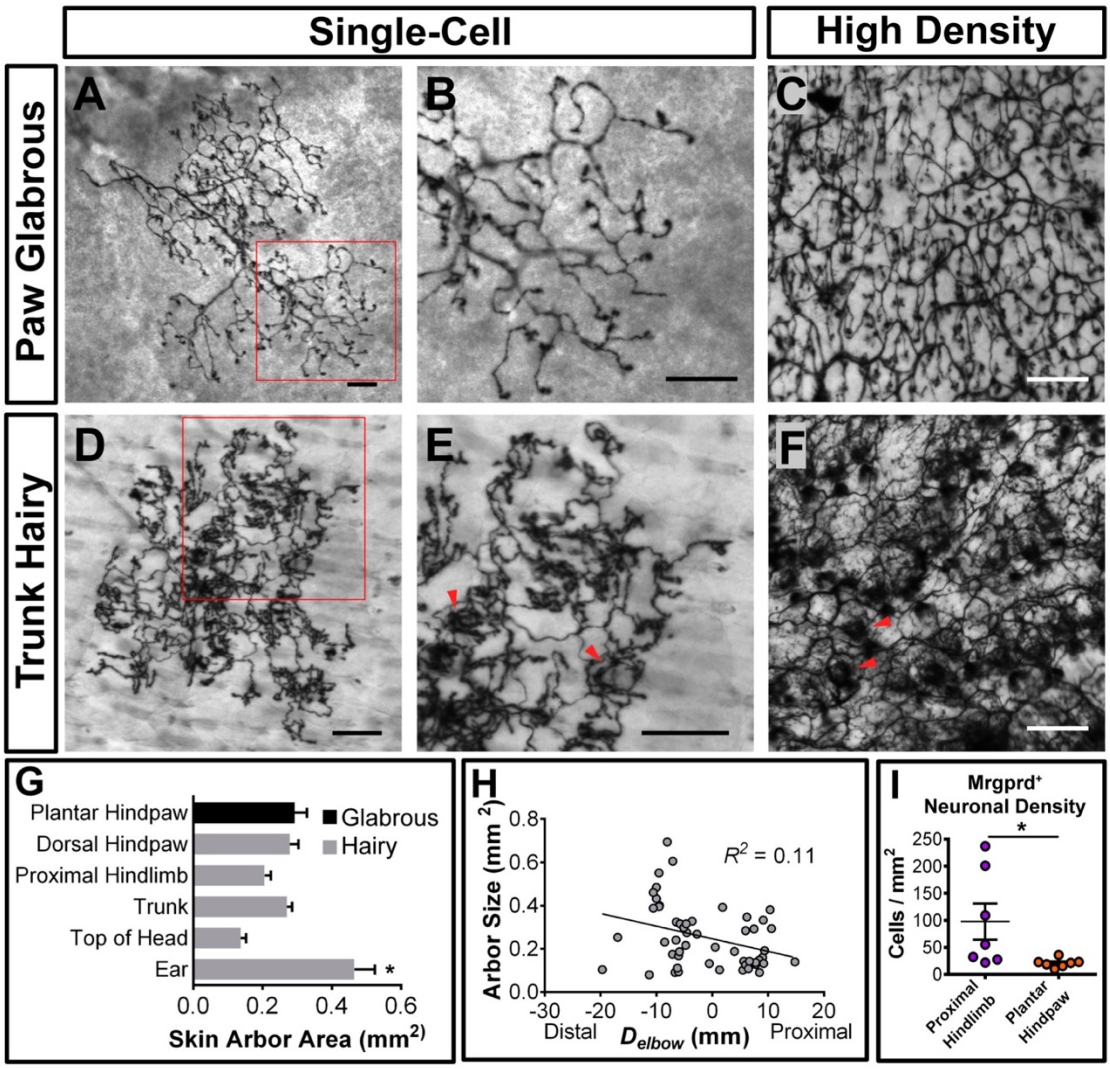

Figure 5. Peripheral organization of non-peptidergic nociceptors in 3-4 pw *Mrgprd*^{CreERT2}; *Rosa*^{iAP} mice. (A, B, D, E) Sparse labeled non-peptidergic nociceptors show bushy-ending structure in the glabrous skin (A-B) and trunk hairy skin (D-E). B, E, high magnification images of regions boxed in A and D, respectively. (C, F) High-density labeled (0.5mg tamoxifen at P11) glabrous and hairy skin. Overall neurite densities are lower in glabrous compared to hairy skin. Red arrowheads in E&F mark neurite clumps that likely surround hair follicles. (G) Arbor areas in different skin regions. n = 173 terminals from 9 animals. * = p<0.05 (one-way ANOVA with Tukey's multiple

comparisons test). (H) Arbor areas in the hind limb skin vs. proximodistal distance (D_{elbow}) from the elbow (point 0, terminals distal to this edge are given negative D_{elbow} values). n = 52 arbors from 4 animals. No clear relationship between proximodistal location and size is evident (linear regression). (I) Mrgprd+ neuron density (number of retrogradely labeled DiI/*Mrgprd*^{EGFPf} double positive neurons / area of DiI labeled skin, see figure supplement 2) is lower in plantar hind paw compared to proximal hind limb skin. * = p<0.05 (Student's t test). Scale bars = 100μm.

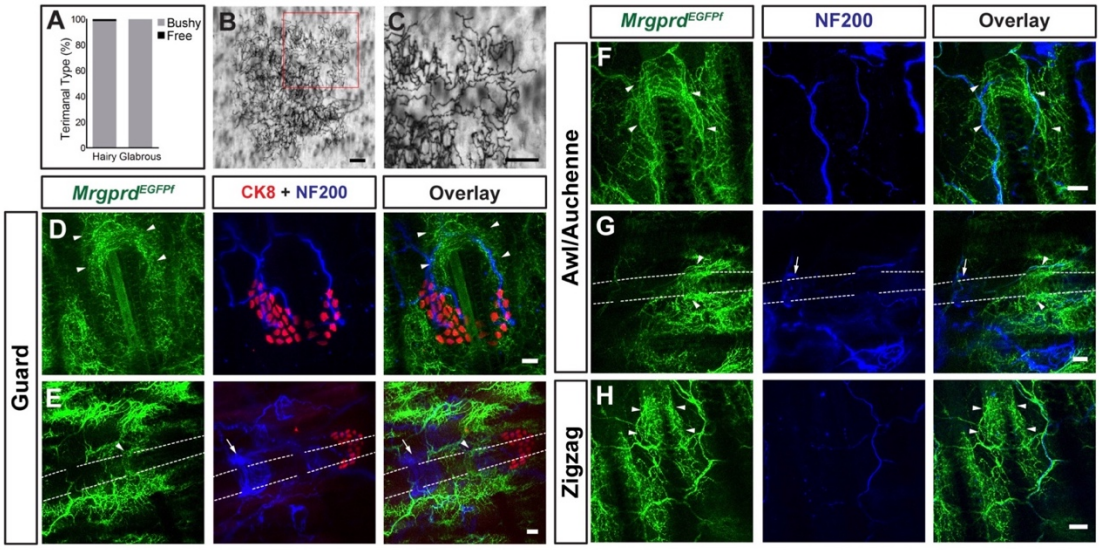

Figure 6. Mrgprd+ fiber hairy skin innervation. (A) Percentage of bushy or free ending type arbors labeled in untreated *Mrgprd*^{CreERT2}; *Rosa*^{iAP} mice by location. *n* = 132 hairy, 22 glabrous terminals from 4 animals. (B&C) Sparse labeled free terminal-type arbor in trunk hairy skin. C is a high magnification view of the region boxed in B. (D-H) Whole mount immunostaining of hair follicle innervation in *Mrgprd*^{EGFPf} skin. Mrgprd+ fibers form circumferential like endings around the necks of all three hair follicle types found in mouse hairy skin: guard (identified by presence of CK8^{+} Merkel cells and innervation by NF200^{+} Aβ mechanoreceptors) (D&E), awl/auchenne (identified by innervation by NF200^{+} fibers but no Merkel cells), and zigzag (identified by a lack of both Merkel cells and NF200^{+} fiber innervation). Mrgprd+ fibers encircle hair follicles close to the skin surface, more superficial than NF200^{+} Aβ fiber circumferential or lanceolate endings (E&G). Arrowheads, Mrgprd+ circumferential endings. Arrows, NF200^{+} Aβ fiber circumferential or lanceolate endings. Scale bars = 100μm (A-C), 20μm (D-H).

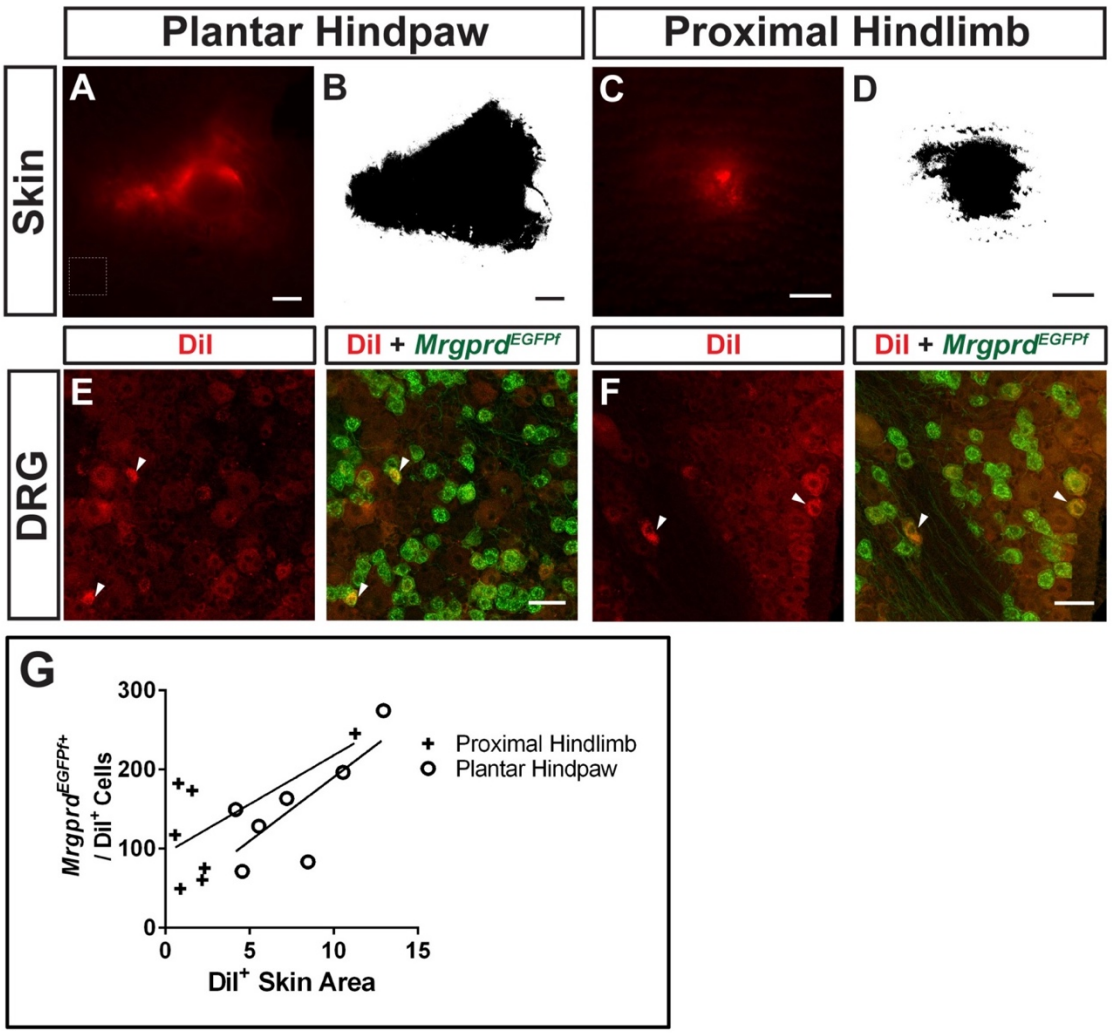

Figure 7. Retrograde DiI labeling of *Mrgprd*^{EGFPf} nociceptors. (A-D). DiI labeled skin areas in plantar hind paw (A) or ventral proximal hind limb (C) skin. DiI+ skin areas (B&D) were identified and quantified based on signal intensity threshold at 10 standard deviations above background fluorescence (representative background shown in dotted line box in A). (E&F) DiI/*Mrgprd*^{EGFPf} double-positive neurons were counted in serial sections. (G) Number of DiI/*Mrgprd*^{EGFPf} double-positive neurons vs. DiI^{+} skin area (Figure 3 – source data 2). Linear regressions: proximal hind limb, R^2 = 0.41, plantar hind paw, R^2 = 0.57. Scale bars = 500μm (A-D), 50μm (E&F).

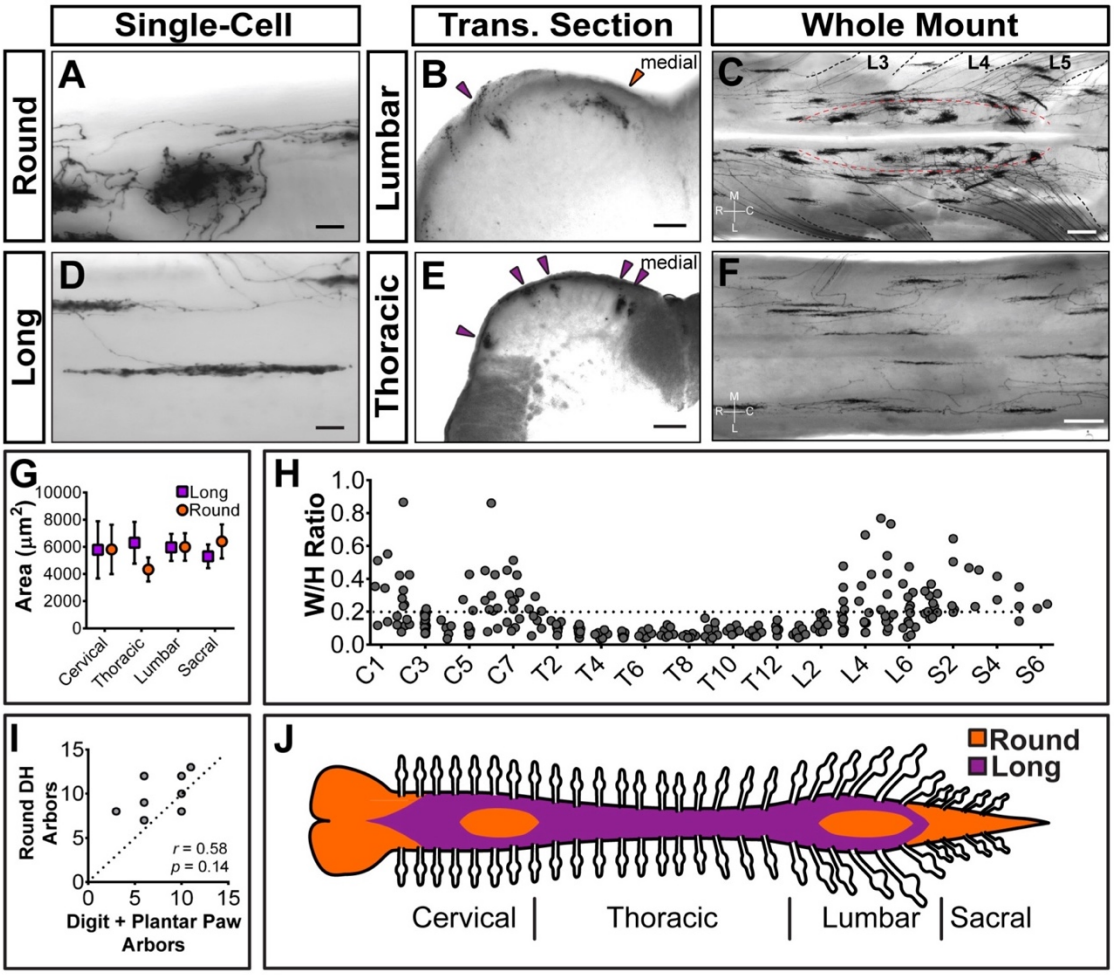

Figure 8. Sparsely labeled *Mrgprd*^{CreERT2}; *Rosa*^{iAP} nociceptors have region-specific central arbor morphologies. (A-F) Round and long non-peptidergic central arbors seen in top-down whole mount (A, C, D, F) and transverse section (B&E) spinal cords. Round arbors are in the medial lumbar enlargement (B&C) while long arbors are in the lateral lumbar enlargement and thoracic spinal cord (B-F). Dorsal roots are outlined and labeled in C. Red dashed lines outline the round arbor zone. Orange arrowhead marks a round arbor, purple arrowheads mark long arbors. M, medial. L, lateral. R, rostral. C, caudal. (G) Round and long (defined by ratio in H) arbor areas are comparable for all regions. (H) Arbor Width/Height ratios by ganglion of origin. Round terminals: W/H > 0.2. *n* =368

arbors from 7 animals (I) Comparison of the number of labeled arbors in the hind limb digit and plantar paw skin with the number of ipsilateral round arbors in the dorsal horn. n = 4 animals, dotted line shows 1:1 relationship. r, p values from Spearman's rank correlation test. (J) Illustration showing the distribution of round (orange zone) and long (purple zone) arbors in the spinal cord. Scale bars = 50μm (A&B, D&E), 250μm (C&F).

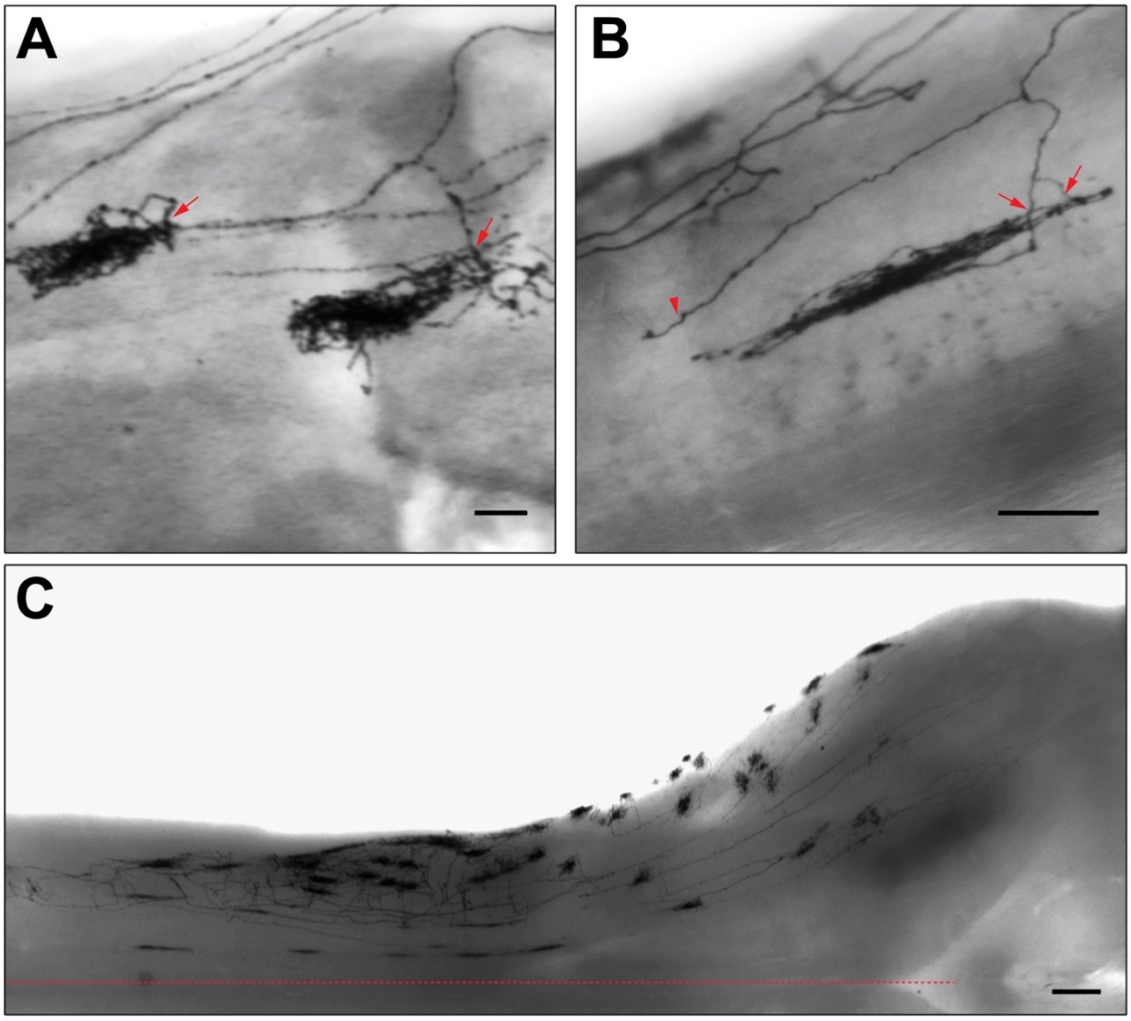

Figure 9. Central arbors of sparsely labeled non-peptidergic neurons in *Mrgprd*^{CreERT2}; *Rosa*^{iAP} mice. (A&B) Examples of bifurcating non-peptidergic nociceptor central projections from 1pw (0.05 mg tamoxifen at E16.5) (A) and 3pw (B) spinal cords. Bifurcated branches sometimes give rise to independent arbors (arrows in A), join other branches to give rise to a common arbor (arrows in B) or end without elaborating an arbor (arrowhead in B). (C) Round arbors in the upper cervical spinal cord and medulla, many of which descend from the TG non-peptidergic neurons. Scale bars, 50μm (A&B), 250μm (C).

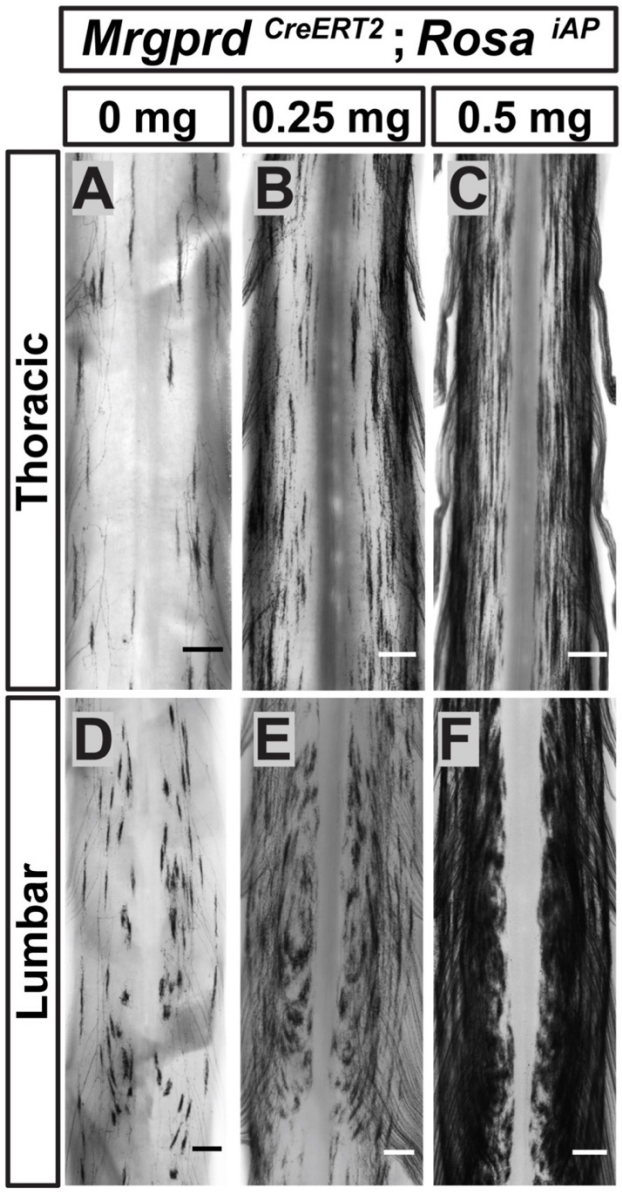

Figure 10. Non-peptidergic nociceptor labeling with increasing densities reveals somatotopic organization of Mrgprd+ central arbors. (A-F) AP staining of *Mrgprd*^{CreERT2}; *Rosa*^{iAP} thoracic (A-C) and lumbar (D-F) spinal cords that received prenatal 0mg (A&D), 0.25mg (B&E) or 0.5mg (C&F) prenatal tamoxifen. Even with increased labeling densities, round and long arbors occupy exclusive zones of the DH. n = 3 animals per treatment. Scale bars = 250μm.

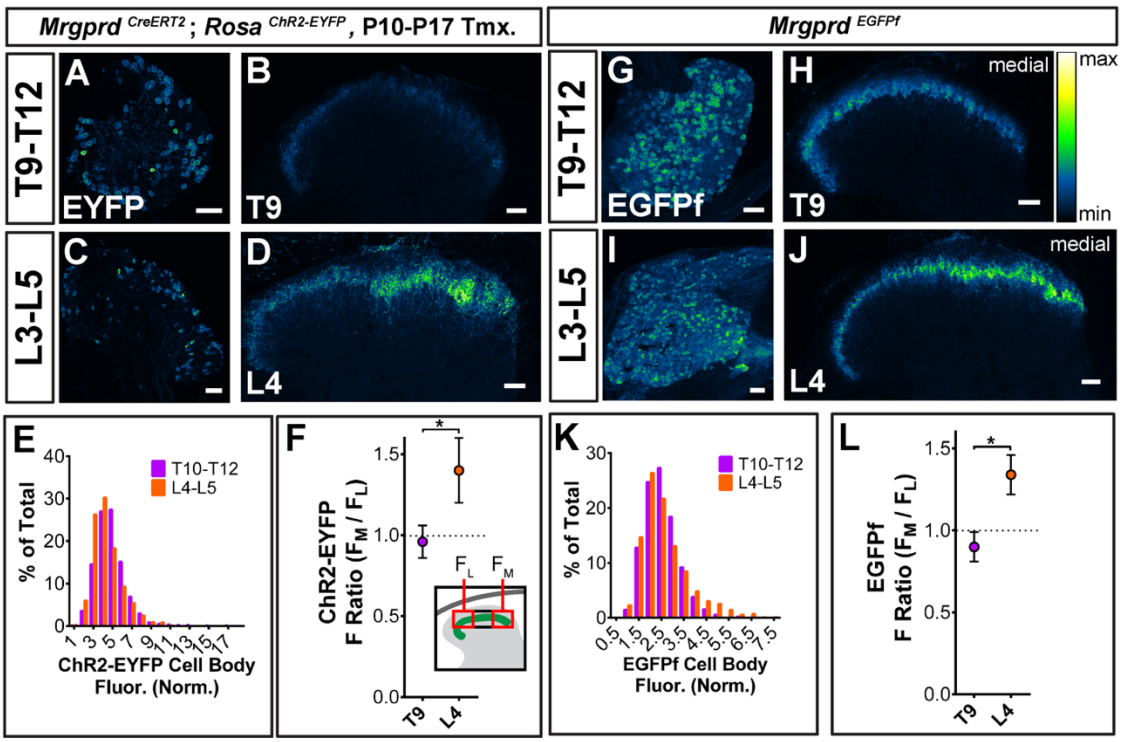

Figure 11. Mrgprd+ cell bodies show no regional difference in *Rosa*$^{ChR2\text{-}EYFP}$ expression, but Mrgprd+ circuits have a higher primary afferent membrane density in medial lumbar DH. (A-F). Native (no immunostaining) ChR2-EYFP fluorescence of *Mrgprd*^{CreERT2}; *Rosa*$^{ChR2\text{-}EYFP}$ (P10-P17 tamoxifen) DRG sections (A&C) and DH sections (B&D). (E) T10-T12 and L4-L4 DRG cell body fluorescence frequency distributions overlap, indicating no regional change in ChR2-EYFP expression level. (F) DH fluorescence ratio (medial third over lateral third) for T9 vs. L4. n = 3 animals for E&F. * = p <0.05, Student's two-tailed t-test. (G-L) Native EGFPf fluorescence in *Mrgprd*^{EGFPf} whole mount DRGs (G&I) or DH sections (H&J). Fluorescence intensity pseudocoloring is shown. (K) T10-T12 and L4-L5 DRG cell body fluorescence frequency distributions overlap (L) DH section fluorescence ratio for T9 vs. L4 levels. n = 3 animals for K&L. * = p <0.05, Student's two-tailed t-test.

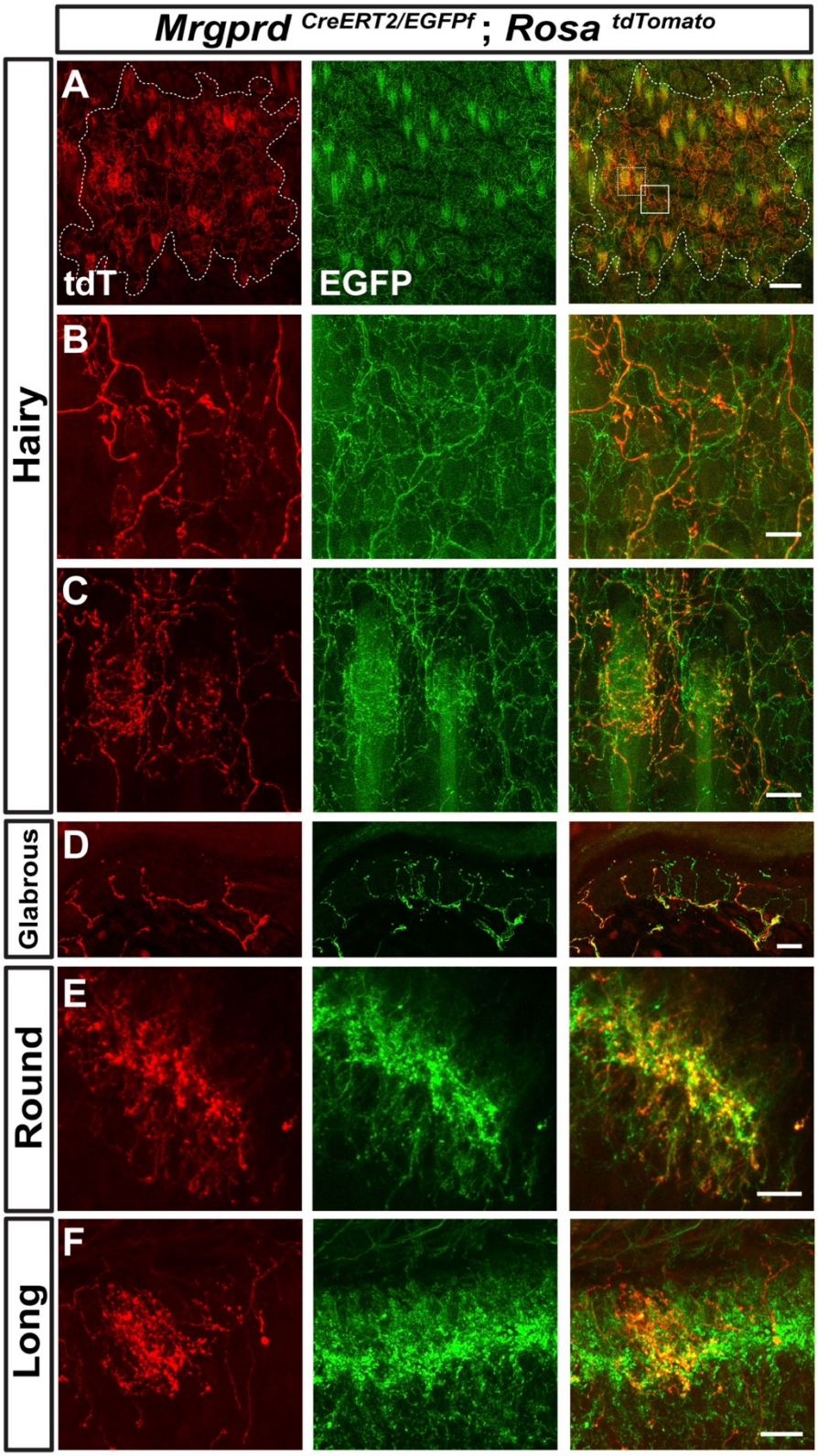
Mrgprd CreERT2/EGFPf ; Rosa tdTomato
Hairy
Glabrous
Round
Long
A
B
C
D
E
F
tdT
EGFP

Figure 12. Neighboring non-peptidergic nociceptors overlap extensively in the skin and spinal cord. (A-C) Whole mount immunostaining of *Mrgprd*$^{CreERT2/EGFPf}$; *Rosa*^{tdTomato} (0.5 mg tamoxifen at E16.5) hairy skin with anti-GFP and anti-RFP antibodies. The terminal field of one non-peptidergic nociceptor is labeled with tdT, as outlined in A. B&C show higher magnifications view of the regions boxed in A (solid line = B, dotted line = C). Innervation of hair follicles is shown in C. (D) Immunostaining of a section of glabrous skin. (E&F) Immunostaining of medial cervical (D) and thoracic (E) spinal cord sections, showing sparse labeled round terminal and long arbors. Scale bars = 100μm (A), 20μm (B-F).

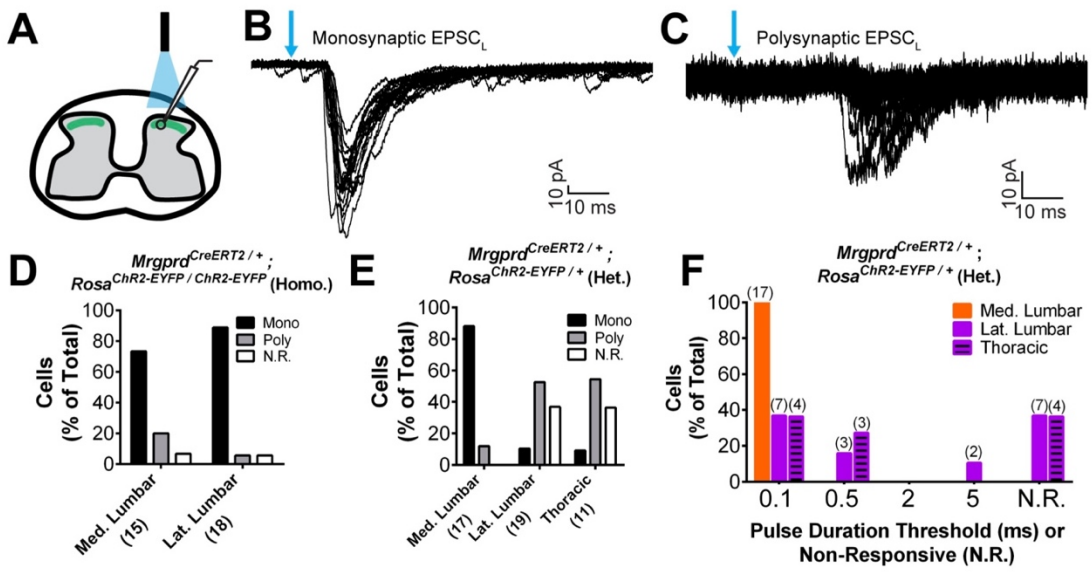

Figure 13. Plantar paw circuits show a heightened signal transmission in the dorsal horn. (A) Illustration of spinal cord slice recording from *Mrgprd*^{CreERT2}; *Rosa*$^{ChR2\text{-}EYFP}$ mice (P14-P21 tamoxifen) using optical stimulation. Neuron cell bodies located in the territory innervated by EYFP^{+} fibers were chosen for recording. (B&C) Monosynaptic (B) and polysynaptic (C) light-induced EPSC (EPSC$_L$) traces recorded from layer II neurons during 0.2 Hz light stimulation (overlay of 20 traces). Light pulses indicated by blue arrows, scale bars shown in lower right. (D) In *Mrgprd*$^{CreERT2/+}$; *Rosa*$^{ChR2\text{-}EYFP/ChR2\text{-}EYFP}$ homozygous slices, similar incidences of light-responsive neurons were found in medial and lateral lumbar regions. (E) In *Mrgprd*$^{CreERT2/+}$; *Rosa*$^{ChR2\text{-}EYFP/+}$ heterozygous slices, a much higher incidence of light-responsive neurons was seen in medial lumbar compared to lateral lumbar or medial thoracic circuits. (F) Frequency distribution of threshold light pulse durations required for eliciting EPSC$_L$s among cells in E. Among responsive cells, postsynaptic neurons in lateral lumbar and thoracic regions require longer pulse

durations to be activated compared to those in medial lumbar region. Cell (*n*) numbers indicated in parentheses in x-axis labels in D&E and above bars in F.

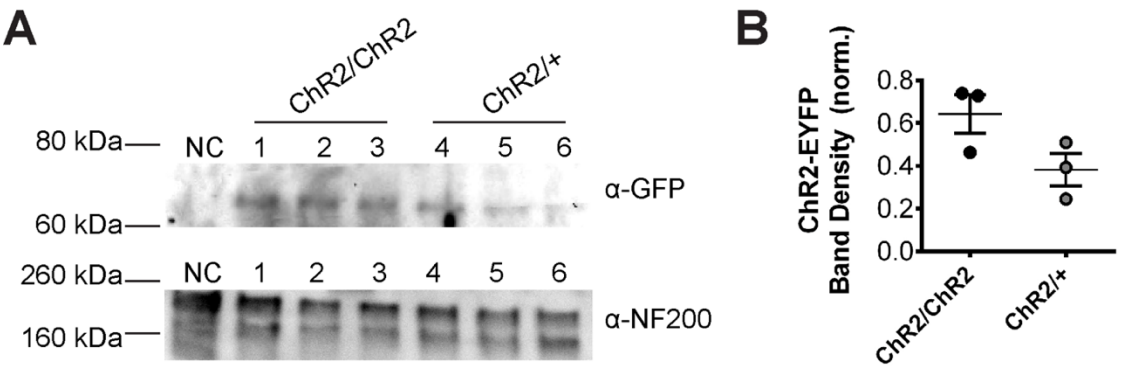

Figure 14. *Rosa*$^{ChR2\text{-}EYFP}$ expression levels. (A) Western blot of DRG lysates from one negative control mouse (CD1 wildtype, NC), 3 *Mrgprd*^{CreERT2}; *Rosa*$^{ChR2\text{-}EYFP/ChR2\text{-}EYFP}$ mice (ChR2/ChR2, 1-3), and 3 *Mrgprd*^{CreERT2}; *Rosa*$^{ChR2\text{-}EYFP/+}$ (ChR2/+, 4-6) mice with anti-GFP antibody (against ChR2-EYFP) and anti-NF200 as a loading control. (B) Quantification of ChR2-EYFP band intensity (normalized to upper NF200 loading control band) shows that ChR2 heterozygous DRGs show a ~40% reduction in ChR2-EYFP expression compared to homozygotes. $p = 0.09$ (Student's t-test).

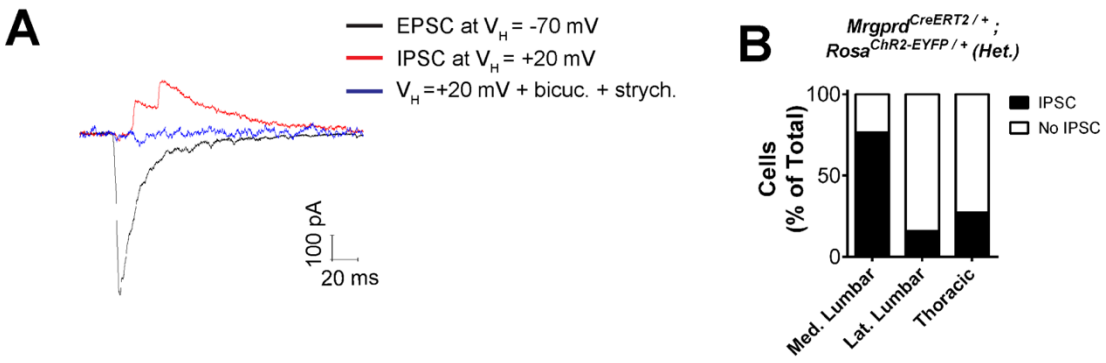

Figure 15. Paw DH regions show stronger activation of Mrgprd-driven inhibitory currents. (A) Representative traces from whole cell recording of a layer II neuron in a *Mrgprd*^{CreERT2}; *Rosa*$^{ChR2\text{-}EYFP}$ (P14-P21 tamoxifen) spinal cord slice upon optical stimulation of Mrgprd+ fibers at various holding potentials (not corrected). This neuron shows mono-synaptic $EPSC_L$ and polysynaptic $IPSC_L$ currents triggered by Mrgprd+ fibers. $IPSC_L$ currents are blocked by bicuculline and strychnine. (B) Incidences of $IPSC_L$ currents in random recordings from medial lumbar, lateral lumbar, thoracic regions. Medial lumbar shows higher incidence of Mrgprd+ triggered inhibitory currents.

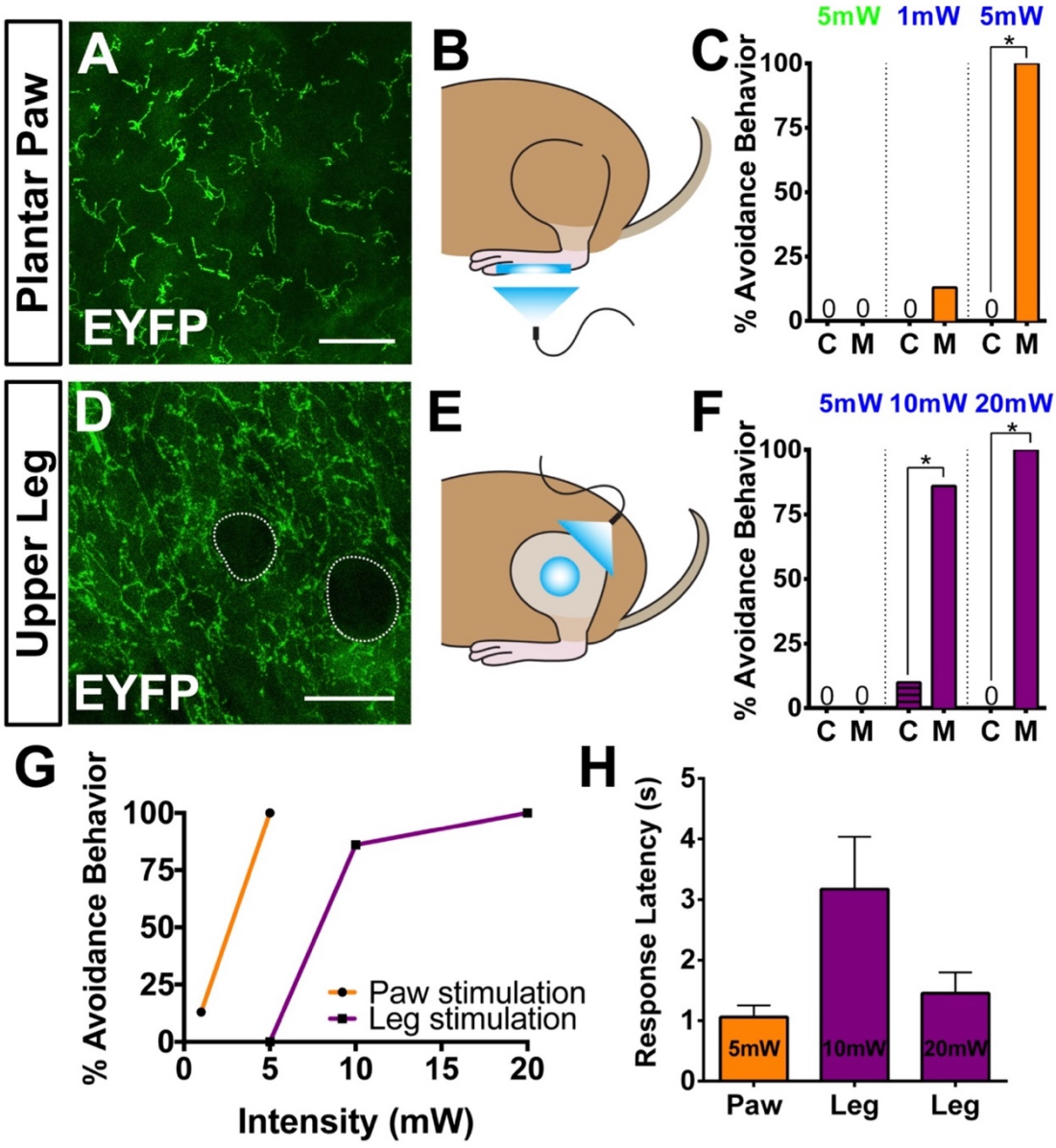

Figure 16. Peripheral optogenetic activation of Mrgprd+ nociceptors reveals regional differences in optical threshold required to elicit withdrawal responses. (A-C) Optical stimulation in the paw. (A) Representative whole-mount immunostaining of plantar paw skin in *Mrgprd*$^{CreERT2/+}$; *Rosa*$^{ChR2\text{-}EYFP/ChR2\text{-}EYFP}$ mice, *n*=3 mice. (B) Schematic of light placement on paw skin, see videos. (C) Histogram showing percentage of mice displaying aversive responses to 5mW green light and 1 or 5mW blue light to littermate control *(C)*

and *Mrgprd*$^{CreERT2/+}$; *Rosa*$^{ChR2\text{-}EYFP/ChR2\text{-}EYFP}$ *(M).* n = 6-10 for each genotype with 1-2 trials per mouse. * = p <0.001 Chi-square test. (D-F) Optical stimulation in the leg. (D) Representative whole-mount immunostaining of upper leg skin in *Mrgprd*$^{CreERT2/+}$; *Rosa*$^{ChR2\text{-}EYFP/ChR2\text{-}EYFP}$ mice, n = 3 mice. Dotted lines outline hair follicles. (E) Schematic of light placement on hair-shaven leg skin, see videos. (F) Histogram showing percentage of mice displaying aversive responses to 5, 10, or 20mW blue light at the leg (see above panel C for genotype description and statistical analyses). (G) A lower activation threshold is required for paw versus leg skin nociceptors. (H) Temporal delay time (seconds) from light onset to the first aversive behavior with 5, 10, or 20mW blue light in paw or leg of *Mrgprd*$^{CreERT2/+}$; *Rosa*$^{ChR2\text{-}EYFP/ChR2\text{-}EYFP}$ mice. Error bars represent SEM.

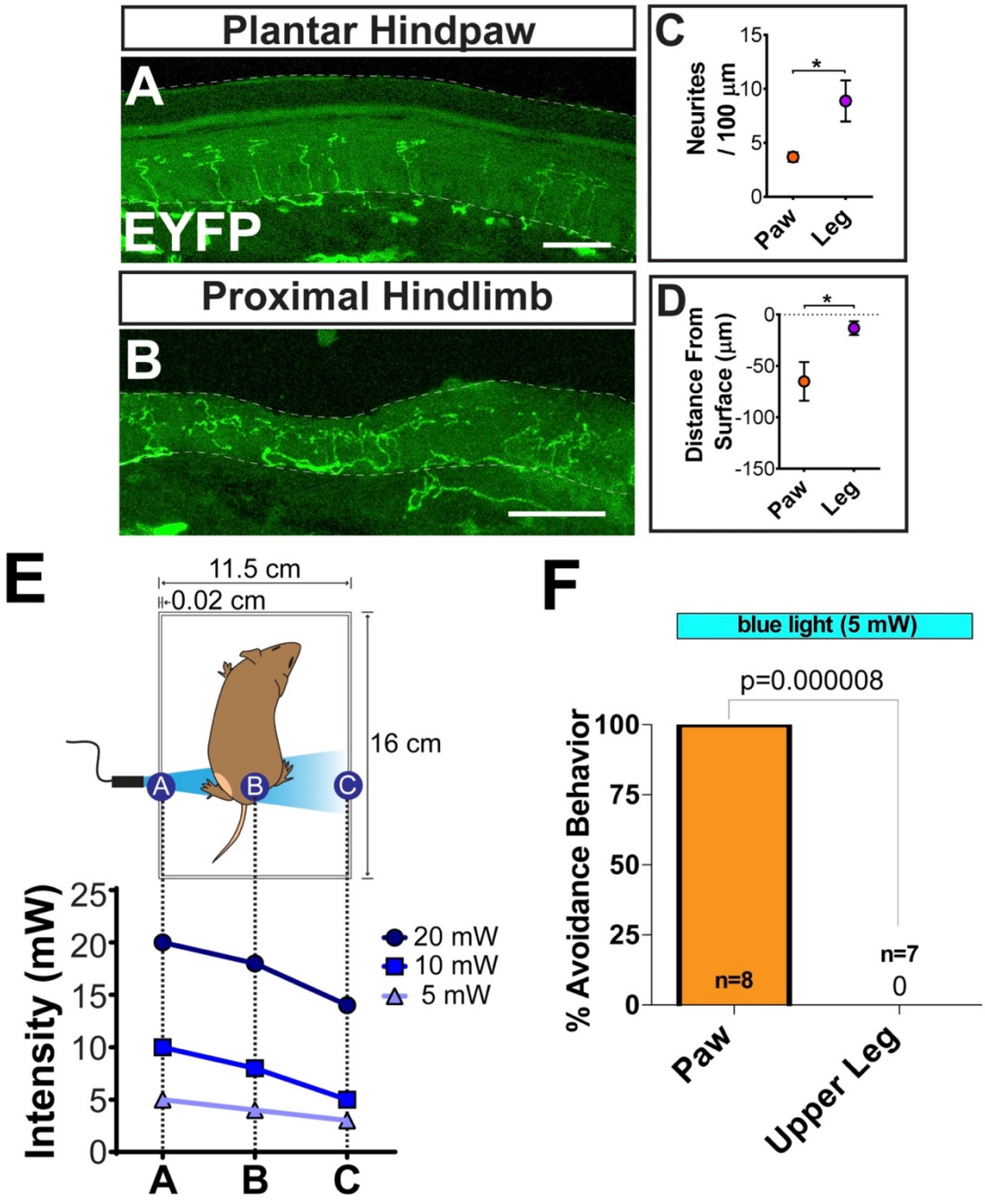

Figure 17. *In vivo* optogenetic peripheral stimulation. (A&B) *Mrgprd*^{CreERT2}; *Rosa*$^{ChR2\text{-}EYFP}$ sectioned upper leg hairy skin (B) and plantar paw glabrous skin (A) shows the lower density and farther distance from the skin surface of plantar paw neurites. Dotted lines indicate dermis/epidermis junction and outer skin surface. (C&D) Quantification of

neurites per 100μm (C) and neurite distance below the skin surface. n = 3 animals, * = p <0.05 (Student's t-test). (E) Measured light power at three locations (closest side, midpoint, farthest side) in the behavior chamber with 5 mW, 10 mW, and 20 mW blue laser intensity. (F) Response rate (% of mice) showing withdrawal responses to 5 mW blue light stimulation at paw or upper leg. n = 6-10 mice, 1-2 trials per mouse. * = p <0.05, Chi-square test. Scale bars = 50 μm (A&B).

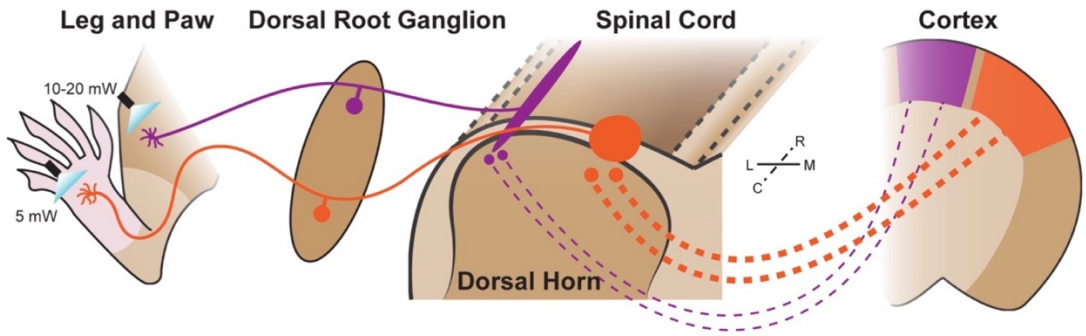

Figure 18. Model of the somatotopic organization of mammalian nociceptive circuitry. Distinct central arbor morphologies ("round versus long") of Mrgprd+ non-peptidergic nociceptors are observed in the medial versus lateral dorsal spinal cord, which correlates well with regional peripheral sensitivity and cortical representation. Scale bars = 50μm.

Tables

Region	n	**Avg area (mm^2)**	SE	Min area (mm^2)	Max area (mm^2)
Plantar hindpaw (glabrous)	22	**0.30**	0.10	0.08	0.86
Dorsal hindpaw	23	**0.29**	0.04	0.15	0.54
Proximal hindlimb*	23	**0.17**	0.03	0.14	0.32
Dorsal forepaw	9	**0.26**	0.07	0.11	0.45
Proximal forelimb*	3	**0.14**	0.01	0.13	0.14
Trunk	76	**0.28**	0.05	0.10	0.71
Top of head*	6	**0.14**	0.04	0.10	0.20
Ear	11	**0.47**	0.11	0.22	0.93

Table 1. Summary of peripheral terminals of sparsely labeled Mrgprd+ non-peptidergic nociceptors. Data pooled from nine 3pw animals. Asterisk (*) indicates a significant difference ($p<0.05$, Student's t-test) in average size when compared to hindpaw plantar (glabrous) skin arbors.

Animal	Proximal Hindlimb		Plantar Hindpaw	
	DiI$^+$ Skin Area (mm^2)	DiI/GFP double$^+$ DRG neurons	DiI$^+$ Skin Area (mm^2)	DiI/GFP double$^+$ DRG neurons
1	1.59	173	5.54	128
2	0.89	49	7.20	163
3	2.32	75	10.54	196
4	11.26	245	4.16	149
5	0.58	117	4.56	71
6	0.77	182	8.46	83
7	**	**	12.95	274
8	2.19	60	**	**

Table 2. Retrograde DiI+ labeling of nociceptors in *Mrgprd*^{EGFPf} mice. Side (right or left) of injection locations were alternated between animals. Asterisks (**) indicate missing tissue.

	n	% of Total
Total neurons	234	
Segments traveled from point of entry		
0	170	72.6
1	54	23.1
2	9	3.8
3	1	0.4
Direction traveled (for axons traveling 1-3 segments)		
Caudal	46	19.7
Rostral	18	7.7
No central branch bifurcations	154	65.8
1 central branch bifurcation	72	30.8
>1 central branch bifurcation	8	3.4
No central terminals	1	0.4
1 central terminals	215	91.9
2 central terminals	16	6.8
3 central terminals	2	0.9

Table 3. Summary of central innervation patterns of sparsely labeled Mrgprd+ non-peptidergic nociceptors. Data pooled from three 3pw animals.

	Round					Long				
	n	**Height (µm)**	SE	**Width (µm)**	SE	n	**Height (µm)**	SE	**Width (µm)**	SE
Cervical	31	**145**	28	**49**	11	45	**259**	56	**28**	5
Thoracic	3	**155**	6	**37**	6	81	**334**	61	**24**	4
Lumbar	99	**157**	20	**48**	5	83	**274**	32	**28**	3
Sacral	19	**162**	22	**51**	7	7	**197**	19	**35**	3

Table 4. Summary of non-peptidergic nociceptor central terminal height and width measurements. Round and long terminals were defined by W/H ratios (round = W/H ratio >0.2, long = W/H ratio <0.2). Data pooled from seven 3pw animals.

Mrgprd^{CreERT2}; *Rosa*$^{ChR2\text{-}EYFP/ChR2\text{-}EYFP}$ (ChR2 Homozygous)

	Transverse			
	n	Mono $EPSC_L$	Poly $EPSC_L$	Non-Responsive
Medial Lumbar	15	11 (73.3%)	3 (20%)	1 (6.7%)
Lateral Lumbar	18	16 (88.9%)	1 (5.6%)	1 (5.6%)

Mrgprd^{CreERT2}; *Rosa*$^{ChR2\text{-}EYFP/+}$ (ChR2 Heterozygous)

	Transverse					
	n	Mono $EPSC_L$	Poly $EPSC_L$	Non-responsive	$IPSC_L$	No $IPSC_L$
Medial Lumbar	17	15 (88.2%)	2 (11.8%)	0 (0%)	13 (76.5%)	4 (23.5%)
Lateral Lumbar	19	2 (10.3%)	10 (52.6%)	7 (36.8%)	3 (15.8%)	16 (84.2%)
Thoracic	11	1 (9.1%)	6 (54.4%)	4 (36.4%)	3 (27.3%)	8 (72.7%)
	Sagittal					
	n	Mono $EPSC_L$	Poly $EPSC_L$	Non-responsive		
Medial Lumbar	13	9 (69.2%)	3 (23.1%)	1 (7.7%)		
Lateral Lumbar	16	0 (0%)	3 (18.8%)	13 (81.3%)		
Thoracic	12	1 (8.3%)	3 (25.0%)	8 (66.7%)		

Table 5. Summary of incidences of light-induced postsynaptic current ($EPSC_L$ or $IPSC_L$) responses recorded from layer II neurons in *Mrgprd*^{CreERT2}; *Rosa*$^{ChR2\text{-}EYFP}$ homozygous and heterozygous mice. Patch clamp recordings were taken from either transverse or sagittal DH slices, as indicated. Responses were classified as mono- or polysynaptic (see text). Shaded boxes show the response of the majority (>50%) of recorded cells.

Chapter 3:

Region-specific nociceptor central terminal arbors develop independent of peripheral innervation

This chapter has been adapted from:

Olson W, Luo W (2018) Somatotopic organization of central arbors from nociceptive afferents develops independently of their peripheral target innervation.(Submitted)

Abstract

Functionally important regions of sensory maps are overrepresented in the sensory pathways and cortex, but the underlying developmental mechanisms are not clear. Given that peripheral and central arbor formation of Mrgprd+ neurons co-occurs around the time of birth, we tested whether peripheral cues from different skin areas and/or postnatal reorganization mechanisms could instruct the somatotopic difference among central arbor morphologies we identified in the spinal cord DH. We found that, while terminal outgrowth/refinement occurs during early postnatal development in both the skin and the DH, postnatal refinement of central terminals precedes that of peripheral terminals. Further, we used single-cell ablation of *Ret* to genetically disrupt epidermal innervation of Mrgprd+ neurons and revealed that the somatotopic difference among their central arbors was unaffected by this manipulation. Finally, we saw that region-specific Mrgprd+ central terminal arbors are present from the earliest postnatal stages, before skin terminals are evident. In summary, we find that region-specific organization of Mrgprd+ neuron central arbors develops independently of peripheral target innervation and is present shortly after initial central terminal formation. Our data suggest that either cell-intrinsic and/or DH local signaling are likely to establish this somatotopic difference.

Introduction

While the somatosensory and other sensory systems use central magnification to meet region-specific functional requirements (Daniel and Whitteridge, 1961; Suga et al., 1987; Ahnelt, 1998; Challis et al., 2015), the developmental mechanisms used to differentially allocate circuit space in this manner have not been clearly defined. In addition to differences in primary neuron density in the periphery (Johansson and Vallbo, 1979; Brown et al., 2004), magnification at downstream circuits are likely to be involved. We identified region-specific central arbor morphology as a likely mechanism used by Mrgprd+ non-peptidergic nociceptors for 'afferent magnification' in DH circuits (Chapter 2). This indicates that Mrgprd+ neurons, which as a population show very similar molecular markers and anatomical features, differentially direct their central terminal arbor formation based on their somatotopic location during development. Given our ability to trace and genetically manipulate this population, this system offers a unique opportunity to gain insight into the mechanisms used by developing sensory systems to magnify important regions.

The mechanisms that direct somatotopically-appropriate wiring of DRG neurons are largely unclear. Somatosensory circuits of the DH have a 'flipped' topographic map: in the lumbar enlargement (innervating the hindlimbs), the distal limbs (foot and toes) are represented in medial DH while the proximal limbs are represented in the lateral DH (Figure 1A) (Brown and Fuchs, 1975a; Swett and Woolf, 1985). Nerve tracing experiments have shown that cutaneous sensory topographic maps formed early in development are similar to the mature pattern (Smith, 1983; Mendelson et al., 1992).

Based on the rough coincidence of peripheral and central target innervation, and based on the proximal-to-distal progression of hind limb epidermal innervation, it was proposed that peripheral innervation could drive correct somatotopic map formation in the DH (Reynolds et al., 1991). However, subsequent studies suggested that peripheral and central somatotopic maps may develop independently of one another (Sharma et al., 1994; Mirnics and Koerber, 1995a; Wang and Scott, 2002).

Despite the interesting information gained from these experiments, the previous work could not resolve the single-cell structure of DRG neurons. Therefore, these studies could not examine the mechanisms for the disproportionate representation (magnification) of paw regions in somatosensory circuits. It remains possible that peripheral cues from different skin regions could instruct the formation of region-specific central arbor morphologies in the DH (Figure 1B). Alternatively, it is also possible that Mrgrd+ neurons form immature, somatotopically homogenous arbors that are postnatally reorganized into region-specific morphologies (Figure 1C). Lastly, DRG afferents may form region-specific arbor morphologies during their initial terminal formation, suggesting pre-patterning mechanisms (Figure 1D). Here, we used population-level tracing to characterize the postnatal development of Mrgprd+ nociceptor central and peripheral terminal arbors. In addition, we performed single-cell ablation of *Ret* to disrupt peripheral target innervation of these neurons and analyze the effect on their central arbor morphology in the DH. Lastly, we performed single-cell tracing of Mrgprd+ neurons in early postnatal animals, right after their initial innervation of the DH. These experiments show that region-specific arbors are present in early postnatal animals

(supporting the 'pre-patterned' model), and that central terminal development slightly precedes, and occurs independently of, peripheral terminal development/refinement. Taken together, our results suggest that somatotopic organization of mammalian nociceptor central terminal arbors is likely to be dictated through mechanisms intrinsic to the DRG neurons themselves and/or by mechanisms within the spinal cord.

Population-level characterization of postnatal development of peripheral and central terminals of Mrgprd+ DRG neurons

To investigate whether region-specific arbor development may be driven by peripheral and/or central mechanisms, we used *Mrgprd*^{EGFPf} knock-in mice (Zylka et al., 2005) to characterize the postnatal (P1 – 3 postnatal weeks, pw) innervation of non-peptidergic nociceptors in the paw glabrous skin and the lumbar spinal cord enlargement DH. *Mrgprd* is first expressed at E16.5 in mice and specifically marks the non-peptidergic nociceptor population (Chen et al., 2006). EGFP expression in this knock-in mouse line faithfully indicates expression of *Mrgprd*. This genetic tool offers advantages over previous approaches since it specifically labels non-peptidergic fibers (unlike nerve filling) and avoids issues related to the dynamic expression of immunostaining markers (Reynolds et al., 1991; Jackman and Fitzgerald, 2000).

Peripherally, mature non-peptidergic nociceptor axons travel to the skin in the cutaneous nerves, grow a fiber plexus parallel to the skin surface in the dermis, and send perpendicular terminals out of the subepidermal plexus that penetrate the epidermis (Zylka et al., 2005; Olson et al., 2017). Most of the paw epidermis is not innervated by

Mrgprd^{EGFPf} fibers at P1, except for few rudimentary terminals (Figure 2A). From P1 to P7, there is a rapid phase of nerve terminal growth, as indicated by a great increase in density of both primary (leaving the subepidermal plexus) as well as secondary/tertiary (branches off primary terminals) Mrgprd+ fiber branches (Figure 2A-C, K, M, N). It is then followed by a refinement phase, as indicated by a decrease in density from P7 to 3pw. By 3pw, no secondary or tertiary branches are present (Figure 2G, H, L-N). This pattern is true when quantified as absolute terminal densities or as growth-normalized values (Figure 2M, N).

Centrally, non-peptidergic nociceptor axons travel through the dorsal roots, grow for 0-2 spinal segments rostrally or caudally in Lisseur's tract at the dorsolateral margin of the spinal cord, and then dive ventrally to innervate layer II of the DH (Zylka et al., 2005; Olson et al., 2017). *Mrgprd*^{EGFPf} fibers have established a thick (in the dorsoventral extent) terminal layer by P1 in the DH (Figure 2D). This layer shows a 4-fold (absolute) decrease in layer thickness, reaching the mature layer thickness by P7 (Figure 2D-F, I, J). This decrease of layer thickness is also true when quantified by growth-normalized values (Figure 2O, P). In summary, while *Mrgprd*^{EGFPf} peripheral terminals are still undergoing initial outgrowth in the epidermis (the first postnatal week), their central terminals are in the process of refining to their mature thickness in the DH. These results indicate that central terminal development of Mrgprd+ neurons precedes peripheral development in the postnatal period.

Non-peptidergic nociceptor central arbor formation is independent of peripheral terminal innervation

Next, we further determined whether non-peptidergic nociceptors utilize peripheral cues or processes to establish region-specific central arbor morphologies with a genetic manipulation. Previous work has shown that, upon DRG-specific deletion of the Glial cell line-derived neurotrophic factor receptor *Ret*, non-peptidergic nociceptors fail to innervate their final peripheral target, the skin epidermis, while their central terminals remain in DH layer II (Luo et al., 2007). However, these experiments did not trace single-cell morphology, so it remains unknown whether their central arbors are altered after this failure in peripheral target innervation. We ablated *Ret* from individual non-peptidergic nociceptors and quantitatively measured their regional single-cell width (mediolateral) in the DH. We used a mouse line in which Cre-dependent inactivation of *Ret* also leads to expression of CFP ($Ret^{f(CFP)}$) (Uesaka et al., 2008). In $Mrgprd^{CreERT2/+}$; $Ret^{f(CFP)/null}$ mice (*Ret* CKO), which carry the $Ret^{f(CFP)}$ allele along with a *Ret* null allele, low-dose prenatal tamoxifen (0.5 mg at E16.5-E17.5) generated sparse *Ret*-null non-peptidergic nociceptors that are labeled with CFP (Figure 3C). In $Mrgprd^{CreERT2/+}$; $Ret^{f(CFP)/+}$ littermate controls (Control), this same treatment sparsely labeled *Ret* heterozygous non-peptidergic neurons with CFP (Figure 3A). As expected for *Ret* deletion, sparsely labeled CFP^+ DRG cell bodies were smaller in $Mrgprd^{CreERT2/+}$; $Ret^{f(CFP)/null}$ mutant mice (data not shown), but the number of CFP^+ neurons was not decreased (average CFP^+ neurons/DRG: control = 58.7 ± 10.3, n = 14 DRGs from 3 animals, mutant = 70.4 ± 24.6 n = 22 DRGs from 3 animals) (Figure 3A, C, I). In addition, while sections of glabrous skin from control mice showed sparsely labeled terminals with mature epidermal endings, sections from mutant

skin showed axon bundles in the dermis but no mature endings in the epidermis, consistent with previous work (Luo et al., 2007) (Figure 3B, D). Lastly, serial sectioning of control and mutant thoracic (T6-T12) and lumbar (L3-L6) spinal cords showed that the round-vs.-long distinction in central terminal morphology was unaffected by *Ret* deletion (Figure 4E-H). We imaged through serial sections and measured the maximum mediolateral width of sparse-labeled neurons. The medial lumbar neurons were roughly twice as wide, on average, as either lateral lumbar or thoracic neurons (thoracic = 28.7 ± 5.2 μm, lateral lumbar = 33.5 ± 6.5 μm, medial lumbar = 64.7 ± 14.2 μm, n = 287 neurons from 3 mice) in control mice (Figure 3E&F, J). A similar difference was also seen in mutant spinal cords (thoracic = 29.0 ± 7.0 μm, lateral lumbar = 33.1 ± 8.7 μm, medial lumbar = 68.6 ± 18.1 μm, n = 239 neurons from 3 mice (Figure 3G&H, J), indicating that the round-vs.-long distinction is maintained in these mutant neurons. Additionally, no difference in the average width of round or long terminals was observed between control and *Ret* null non-peptidergic neurons (Figure 3J), suggesting that Mrgprd+ neurons grow normal central terminal arbor morphologies in the absence of *Ret*.

Sparse labeling reveals region-specific Mrgprd+ central arbors from the earliest stages of central innervation

Lastly, we asked whether the region-specific central terminal arbors of non-peptidergic DRG neurons might be established through postnatal reorganization (Figure 1C), or instead are present from the earliest stages of DH innervation (Figure 1D). We performed sparse genetic tracing of non-peptidergic neurons at early postnatal stages by crossing tamoxifen-dependent $Mrgprd^{CreERT2}$ mice with $Rosa^{iAP}$ alkaline phosphatase reporter mice

(0.25 mg of tamoxifen was given at E17.5) (Olson et al., 2017). Sparse terminals were seen after AP staining of skin and spinal cord tissue. Immature skin terminals could be seen at P3 but not P1 (Figure 4E&F), consistent with the few *Mrgprd*^{EGFPf} fibers in the epidermis at P1 (Figure 2). In addition, while their central arbors still appear immature at P1 and P3, region-specific arbor morphologies (the somatotopic organization of central arbors) are seen in both P1 and P3 spinal cords (Figure 4A-D). Like the mature DH organization of these afferents (Olson et al., 2017), medial lumbar enlargement (paw representation, outlined in Figure 4B, D) regions contain mediolaterally wide arbors while lateral lumbar enlargement and thoracic (proximal hindlimb, trunk) regions contain mediolaterally thin arbors (Figure 1A). It should be noted that the genetic targeting strategy utilized for this experiment may label two *Mrgprd*-lineage non-peptidergic DRG populations, one expressing *Mrgprd* in adulthood and the other expressing *Mrgpra/b/c* genes in adulthood (Liu et al., 2008; Olson et al., 2017). Given that the *Mrgpra/b/c* population only represents <20% of targeted neurons (Olson et al., 2017), we believe that most if not all AP+ neurons belong to the mature Mrgprd+ population.

Discussion

In summary, we found that (1) postnatal development/refinement of central terminals precedes development/refinement in the periphery, (2) genetic disruption of peripheral terminal wiring had a negligible effect on region-specific central arbors, and (3) region-specific arbors are present from the earliest postnatal stages. Though trophic factor signaling functions to control neurite arbor morphogenesis in some cell types (Xu et al., 2000; Joo et al., 2014), here we found that deletion of the major trophic factor receptor, *Ret*, expressed by Mrgprd+ neurons (Luo et al., 2007), did not affect their DH arbor morphology. Earlier work indicated that spinal cord somatotopic map formation of DRG afferents does not rely on cues from the periphery (Sharma et al., 1994; Wang and Scott, 2002). Our findings expand upon this work to show that region-specific arbor morphology development (and thereby magnification of paw regions) also occurs independent of peripheral innervation.

While non-peptidergic central terminal arbors do show very clear postnatal layer thickness refinement (the dorsoventral axis) (Figure 2), and while early postnatal arbors have a somewhat immature morphology (Figure 4), their region-specific structure is apparent from the earliest stages of DH innervation. Earlier spinal nerve backfilling experiments indicated that DRG central projections form somatotopically appropriate innervation patterns from the earliest stages of innervation (Smith, 1983; Mendelson et al., 1992). Our work expands upon this to show that region-specific single-cell morphologies are also apparent shortly after the initial terminal formation (Figure 1D). This suggests that pre-patterning mechanisms may underlie the regional magnification of

paw representations in the primary afferent neuropil. While a rostrocaudal progression of expression for different *Hox* genes has been demonstrated to underlie segmental patterning in the spinal cord (Dasen et al., 2005), less is understood regarding mediolateral patterning in the spinal cord or regarding proximodistal patterning of somatotsensory afferents. Future work should examine what kinds of DRG cell intrinsic and/or DH patterning mechanisms might direct region-specific wiring of somatosensory afferents.

While peripheral receptor density is a major contributor to central magnification for some sensory systems (Kossl and Vater, 1985; Stanley, 1991), afferent magnification at in the CNS can also magnify sensory regions (Catania and Kaas, 1997; Catania et al., 2011). Given that paw skin shows a low density of non-peptidergic fibers, magnification for peripheral nociceptor circuits likely utilizes such afferent magnification. In combination with earlier work, our results support a model in which somatotopic map formation (including both topographic innervation and region-specific magnification) in the CNS does not depend on peripheral mechanisms. Our results do not rule out a role for spontaneous activity in afferents that could have been spared by our genetic manipulation, which are known to play critical roles in visual map formation (Assali et al., 2014). It remains to be seen if centrally-driven patterning mechanisms might underlie region-specific afferent morphologies in other systems.

Materials and Methods

Mouse strains:

Mice were raised in a barrier facility in Hill Pavilion, University of Pennsylvania. All procedures were conducted according to animal protocols approved by Institutional Animal Care and Use Committee (IACUC) of the University of Pennsylvania and National Institutes of Health guidelines. *Mrgprd*^{EGFPf}, *Mrgprd*^{CreERT2}, *Rosa*^{iAP}, and *Ret*$^{f(CFP)}$ mice have been previously described (Zylka et al., 2005; Uesaka et al., 2008; Badea et al., 2009; Olson et al., 2017). *Ret*^{null} allele mice were generated by crossing a conditional *Ret* line (*Ret*$^{f/f}$) (Luo et al., 2007) with a germline Cre mouse line (*Sox2*^{Cre}) (Hayashi et al., 2002).

Genetic labeling of Mrgprd+ nociceptors:

To sparsely label Mrgprd+ nociceptors, we set up timed pregnancy matings of *Mrgprd*^{CreERT2} mice with *Rosa*^{iAP} or *Ret*$^{f(CFP)}$ mice. Population-level labeling was achieved through either prenatal or postnatal tamoxifen treatment. For prenatal treatment, pregnant females were given tamoxifen (Sigma, T5648) along with estradiol (Sigma, E8875, at a 1:1000 mass estradiol: mass tamoxifen ratio) and progesterone (Sigma, P3972, at a 1:2 mass progesterone: mass tamoxifen ratio) in sunflower seed oil via oral gavage at E16.5-E17.5, when *Mrgprd* is highly expressed in mouse non-peptidergic nociceptors (Chen et al., 2006).

Tissue preparation and histology:

Procedures were conducted as previously described (Fleming et al., 2012; Niu et al., 2013). Briefly, mice were euthanized with CO_2 and transcardially perfused with 4% PFA/PBS, and dissected tissue (skin, spinal cord, DRG) was post-fixed for 2 hr in 4% PFA/PBS at 4° C. Tissue used for section immunostaining was cryo-protected in 30% sucrose/PBS (4% overnight). Frozen glabrous skin and DRG/spinal cord sections (20-30 μm) were cut on a Leica CM1950 cryostat. Immunostaining was performed as described previously. DRGs for whole mount immunostaining were treated as described directly after post-fixation. The following antibodies were used: chicken anti-GFP (Aves, GFP-1020), rabbit anti-GFP (Invitrogen, A-11122). Tissue (skin or spinal cord with attached DRGs) for whole mount AP color reaction with BCIP/NBT substrate was treated as previously described. Following AP color reaction labeling, tissue was cleared in 1:2 (v:v) benzyl alcohol + benzyl benzoate (BABB) for imaging (Niu et al., 2013).

Image acquisition and data analysis:

Images were acquired either on a Leica DM5000B microscope (brightfield with a Leica DFC 295 camera and fluorescent with a Leica 345 FX camera), on a Lecia SP5II confocal microscope (fluorescent), or on a Leica M205 C stereoscope with a Leica DFC 450 C camera (brightfield). Image quantification was performed in ImageJ. Graphs and statistical analyses were created in GraphPad Prism5.

For growth normalization of skin terminal densities (Figure 2), plantar paws (n=3 animals for each age) were imaged and fitted ellipses were drawn over the six mouse foot

pads. Major axis lengths (proximodistal axis) were averaged across animals. Absolute skin terminal densities were multiplied by a normalization factor: Growth-normalized density (Age) = Absolute density (Age) X (Mean paw length (Age) / Mean paw length (3 pw)).

For growth normalization of DH layer thickness (Figure 2), the maximum mediolateral width of the *Mrgprd*^{EGFPf} innervation layer was measured (n=3 sections from separate animals for each age). Absolute layer thickness measurements were multiplied by a normalization factor: Growth-normalized thickness (Age) = Absolute thickness (Age) X (Mean DH width (Age) / Mean DH width (3 pw)).

For single-cell width measurements in sectioned DH tissue (Figure 3), serial DH sections were imaged, and individual arbors were identified by comparing adjacent sections. The DH of lumbar enlargement sections (L3-L5) were divided into thirds based on the maximum mediolateral width of the DH. Cells with most of their width lying in the medial third were classified as "Medial Lumbar", cells were otherwise classified as "Lateral Lumbar".

Figures

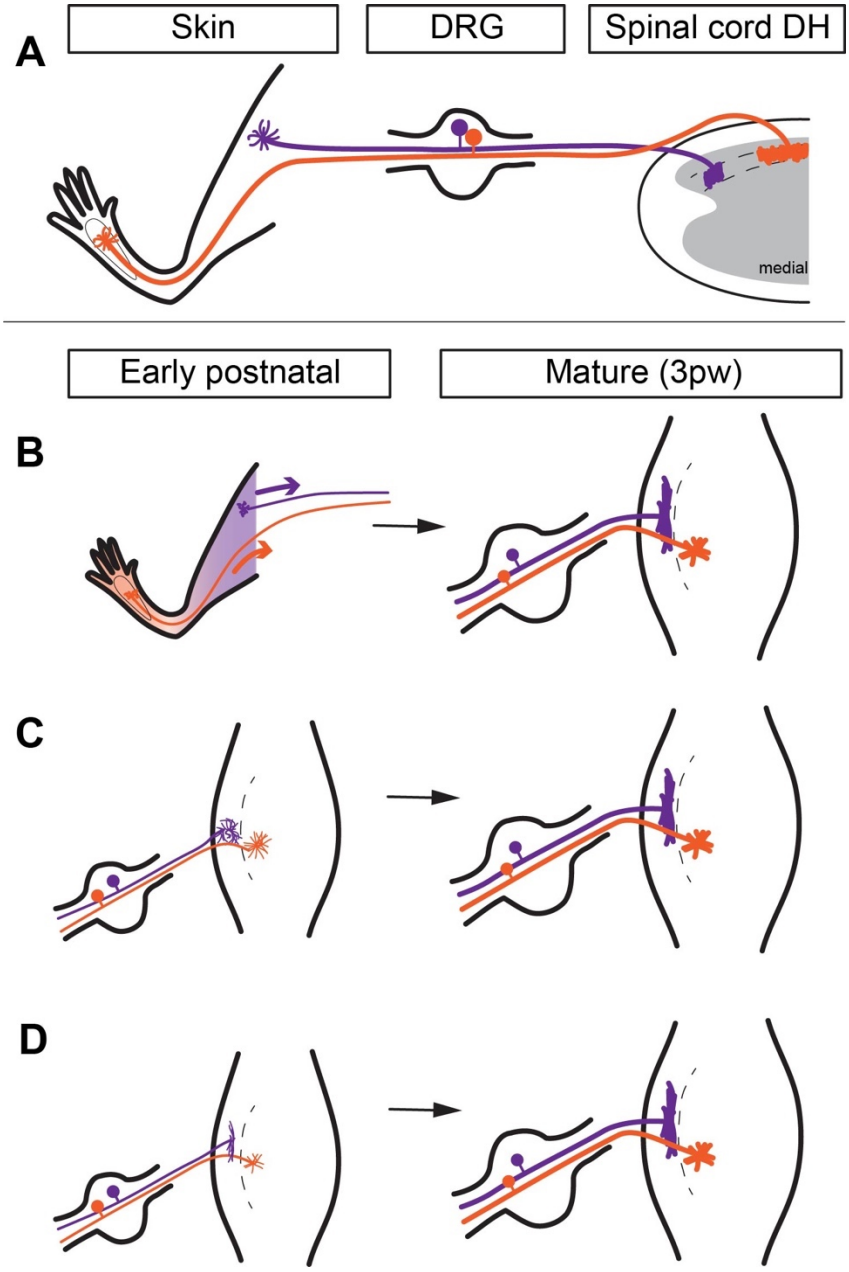

Figure 1. Models of hypothesized developmental mechanisms for region-specific Mrgprd+ central arbors. A, Mature somatotopic organization of Mrgprd+ afferents. Proximal hind limb afferents (purple) grow 'long and thin' central arbors in the lateral DH, while plantar paw afferents (orange) grow 'round and wide' central arbors in the medial DH. DH is drawn as a transverse section. B, Peripheral cues model. Upon

innervation of the skin around birth, cues from different skin regions direct region-specific developmental of central terminal arbors. DH is drawn from a top-down view. C, Central reorganization model. Afferents grow immature, somatotopically homogenous arbors that are postnatally reorganized into region-specific arbor morphologies. D, Pre-patterned model. Afferents grow somatotopically distinct arbor morphologies during their initial innervation of the DH.

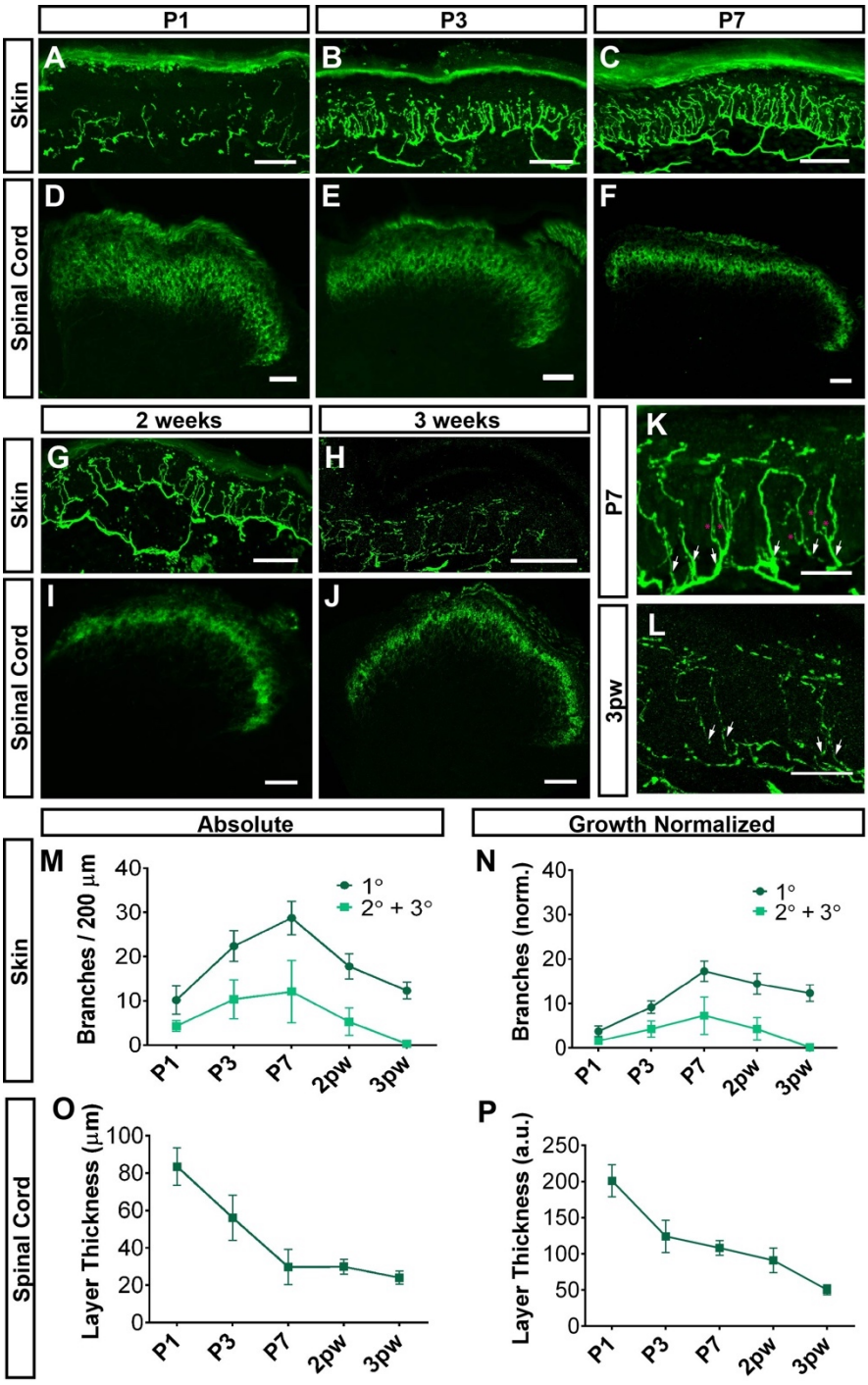

Figure 2. Postnatal central and peripheral terminal development of *Mrgprd*^{EGFPf} non-peptidergic nociceptors. A-J, GFP immunostaining of glabrous skin (A-C, G, H) and DH (D-F, I, J) sections from *Mrgprd*^{EGFPf} mice at the indicated ages. K, L, Higher magnification views of peripheral terminals, indicating secondary/tertiary branches (pink

asterisks) growing off primary branches (white arrows) in P7 but not 3pw skin. M, N, Quantification of densities of absolute (M) and growth-normalized (N, see Methods) glabrous skin primary, secondary and tertiary branches during postnatal development. Skin terminals show overgrowth during the first week. O, P, Quantification of absolute (O) and growth-normalized (P, see Methods) DH layer thickness at the indicated ages. DH terminals show a refinement during the first week, at which point they remain at their mature thickness. n = 3 animals per stage. Scale bars = 50 μm (A-J), 20 μm (K, L).

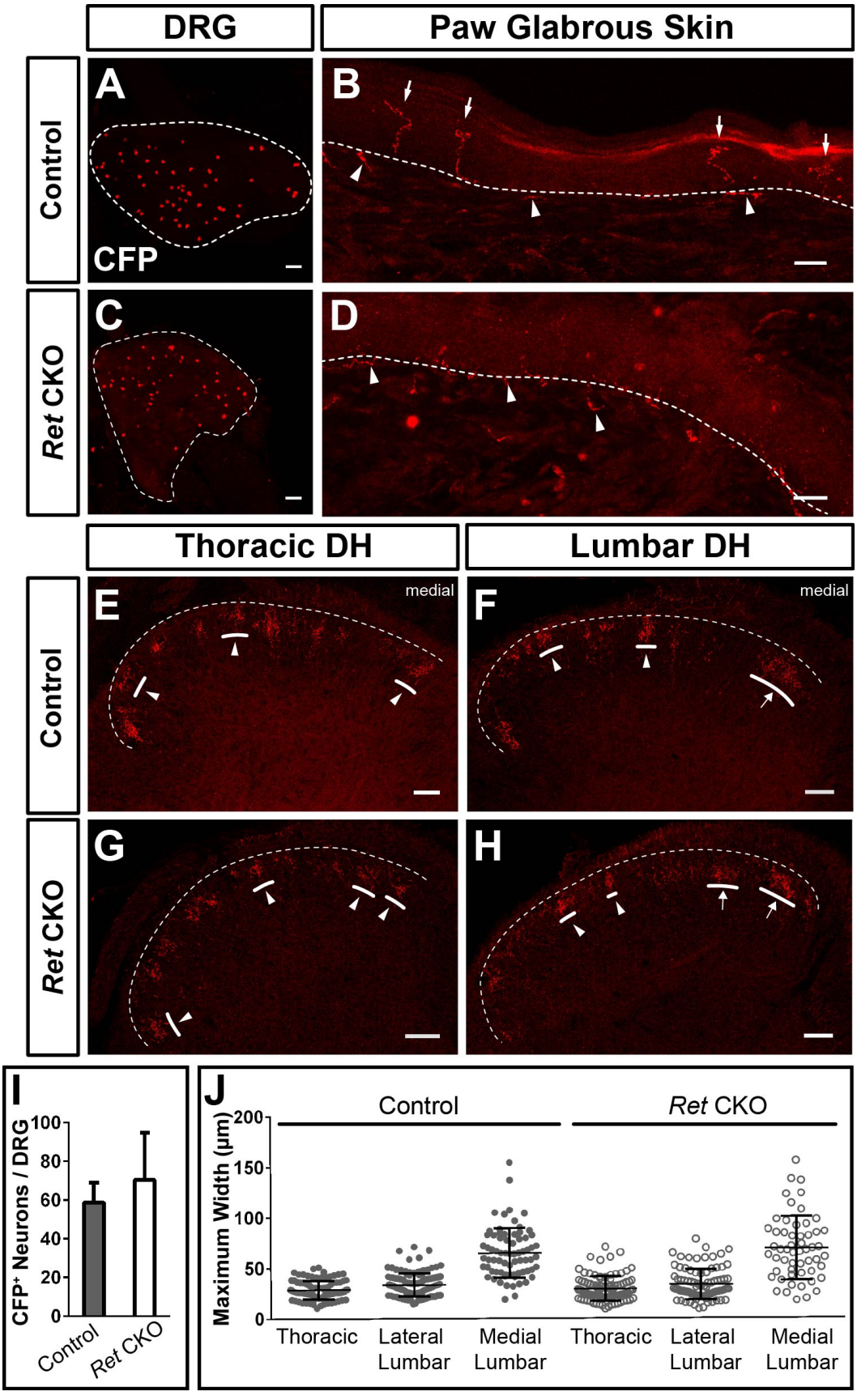
DRG
Paw Glabrous Skin
Control
Ret CKO
A
B
C
D
CFP
Thoracic DH
Lumbar DH
E
F
G
H
medial
I
CFP+ Neurons / DRG
100
80
60
40
20
0
Control
Ret CKO
J
Maximum Width (μm)
200
150
100
50
0
Control
Ret CKO
Thoracic
Lateral Lumbar
Medial Lumbar

Figure 3. Genetic disruption of peripheral target innervation does not affect region-specific central arbor morphologies. A, C, Whole mount CFP immunostaining of sparse labeled 2-3pw MrgprdCreERT2; Ret f(CFP) / + (control, A) and MrgprdCreERT2; Ret f(CFP) / null (mutant, C) DRGs (0.5 mg tamoxifen at E16.5-E17.5). B, D, CFP immunostaining of sectioned glabrous skin shows epidermal endings in control (B) but not mutant (D) mice, indicating a lack of peripheral terminals in Ret null nociceptors. White arrows, mature epidermal endings. White arrowheads, dermal axonal bundles. E-H, CFP immunostaining of serial DH sections from control (E&F) and mutant (G&H) mice shows sparse labeled terminals. I, Quantification of the number of CFP+ neurons / DRG. n = 14-22 DRGs from 3 animals per genotype. J, Maximal mediolateral width of sparse labeled neurons from control and mutant mice shows that the round-vs.-long distinction is still present in mutant mice. n = 239 (mutant), 287 (control) neurons from 3 mice per genotype. Scale bars = 100 μm (A&C), 20 μm (B&D), 50 μm (E-H).

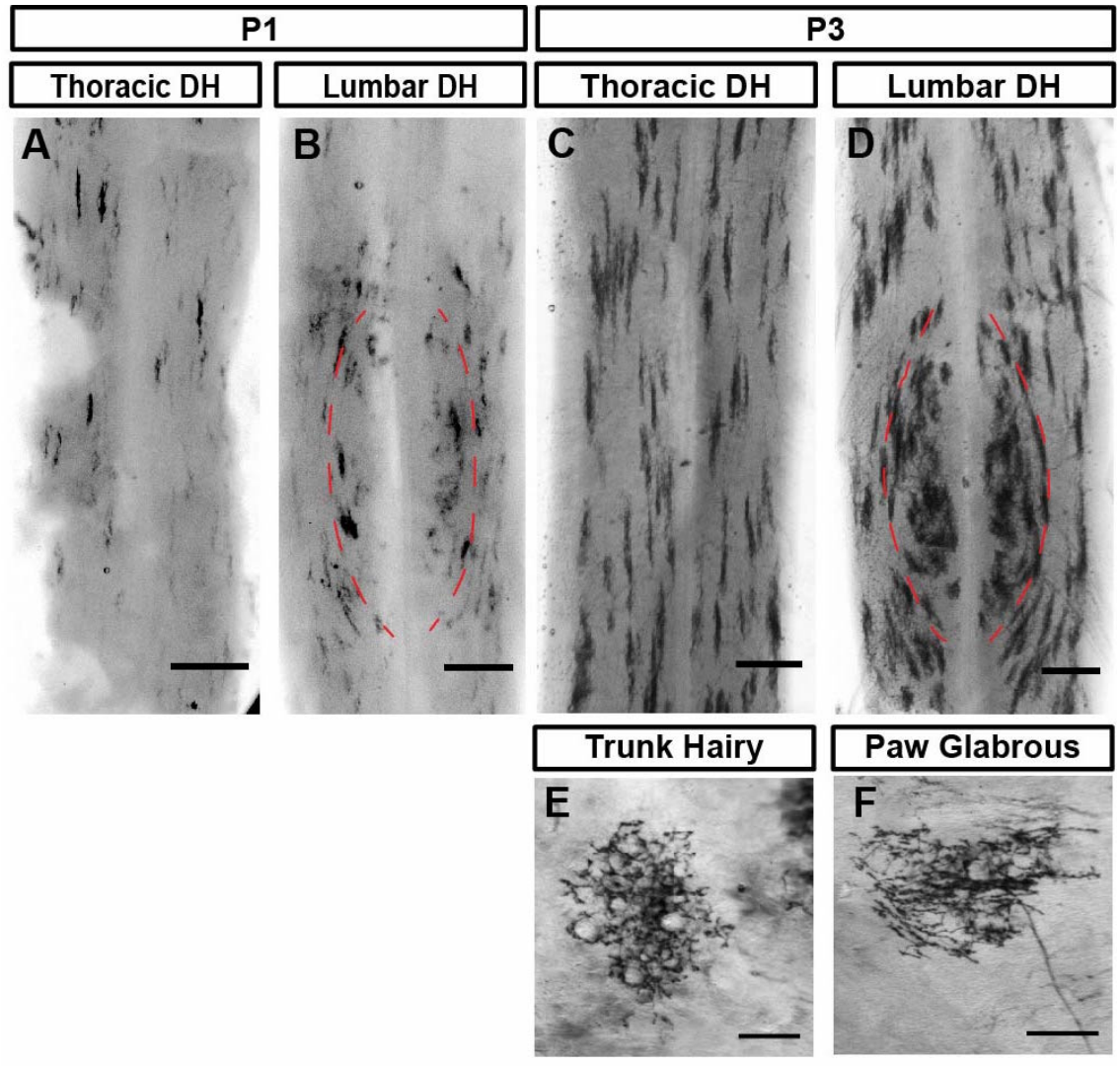

Figure 4. Region-specific Mrgprd+ DH arbors are evident during the earliest stages of innervation. A-F, AP color reaction of spinal cord (A-D) and skin (E&F) tissue from P1 or P3 MrgprdCreERT2; RosaiAP mice (0.25 mg tamoxifen at E17.5). Sparse skin terminals were not seen at P1. While early postnatal nociceptors are still immature, the round vs. long distinction can be seen in B & D. Scale bars = 250 μm (A-D), 100 μm (E&F).

CHAPTER 4

Conclusions and Future Directions

Region-specific mechanisms for the pain fovea: comparison with other sensory modalities

Using sparse genetic tracing of mouse non-peptidergic nociceptors, we found no obvious peripheral mechanisms for high pain sensitivity in the distal limbs, but instead found major somatotopic differences in spinal cord arbor morphology that could underlie the pain fovea. The high sensitivity of the distal limbs for touch stimuli has long been recognized, and classic work has defined mechanisms. This work has suggested that an increase in peripheral receptor density and a decrease in RF size for distal limb regions are likely to be key mechanisms for the central magnification and the high sensitivity of these regions. Our results, consistent with previous human skin biopsy data, indicate that nociceptor density does not increase in the distal limbs for non-peptidergic nociceptors. We cannot exclude the possibility that untested peripheral mechanisms contribute to the high sensitivity to optogenetic stimulation we identified for paw non-peptidergic circuits. However, a comparison of our results to past literature suggests that pain, in contrast to the touch system, pain relies more on central organization mechanisms to facilitate region-specific sensation.

Similar to our results in the pain system, past work has reported that DH arbors of LTMRs are also wider in the mediolateral axis for the paw region of the DH (Shortland et al., 1989; Brown et al., 1991; Millecchia et al., 1991), and this likely contributes to the DH magnification of the paw for touch somatotopic maps. The relationship of this result to the touch fovea is unclear for two reasons: (1) unlike pain, the second-order locus for central relay of touch information is the dorsal column nuclei of the brainstem, not the

DH(Fleming and Luo, 2013; Olson et al., 2016); (2) unlike nociceptors, individual LTMRs send DH projections to many segments rostral and caudal from their segment of entry (Fleming and Luo, 2013; Niu et al., 2013; Olson et al., 2016), meaning that many of the touch primary afferents in the paw region of the DH have peripheral RFs in separate dermatomes. Nevertheless, the finding of similar somatotopic differences in the touch primary afferents, along with the identification of somatotopic differences in heat pain spatial acuity in humans (likely mediated through peptidergic circuits) suggests that these are general structural principles for the somatosensory circuits of the DH. Further, given that these findings are collected from rodent, cat, and human data, the somatotopic differences we identified are likely to be conserved across species.

Interestingly, in addition to the medial cervical and lumbar enlargements, we found 'round' morphology terminals in the medulla (spinal trigeminal nucleus) and the sacral spinal cord. The DRG and trigeminal somatosensory systems feature very different organization in many aspects. Based on this, it is difficult to assess the extent to which our results from the DRG afferents may apply to the trigeminal system. Nevertheless, it is interesting to note that round arbor morphologies are found in all regions that are 'extremities' in quadrupeds, consistent with the fact that these are likely sites of first contact with somatosensory stimuli. Further, the face and lips(and especially the whisker pads of cats and mice) are sensory foveae for both touch and pain(Mancini et al., 2014).

Given our findings, we suggest that region-specific nociceptor central arbors are a mechanism for afferent magnification of distal limb regions. This is analogous to the

touch fovea of the star-nosed mole ventral ray, which similarly shows high spatial acuity despite a low density of peripheral receptors (Catania and Kaas, 1997; Catania et al., 2011). Central magnification of important regions is a common feature of sensory systems, and peripheral receptor density is likely a major mechanism for this magnification in many cases (i.e. visual (Stanley, 1991), auditory (Kossl and Vater, 1985), and tactile (Brown et al., 2004) systems). However, single-cell tracing at multiple loci could identify whether afferent magnification along the sensory pathways might also be seen in these sensory systems.

What is the function of Mrgprd+ non-peptidergic nociceptors?

Based on classic physiological criteria (i.e. mechanical and thermal thresholds), Mrgprd+ neurons have been classified as CMH or CM nociceptors (Rau et al., 2009; Liu et al., 2012). Further, neuronal ablation has shown mechanical sensation deficits (Cavanaugh et al., 2009), supporting a role for this population in noxious mechanosensation. Building on this work, use of targeted optogenetic activation allows for investigation of the sufficiency of these afferents for pain behavior (i.e. what sensation is evoked when they are activated?). Interestingly, findings from our own lab (unpublished data) and from another group (Beaudry et al., 2017) have called into question the role of this population in pain behavior. Specifically, the behavior elicited by peripheral optogenetic stimulation of Mrgprd+ afferents (Figure 16) is more similar to light touch than pain behavior when compared using high-speed imaging and multiparameter analysis (data not shown). Further, optogenetic activation does not induce conditioned place avoidance (data not shown and (Beaudry et al., 2017)). This contrasts with activation of peptidergic

nociceptors, which induces more 'pain-like' withdrawal behavior and does induce conditioned place avoidance (data not shown and (Beaudry et al., 2017)).

Pain pathways are sometimes divided into Discriminative and Affective systems. In this scheme, the discriminative pain pathway will send information to the thalamus and primary somatosensory cortex to localized noxious stimuli, while the affective pain pathway will send information to many limbic system nuclei to induce negative valence emotional sensations. As mentioned above, peptidergic and non-peptidergic fibers have distinct connectivity, with non-peptidergic fibers terminating more superficially in the skin and peptidergic fibers innervating both cutaneous and deep targets (Zylka et al., 2005). Given (1) our identification of somatotopic organization in non-peptidergic fibers that we propose to be related to pain localization, and (2) the differences between peptidergic vs. non-peptidergic activation with regards to induction of conditioned place avoidance, one fascinating question for future research is whether these afferent groups might differentially contribute to discriminative vs affective pain pathways. Hypothetically, superficial non-peptidergic fibers might provide a 'warning' signal to the discriminative pathway to localize potential noxious stimuli, whereas deep peptidergic fibers might signal to the affective pathway that a stimulus has already caused tissue damage. Such a model could both expand upon and clarify past findings regarding the response properties and behavior necessities of these populations. This remains a critical area for future work.

Are region-specific disease processes a component of chronic pain?

Chronic pain conditions (which feature long-lasting, abnormal activation of the pain system in the absence of external damaging stimuli) are devastating disorders comprising a major public health problem. Though pre-clinical research has identified many molecules and substances that can alleviate chronic pain in animal models, very few of them have been successfully translated to human patients. Notably, preclinical pain research has historically relied very heavily on rodent models using paw withdrawal latency/frequency or tail flick frequency, both of which involve noxious stimuli applied to distal somatotopic areas (Le Bars et al., 2001). In addition, past physiological studies of dorsal spinal cord nociceptive circuits typically used recording from lumbar enlargement slices (Lu and Perl, 2003, 2005; Deng and Xu, 2012), likely the medial part of the lumbar enlargement. Furthermore, the most widely used animal models of chronic pain (the spared nerve ligation/injury model, the chronic constriction injury model, and paw application of Complete Freund's Adjuvant model) all focus on nociception mediated by distal hindlimb/lumbar enlargement circuits (Jaggi et al., 2011).

Therefore, most of the current pre-clinical research has revealed nociceptive mechanisms in the distal skin regions and "round terminal" spinal cord circuits. Our findings demonstrating region-specific functional organization of mammalian nociceptive circuits may explain part of the difficulty in translating animal work on chronic pain to patient conditions. Future work is needed to determine whether pain pharmacology, descending gain control, pain pathophysiology, etc. might systematically differ between somatotopic

regions. Such research could suggest ways in which chronic pain conditions might share certain etiological similarities to other conditions that are similarly localized, and might differ between conditions localized to other areas. This could provide insight into which aspects of preclinical research may or may not translate to specific clinical conditions.

BIBLIOGRAPHY

Abraira VE et al. (2017) The Cellular and Synaptic Architecture of the Mechanosensory Dorsal Horn. Cell 168:295-310 e219.

Ahnelt PK (1998) The photoreceptor mosaic. Eye 12 (Pt 3b:531-540.

Assali A, Gaspar P, Rebsam A (2014) Activity dependent mechanisms of visual map formation--from retinal waves to molecular regulators. Semin Cell Dev Biol 35:136-146.

Badea TC, Williams J, Smallwood P, Shi M, Motajo O, Nathans J (2012) Combinatorial expression of Brn3 transcription factors in somatosensory neurons: genetic and morphologic analysis. J Neurosci 32:995-1007.

Badea TC, Hua ZL, Smallwood PM, Williams J, Rotolo T, Ye X, Nathans J (2009) New mouse lines for the analysis of neuronal morphology using CreER(T)/loxP-directed sparse labeling. PLoS One 4:e7859.

Beaudry H, Daou I, Ase AR, Ribeiro-da-Silva A, Seguela P (2017) Distinct behavioral responses evoked by selective optogenetic stimulation of the major TRPV1+ and MrgD+ subsets of C-fibers. Pain 158:2329-2339.

Beitel RE, Dubner R (1976) Response of unmyelinated (C) polymodal nociceptors to thermal stimuli applied to monkey's face. Journal of neurophysiology 39:1160-1175.

Bessou P, Perl ER (1969) Response of cutaneous sensory units with unmyelinated fibers to noxious stimuli. Journal of neurophysiology 32:1025-1043.

Bourane S, Duan B, Koch SC, Dalet A, Britz O, Garcia-Campmany L, Kim E, Cheng L, Ghosh A, Ma Q, Goulding M (2015) Gate control of mechanical itch by a subpopulation of spinal cord interneurons. Science 350:550-554.

Braz JM, Nassar MA, Wood JN, Basbaum AI (2005) Parallel "pain" pathways arise from subpopulations of primary afferent nociceptor. Neuron 47:787-793.

Brown AG (1982) The dorsal horn of the spinal cord. Q J Exp Physiol 67:193-212.

Brown PB, Fuchs JL (1975a) Somatotopic representation of hindlimb skin in cat dorsal horn. Journal of neurophysiology 38:1-9.

Brown PB, Fuchs JL (1975b) Somatotopic representation of hindlimb skin in cat dorsal horn. J Neurophysiol 38:1-9.

Brown PB, Koerber HR (1978) Cat hindlimb tactile dermatomes determined with single-unit recordings. Journal of neurophysiology 41:260-267.

Brown PB, Koerber HR, Millecchia R (2004) From innervation density to tactile acuity: 1. Spatial representation. Brain Res 1011:14-32.

Brown PB, Gladfelter WE, Culberson JC, Covalt-Dunning D, Sonty RV, Pubols LM, Millecchia RJ (1991) Somatotopic organization of single primary afferent axon projections to cat spinal cord dorsal horn. J Neurosci 11:298-309.

Burgess PR, Perl ER (1967) Myelinated afferent fibres responding specifically to noxious stimulation of the skin. The Journal of physiology 190:541-562.

Campbell JN, Meyer RA (1983) Sensitization of unmyelinated nociceptive afferents in monkey varies with skin type. J Neurophysiol 49:98-110.
Catania KC, Kaas JH (1997) Somatosensory fovea in the star-nosed mole: behavioral use of the star in relation to innervation patterns and cortical representation. J Comp Neurol 387:215-233.
Catania KC, Leitch DB, Gauthier D (2011) A star in the brainstem reveals the first step of cortical magnification. PLoS One 6:e22406.
Cauna N (1973) The free penicillate nerve endings of the human hairy skin. J Anat 115:277-288.
Cauna N (2008) Fine Structure of the Receptor Organs and its Probable Functional Significance. Ciba Foundation Symposium - Hormonal Factors in Carbohydrate Metabolism (Colloquia on Endocrinology).
Cavanaugh DJ, Lee H, Lo L, Shields SD, Zylka MJ, Basbaum AI, Anderson DJ (2009) Distinct subsets of unmyelinated primary sensory fibers mediate behavioral responses to noxious thermal and mechanical stimuli. Proc Natl Acad Sci U S A 106:9075-9080.
Cervero F, Connell LA (1984) Distribution of somatic and visceral primary afferent fibres within the thoracic spinal cord of the cat. J Comp Neurol 230:88-98.
Challis RC, Tian H, Wang J, He J, Jiang J, Chen X, Yin W, Connelly T, Ma L, Yu CR, Pluznick JL, Storm DR, Huang L, Zhao K, Ma M (2015) An olfactory cilia pattern in the mammalian nose ensures high sensitivity to odors. Current Biology 25:2503-2512.
Chen CL, Broom DC, Liu Y, de Nooij JC, Li Z, Cen C, Samad OA, Jessell TM, Woolf CJ, Ma Q (2006) Runx1 determines nociceptive sensory neuron phenotype and is required for thermal and neuropathic pain. Neuron 49:365-377.
Croze S, Duclaux R, Kenshalo DR (1976) The thermal sensitivity of the polymodal nociceptors in the monkey. The Journal of physiology 263:539-562.
Crozier R, Ajit S, Kaftan E, Pausch M (2007) {MrgD} activation inhibits {KCNQ/M-currents} and contributes to enhanced neuronal excitability. The Journal of neuroscience : the official journal of the Society for Neuroscience 27:4492-4496.
Cui L, Kim YR, Kim HY, Lee SC, Shin HS, Szabo G, Erdelyi F, Kim J, Kim SJ (2011) Modulation of synaptic transmission from primary afferents to spinal substantia gelatinosa neurons by group III mGluRs in GAD65-EGFP transgenic mice. J Neurophysiol 105:1102-1111.
Cui L, Miao X, Liang L, Abdus-Saboor I, Olson W, Fleming MS, Ma M, Tao YX, Luo W (2016) Identification of Early RET+ Deep Dorsal Spinal Cord Interneurons in Gating Pain. Neuron 91:1137-1153.
Daniel PM, Whitteridge D (1961) The representation of the visual field on the cerebral cortex in monkeys. The Journal of physiology 159:203-221.
Dasen JS, Jessell TM (2009) Hox networks and the origins of motor neuron diversity. Curr Top Dev Biol 88:169-200.
Dasen JS, Tice BC, Brenner-Morton S, Jessell TM (2005) A Hox regulatory network establishes motor neuron pool identity and target-muscle connectivity. Cell 123:477-491.

De Marco Garcia NV, Jessell TM (2008) Early motor neuron pool identity and muscle nerve trajectory defined by postmitotic restrictions in Nkx6.1 activity. Neuron 57:217-231.
Deng P, Xu ZC (2012) Whole-cell patch-clamp recordings on spinal cord slices. Methods Mol Biol 851:65-72.
Dong X, Han S, Zylka MJ, Simon MI, Anderson DJ (2001) A diverse family of GPCRs expressed in specific subsets of nociceptive sensory neurons. Cell 106:619-632.
Doyle MW, Andresen MC (2001) Reliability of monosynaptic sensory transmission in brain stem neurons in vitro. J Neurophysiol 85:2213-2223.
Duan B, Cheng L, Bourane S, Britz O, Padilla C, Garcia-Campmany L, Krashes M, Knowlton W, Velasquez T, Ren X, Ross SE, Lowell BB, Wang Y, Goulding M, Ma Q (2014) Identification of spinal circuits transmitting and gating mechanical pain. Cell 159:1417-1432.
Duncan D, Morales R (1978) Relative numbers of several types of synaptic connections in the substantia gelatinosa of the cat spinal cord. The Journal of comparative neurology 182:601-610.
Eggan K, Akutsu H, Loring J, Jackson-Grusby L, Klemm M, Rideout WM, 3rd, Yanagimachi R, Jaenisch R (2001) Hybrid vigor, fetal overgrowth, and viability of mice derived by nuclear cloning and tetraploid embryo complementation. Proc Natl Acad Sci U S A 98:6209-6214.
Fedtsova NG, Turner EE (1995) Brn-3.0 expression identifies early post-mitotic CNS neurons and sensory neural precursors. Mechanisms of development 53:291-304.
Fitzgerald M, Lynn B (1977) The sensitization of high threshold mechanoreceptors with myelinated axons by repeated heating. The Journal of physiology 265:549-563.
Fleischer E, Handwerker HO, Joukhadar S (1983) Unmyelinated nociceptive units in two skin areas of the rat. Brain Res 267:81-92.
Fleming MS, Luo W (2013) The anatomy, function, and development of mammalian Aβ low-threshold mechanoreceptors. Frontiers in biology 8:1-20.
Fleming MS, Ramos D, Han SB, Zhao J, Son YJ, Luo W (2012) The majority of dorsal spinal cord gastrin releasing peptide is synthesized locally whereas neuromedin B is highly expressed in pain- and itch-sensing somatosensory neurons. Mol Pain 8:52.
Fleming MS, Vysochan A, Paixao S, Niu J, Klein R, Savitt JM, Luo W (2015) Cis and trans RET signaling control the survival and central projection growth of rapidly adapting mechanoreceptors. Elife 4:e06828.
Fode C, Gradwohl G, Morin X, Dierich A, LeMeur M, Goridis C, Guillemot F (1998) The bHLH protein NEUROGENIN 2 is a determination factor for epibranchial placode-derived sensory neurons. Neuron 20:483-494.
Garell PC, McGillis SL, Greenspan JD (1996) Mechanical response properties of nociceptors innervating feline hairy skin. Journal of neurophysiology 75:1177-1189.

Georgopoulos aP (1976) Functional properties of primary afferent units probably related to pain mechanisms in primate glabrous skin. Journal of neurophysiology 39:71-83.
Georgopoulos AP (1977) Stimulus-response relations in high-threshold mechanothermal fibers innervating primate glabrous skin. 128:547-552.
Ghitani N, Barik A, Szczot M, Thompson JH, Li C, Le Pichon CE, Krashes MJ, Chesler AT (2017) Specialized Mechanosensory Nociceptors Mediating Rapid Responses to Hair Pull. Neuron 95:944-954 e944.
Gobel S (1974) Synaptic organization of the substantia gelatinosa glomeruli in the spinal trigeminal nucleus of the adult cat. J Neurocytol 3:219-243.
Gobel S (1976) Dendroaxonic synapses in the substantia gelatinosa glomeruli of the spinal trigeminal nucleus of the cat. J Comp Neurol 167:165-176.
Goetz C, Pivetta C, Arber S (2015) Distinct limb and trunk premotor circuits establish laterality in the spinal cord. Neuron 85:131-144.
Grudt TJ, Perl ER (2002) Correlations between neuronal morphology and electrophysiological features in the rodent superficial dorsal horn. J Physiol 540:189-207.
Grueber WB, Jan LY, Jan YN (2002) Tiling of the Drosophila epidermis by multidendritic sensory neurons. Development 129:2867-2878.
Han L, Ma C, Liu Q, Weng HJ, Cui Y, Tang Z, Kim Y, Nie H, Qu L, Patel KN, Li Z, McNeil B, He S, Guan Y, Xiao B, Lamotte RH, Dong X (2013) A subpopulation of nociceptors specifically linked to itch. Nat Neurosci 16:174-182.
Hayashi S, Lewis P, Pevny L, McMahon AP (2002) Efficient gene modulation in mouse epiblast using a Sox2Cre transgenic mouse strain. Gene Expr Patterns 2:93-97.
Hillman P, Wall PD (1969) Inhibitory and excitatory factors influencing the receptive fields of lamina 5 spinal cord cells. Experimental brain research 9:284-306.
Hoheisel U, Mense S (1987) Observations on the morphology of axons and somata of slowly conducting dorsal root ganglion cells in the cat. Brain Research 423:269-278.
Iggo A (1959) Cutaneous heat and cold receptors with slowly conducting (C) afferent fibres. Experimental Physiology 44:362-370.
Iggo A (1960) Cutaneous mechanoreceptors with afferent C fibres. J Physiol 152:337-353.
Jackman A, Fitzgerald M (2000) Development of peripheral hindlimb and central spinal cord innervation by subpopulations of dorsal root ganglion cells in the embryonic rat. J Comp Neurol 418:281-298.
Jaggi AS, Jain V, Singh N (2011) Animal models of neuropathic pain. Fundam Clin Pharmacol 25:1-28.
Johansson RS, Vallbo AB (1979) Tactile sensibility in the human hand: relative and absolute densities of four types of mechanoreceptive units in glabrous skin. The Journal of physiology 286:283-300.
Johansson RS, Vallbo AB (1980) Spatial properties of the population of mechanoreceptive units in the glabrous skin of the human hand. Brain Res 184:353-366.

Joo W, Hippenmeyer S, Luo L (2014) Neurodevelopment. Dendrite morphogenesis depends on relative levels of NT-3/TrkC signaling. Science 346:626-629.
Kardon AP, Polgar E, Hachisuka J, Snyder LM, Cameron D, Savage S, Cai X, Karnup S, Fan CR, Hemenway GM, Bernard CS, Schwartz ES, Nagase H, Schwarzer C, Watanabe M, Furuta T, Kaneko T, Koerber HR, Todd AJ, Ross SE (2014) Dynorphin acts as a neuromodulator to inhibit itch in the dorsal horn of the spinal cord. Neuron 82:573-586.
Kato G, Kosugi M, Mizuno M, Strassman AM (2011) Separate inhibitory and excitatory components underlying receptive field organization in superficial medullary dorsal horn neurons. The Journal of neuroscience : the official journal of the Society for Neuroscience 31:17300-17305.
Kennedy WR (2004) Opportunities afforded by the study of unmyelinated, nerves in skin and other organs. Muscle and Nerve 29:756-767.
Kirchhoff C, Jung S, Reeh PW, Handwerker HO (1990) Carrageenan inflammation increases bradykinin sensitivity of rat cutaneous nociceptors. Neuroscience Letters 111:206-210.
Koch SC, Acton D, Goulding M (2018) Spinal Circuits for Touch, Pain, and Itch. Annu Rev Physiol 80:189-217.
Koerber HR, Brown PB (1982) Somatotopic organization of hindlimb cutaneous nerve projections to cat dorsal horn. J Neurophysiol 48:481-489.
Kolb H (1994) The architecture of functional neural circuits in the vertebrate retina. The Proctor Lecture. Investigative ophthalmology & visual science 35:2385-2404.
Kolb H (1995) Circuitry for Rod Signals through the Retina. In: Webvision: The Organization of the Retina and Visual System (Kolb H, Fernandez E, Nelson R, eds). Salt Lake City (UT).
Kossl M, Vater M (1985) The cochlear frequency map of the mustache bat, Pteronotus parnellii. J Comp Physiol A 157:687-697.
Kosugi M, Kato G, Lukashov S, Pendse G, Puskar Z, Kozsurek M, Strassman AM (2013) Subpopulation-specific patterns of intrinsic connectivity in mouse superficial dorsal horn as revealed by laser scanning photostimulation. J Physiol 591:1935-1949.
Kruger L, Perl ER, Sedivec MJ (1981) Fine structure of myelinated mechanical nociceptor endings in cat hairy skin. Journal of Comparative Neurology 198:137-154.
Kruger L, Silverman JD, Mantyh PW, Sternini C, Brecha NC (1989) Peripheral patterns of calcitonin-gene-related peptide general somatic sensory innervation: Cutaneous and deep terminations. Journal of Comparative Neurology 280:291-302.
Köppl C, Gleich O, Manley GA (1993) An auditory fovea in the barn owl cochlea. Journal of Comparative Physiology A 171:695-704.
Kössl M, Vater M (1985) The cochlear frequency map of the mustache bat, Pteronotus parnellii. Journal of comparative physiology A, Sensory, neural, and behavioral physiology 157:687-697.
Lanier J, Dykes IM, Nissen S, Eng SR, Turner EE (2009) Brn3a regulates the transition from neurogenesis to terminal differentiation and represses non-neural gene expression in the trigeminal ganglion. Developmental Dynamics 238:3065-3079.

Lawson SN, Biscoe TJ (1979) Development of mouse dorsal root ganglia: an autoradiographic and quantitative study. J Neurocytol 8:265-274.
Le Bars D, Gozariu M, Cadden SW (2001) Animal models of nociception. Pharmacol Rev 53:597-652.
Leem JW, Willis WD, Chung JM (1993) Cutaneous sensory receptors in the rat foot. Journal of neurophysiology 69:1684-1699.
Li L, Rutlin M, Abraira VE, Cassidy C, Kus L, Gong S, Jankowski MP, Luo W, Heintz N, Koerber HR, Woodbury CJ, Ginty DD (2011) The functional organization of cutaneous low-threshold mechanosensory neurons. Cell 147:1615-1627.
Light AR, Perl ER (1979) Spinal termination of functionally identified primary afferent neurons with slowly conducting myelinated fibers. The Journal of comparative neurology 186:133-150.
Light AR, Shults RC, Jones SL (1992) The initial processing of pain and its descending control: spinal and trigeminal systems: Karger Basel.
Lima D, Coimbra A (1988) The spinothalamic system of the rat: structural types of retrogradely labelled neurons in the marginal zone (lamina I). Neuroscience 27:215-230.
Liu Q, Vrontou S, Rice FL, Zylka MJ, Dong X, Anderson DJ (2007) Molecular genetic visualization of a rare subset of unmyelinated sensory neurons that may detect gentle touch. Nat Neurosci 10:946-948.
Liu Q, Sikand P, Ma C, Tang Z, Han L, Li Z, Sun S, LaMotte RH, Dong X (2012) Mechanisms of itch evoked by beta-alanine. J Neurosci 32:14532-14537.
Liu Q, Tang Z, Surdenikova L, Kim S, Patel KN, Kim A, Ru F, Guan Y, Weng HJ, Geng Y, Undem BJ, Kollarik M, Chen ZF, Anderson DJ, Dong X (2009) Sensory neuron-specific GPCR Mrgprs are itch receptors mediating chloroquine-induced pruritus. Cell 139:1353-1365.
Liu Y, Yang FC, Okuda T, Dong X, Zylka MJ, Chen CL, Anderson DJ, Kuner R, Ma Q (2008) Mechanisms of compartmentalized expression of Mrg class G-protein-coupled sensory receptors. J Neurosci 28:125-132.
Lu Y, Perl ER (2003) A specific inhibitory pathway between substantia gelatinosa neurons receiving direct C-fiber input. J Neurosci 23:8752-8758.
Lu Y, Perl ER (2005) Modular organization of excitatory circuits between neurons of the spinal superficial dorsal horn (laminae I and II). J Neurosci 25:3900-3907.
Luo W, Wickramasinghe SR, Savitt JM, Griffin JW, Dawson TM, Ginty DD (2007) A hierarchical NGF signaling cascade controls Ret-dependent and Ret-independent events during development of nonpeptidergic DRG neurons. Neuron 54:739-754.
Lynn B, Carpenter SE (1982) Primary afferent units from the hairy skin of the rat hind limb. Brain Res 238:29-43.
Lynn B, Shakhanbeh J (1988) Properties of A delta high threshold mechanoreceptors in the rat hairy and glabrous skin and their response to heat. Neurosci Lett 85:71-76.
Ma Q, Fode C, Guillemot F, Anderson DJ (1999) Neurogenin1 and neurogenin2 control two distinct waves of neurogenesis in developing dorsal root ganglia. Genes & development 13:1717-1728.

Madisen L, Zwingman TA, Sunkin SM, Oh SW, Zariwala HA, Gu H, Ng LL, Palmiter RD, Hawrylycz MJ, Jones AR, Lein ES, Zeng H (2010) A robust and high-throughput Cre reporting and characterization system for the whole mouse brain. Nat Neurosci 13:133-140.
Madisen L et al. (2012) A toolbox of Cre-dependent optogenetic transgenic mice for light-induced activation and silencing. Nat Neurosci 15:793-802.
Mancini F, Haggard P, Iannetti GD, Longo MR, Sereno MI (2012) Fine-grained nociceptive maps in primary somatosensory cortex. J Neurosci 32:17155-17162.
Mancini F, Sambo CF, Ramirez JD, Bennett DL, Haggard P, Iannetti GD (2013) A fovea for pain at the fingertips. Curr Biol 23:496-500.
Mancini F, Bauleo A, Cole J, Lui F, Porro CA, Haggard P, Iannetti GD (2014) Whole-body mapping of spatial acuity for pain and touch. Annals of Neurology 75:917-924.
Marshall GE, Shehab SA, Spike RC, Todd AJ (1996) Neurokinin-1 receptors on lumbar spinothalamic neurons in the rat. Neuroscience 72:255-263.
Masland RH (2001) The fundamental plan of the retina. Nature neuroscience 4:877-886.
Mason P (2012) Medullary circuits for nociceptive modulation. Current Opinion in Neurobiology 22:640-645.
McCoy ES, Taylor-Blake B, Zylka MJ (2012) CGRPalpha-expressing sensory neurons respond to stimuli that evoke sensations of pain and itch. PLoS One 7:e36355.
McCoy ES, Taylor-Blake B, Street SE, Pribisko AL, Zheng J, Zylka MJ (2013) Peptidergic CGRPalpha primary sensory neurons encode heat and itch and tonically suppress sensitivity to cold. Neuron 78:138-151.
Mendelson B, Koerber HR, Frank E (1992) Development of cutaneous and proprioceptive afferent projections in the chick spinal cord. Neuroscience Letters 138:72-76.
Mense S (2009) Anatomy of Nociceptors. In: Science of Pain (Basbaum AI, Bushnell MC, eds), pp 11-41: Elsevier.
Meyer RA, Davis KD, Cohen RH, Treede RD, Campbell JN (1991) Mechanically insensitive afferents (MIAs) in cutaneous nerves of monkey. Brain Research 561:252-261.
Millecchia RJ, Pubols LM, Sonty RV, Culberson JL, Gladfelter WE, Brown PB (1991) Influence of map scale on primary afferent terminal field geometry in cat dorsal horn. Journal of neurophysiology 66:696-704.
Mirnics K, Koerber HR (1995a) Prenatal development of rat primary afferent fibers: II. Central projections. The Journal of comparative neurology 355:601-614.
Mirnics K, Koerber HR (1995b) Prenatal development of rat primary afferent fibers: I. Peripheral projections. The Journal of comparative neurology 355:589-600.
Molander C, Grant G (1985) Cutaneous projections from the rat hindlimb foot to the substantia gelatinosa of the spinal cord studied by transganglionic transport of WGA-HRP conjugate. J Comp Neurol 237:476-484.
Molliver DC, Wright DE, Leitner ML, Parsadanian AS, Doster K, Wen D, Yan Q, Snider WD (1997) IB4-binding DRG neurons switch from NGF to GDNF dependence in early postnatal life. Neuron 19:849-861.

Montelius A, Marmigère F, Baudet C, Aquino JB, Enerbäck S, Ernfors P (2007) Emergence of the sensory nervous system as defined by Foxs1 expression. Differentiation 75:404-417.
Nagy JI, Hunt SP (1982) Fluoride-resistant acid phosphatase-containing neurones in dorsal root ganglia are separate from those containing substance P or somatostatin. Neuroscience 7:89-97.
Niu J, Ding L, Li JJ, Kim H, Liu J, Li H, Moberly A, Badea TC, Duncan ID, Son YJ, Scherer SS, Luo W (2013) Modality-based organization of ascending somatosensory axons in the direct dorsal column pathway. J Neurosci 33:17691-17709.
Norrsell U, Finger S, Lajonchere C (1999) Cutaneous sensory spots and the "law of specific nerve energies": history and development of ideas. Brain Res Bull 48:457-465.
Olson W, Dong P, Fleming M, Luo W (2016) The specification and wiring of mammalian cutaneous low-threshold mechanoreceptors. Wiley Interdiscip Rev Dev Biol 5:389-404.
Olson W, Abdus-Saboor I, Cui L, Burdge J, Raabe T, Ma M, Luo W (2017) Sparse genetic tracing reveals regionally specific functional organization of mammalian nociceptors. Elife 6.
Orefice LL, Zimmerman AL, Chirila AM, Sleboda SJ, Head JP, Ginty DD (2016) Peripheral Mechanosensory Neuron Dysfunction Underlies Tactile and Behavioral Deficits in Mouse Models of ASDs. Cell 166:299-313.
Ozaki S, Snider WD (1997) Initial trajectories of sensory axons toward laminar targets in the developing mouse spinal cord. J Comp Neurol 380:215-229.
Pare M, Smith AM, Rice FL (2002) Distribution and terminal arborizations of cutaneous mechanoreceptors in the glabrous finger pads of the monkey. J Comp Neurol 445:347-359.
Patel T, Jackman A, Rice F, Kucera J, Snider W (2000) Development of sensory neurons in the absence of {NGF/TrkA} signaling in vivo. Neuron 25:345-357.
Penfield BYW (1937) SOMATIC MOTOR AND SENSORY REPRESENTATION IN.
Perl ER (1968) Myelinated afferent fibres innervating the primate skin and their response to noxious stimuli. The Journal of physiology 197:593-615.
Pogorzala L, Mishra SK, Hoon Ma (2013) The cellular code for mammalian thermosensation. The Journal of neuroscience : the official journal of the Society for Neuroscience 33:5533-5541.
Pollak GD, Bodenhamer RD (1981) Specialized characteristics of single units in inferior colliculus of mustache bat: frequency representation, tuning, and discharge patterns. Journal of neurophysiology 46:605-620.
Price DD (1972) Characteristics of second pain and flexion reflexes indicative of prolonged central summation. Experimental Neurology 37:371-387.
Price DD, Hu JW, Dubner R, Gracely RH (1977) Peripheral suppression of first pain and central summation of second pain evoked by noxious heat pulses. Pain 3:57-68.
Ramón y Cajal S (1909) Histologie du système nerveux de l'homme & des vertébrés. Paris: Maloine.

Rau K, Sabrina M, Wang H, Lawson J, Jankowski M, Zylka M, Anderson D, Koerber H (2009) Mrgprd enhances excitability in specific populations of cutaneous murine polymodal nociceptors. The Journal of neuroscience : the official journal of the Society for Neuroscience 29:8612-8619.

Rethelyi M (1977) Preterminal and terminal axon arborizations in the substantia gelatinosa of cat's spinal cord. J Comp Neurol 172:511-521.

Rexed B (1952) The cytoarchitectonic organization of the spinal cord in the cat. The Journal of comparative neurology 96:414-495.

Rexed B (1954) A cytoarchitectonic atlas of the spinal cord in the cat. The Journal of comparative neurology 100:297-379.

Reynolds ML, Fitzgerald M, Benowitz LI (1991) GAP-43 expression in developing cutaneous and muscle nerves in the rat hindlimb. Neuroscience 41:201-211.

Ribeiro-da-Silva A (1995) Ultrastructural features of the colocalization of calcitonin gene related peptide with substance P or somatostatin in the dorsal horn of the spinal cord. Can J Physiol Pharmacol 73:940-944.

Ribeiro-da-Silva A, Coimbra A (1982) Two types of synaptic glomeruli and their distribution in laminae I-III of the rat spinal cord. The Journal of comparative neurology 209:176-186.

Rice FL, Kinnman E, Aldskogius H, Johansson O, Arvidsson J (1993) The innervation of the mystacial pad of the rat as revealed by PGP 9.5 immunofluorescence. J Comp Neurol 337:366-385.

Sagasti A, Guido MR, Raible DW, Schier AF (2005) Repulsive interactions shape the morphologies and functional arrangement of zebrafish peripheral sensory arbors. Curr Biol 15:804-814.

Scheibel ME, Scheibel AB (1968) Terminal axonal patterns in cat spinal cord. II. The dorsal horn. Brain Res 9:32-58.

Scheibel ME, Schiebel AB (1969) Terminal patterns in cat spinal cord III. Primary afferent collaterals. Brain Res 13:417-443.

Schmidt R, Schmelz M, Torebjörk HE, Handwerker HO (2000) Mechano-insensitive nociceptors encode pain evoked by tonic pressure to human skin. Neuroscience 98:793-800.

Schmidt R, Schmelz M, Ringkamp M, Handwerker HO, Torebjork HE (1997) Innervation territories of mechanically activated C nociceptor units in human skin. J Neurophysiol 78:2641-2648.

Schmidt R, Schmelz M, Weidner C, Handwerker HO, Torebjork HE (2002) Innervation territories of mechano-insensitive C nociceptors in human skin. J Neurophysiol 88:1859-1866.

Schmidt R, Schmelz M, Forster C, Ringkamp M, Torebjörk E, Handwerker H (1995) Novel classes of responsive and unresponsive C nociceptors in human skin. The Journal of neuroscience : the official journal of the Society for Neuroscience 15:333-341.

Sharma K, Korade Z, Frank E (1994) Development of specific muscle and cutaneous sensory projections in cultured segments of spinal cord. Development (Cambridge, England) 120:1315-1323.

Sherrington CS (1906) The integrative action of the nervous system. New York,: C. Scribner's sons.
Shortland P, Woolf CJ, Fitzgerald M (1989) Morphology and somatotopic organization of the central terminals of hindlimb hair follicle afferents in the rat lumbar spinal cord. J Comp Neurol 289:416-433.
Silverman JD, Kruger L (1990) Selective neuronal glycoconjugate expression in sensory and autonomic ganglia: relation of lectin reactivity to peptide and enzyme markers. J Neurocytol 19:789-801.
Simone DA, Kajander KC (1996) Excitation of rat cutaneous nociceptors by noxious cold. Neuroscience Letters 213:53-56.
Simone Da, Kajander KC (1997) Responses of cutaneous A-fiber nociceptors to noxious cold. Journal of neurophysiology 77:2049-2060.
Smith CL (1983) The development and postnatal organization of primary afferent projections to the rat thoracic spinal cord. The Journal of comparative neurology 220:29-43.
Sommer EW, Kazimierczak J, Droz B (1985) Neuronal subpopulations in the dorsal root ganglion of the mouse as characterized by combination of ultrastructural and cytochemical features. Brain Research 346:310-326.
Spike RC, Puskar Z, Andrew D, Todd AJ (2003) A quantitative and morphological study of projection neurons in lamina I of the rat lumbar spinal cord. Eur J Neurosci 18:2433-2448.
Stanley OH (1991) Cortical development and visual function. Eye (Lond) 5 (Pt 1):27-30.
Stucky CL, Lewin GR (1999) Isolectin B(4)-positive and -negative nociceptors are functionally distinct. The Journal of neuroscience 19:505.
Suga N, Niwa H, Taniguchi I, Margoliash D (1987) The personalized auditory cortex of the mustached bat: adaptation for echolocation. Journal of neurophysiology 58:643-654.
Sugiura Y, Lee CL, Perl ER (1986) Central projections of identified, unmyelinated (C) afferent fibers innervating mammalian skin. Science 234:358-361.
Sugiura Y, Terui N, Hosoya Y (1989) Difference in distribution of central terminals between visceral and somatic unmyelinated (C) primary afferent fibers. J Neurophysiol 62:834-840.
Sun S, Xu Q, Guo C, Guan Y, Liu Q, Dong X (2017) Leaky Gate Model: Intensity-Dependent Coding of Pain and Itch in the Spinal Cord. Neuron 93:840-853.e845.
Sun Y, Dykes IM, Liang X, Eng SR, Evans SM, Turner EE (2008) A central role for Islet1 in sensory neuron development linking sensory and spinal gene regulatory programs. Nature neuroscience 11:1283-1293.
Swett JE, Woolf CJ (1985) The somatotopic organization of primary afferent terminals in the superficial laminae of the dorsal horn of the rat spinal cord. J Comp Neurol 231:66-77.
Szentagothai J (1964) Neuronal and Synaptic Arrangement in the Substantia Gelatinosa Rolandi. J Comp Neurol 122:219-239.
Takahashi Y, Aoki Y, Doya H (2007) Segmental somatotopic organization of cutaneous afferent fibers in the lumbar spinal cord dorsal horn in rats. Anat Sci Int 82:24-30.

Takahashi Y, Chiba T, Sameda H, Ohtori S, Kurokawa M, Moriya H (2002) Organization of cutaneous ventrodorsal and rostrocaudal axial lines in the rat hindlimb and trunk in the dorsal horn of the spinal cord. J Comp Neurol 445:133-144.

Todd AJ (1996) GABA and glycine in synaptic glomeruli of the rat spinal dorsal horn. European Journal of Neuroscience 8:2492-2498.

Torebjörk HE (1974) Afferent C units responding to mechanical, thermal and chemical stimuli in human non-glabrous skin. Acta physiologica Scandinavica 92:374-390.

Torebjörk HE, Hallin RG (1973) Perceptual changes accompanying controlled preferential blocking of A and C fibre responses in intact human skin nerves. Experimental brain research 16:321-332.

Treede R, Meyer R, Campbell J (1990) Comparison of heat and mechanical receptive fields of cutaneous C-fiber nociceptors in monkey. Journal of neurophysiology 64:1502-1513.

Treede R-dD, Meyer RA, Campbell JN, Johns T, Meyer RA, Camp- JN (1998) Myelinated mechanically insensitive afferents from monkey hairy skin: heat-response properties. JNeurophysiol 80:1082-1093.

Treede RD, Meyer RA, Raja SN, Campbell JN (1992) Peripheral and central mechanisms of cutaneous hyperalgesia. Prog Neurobiol 38:397-421.

Uesaka T, Nagashimada M, Yonemura S, Enomoto H (2008) Diminished Ret expression compromises neuronal survival in the colon and causes intestinal aganglionosis in mice. J Clin Invest 118:1890-1898.

Usoskin D, Furlan A, Islam S, Abdo H, Lönnerberg P, Lou D, Hjerling-Leffler J, Haeggström J, Kharchenko O, Kharchenko PV, Linnarsson S, Ernfors P (2014) Unbiased classification of sensory neuron types by large-scale single-cell RNA sequencing. Nature Neuroscience 18:145-153.

Vallbo AB, Johansson RS (1984) Properties of cutaneous mechanoreceptors in the human hand related to touch sensation. Human neurobiology 3:3-14.

Van Hees J, Gybels J (1972) Pain related to single afferent C-fibers from human skin. Brain Res 48:397-400.

Van Hees J, Gybels J (1981) C nociceptor activity in human nerve during painful and non painful skin stimulation. Journal of neurology, neurosurgery, and psychiatry 44:600-607.

Vandewauw I, De Clercq K, Mulier M, Held K, Pinto S, Van Ranst N, Segal A, Voet T, Vennekens R, Zimmermann K, Vriens J, Voets T (2018) A TRP channel trio mediates acute noxious heat sensing. Nature.

Vater M, Feng AS, Betz M (1985) An HRP-study of the frequency-place map of the horseshoe bat cochlea: morphological correlates of the sharp tuning to a narrow frequency band. Journal of comparative physiology A, Sensory, neural, and behavioral physiology 157:671-686.

Vriens J, Owsianik G, Hofmann T, Philipp SE, Stab J, Chen X, Benoit M, Xue F, Janssens A, Kerselaers S, Oberwinkler J, Vennekens R, Gudermann T, Nilius B, Voets T (2011) TRPM3 Is a Nociceptor Channel Involved in the Detection of Noxious Heat. Neuron 70:482-494.

Wang G, Scott SA (2002) Development of "normal" dermatomes and somatotopic maps by "abnormal" populations of cutaneous neurons. Dev Biol 251:424-433.
Wang H, Zylka MJ (2009) Mrgprd-expressing polymodal nociceptive neurons innervate most known classes of substantia gelatinosa neurons. J Neurosci 29:13202-13209.
Wang L, Millecchia R, Brown PB (1997) Correlation of peripheral innervation density and dorsal horn map scale. Journal of neurophysiology 78:689-702.
Weber EH (1834) De pulsu, resorptione, auditu et tactu: Annotationes anatomicae et physiologicae, auctore: prostat apud C.F. Koehler.
Weinstein S (1968) Intensive and extensive aspects of tactile sensitivity as a function of body part, sex, and laterality. In: The Skin Senses (Kenshalo DR, ed), pp 195-222. Springfield, IL: Thomas.
White DM, Basbaum AI, Goetzl EJ, Levine JD (1990) The 15-lipoxygenase product, 8R,15S-diHETE, stereospecifically sensitizes C-fiber mechanoheat nociceptors in hairy skin of rat. Journal of Neurophysiology 63:966-970.
White F, Silos-Santiago I, Molliver DC, Nishimura M, Phillips H, Barbacid M, Snider WD (1996) Synchronous onset of NGF and TrkA survival dependence in developing dorsal root ganglia. The Journal of neuroscience : the official journal of the Society for Neuroscience 16:4662-4672.
Woolf CJ, Fitzgerald M (1986) Somatotopic organization of cutaneous afferent terminals and dorsal horn neuronal receptive fields in the superficial and deep laminae of the rat lumbar spinal cord. J Comp Neurol 251:517-531.
Wooten M, Weng H-J, Hartke TV, Borzan J, Klein AH, Turnquist B, Dong X, Meyer RA, Ringkamp M (2014) Three functionally distinct classes of C-fibre nociceptors in primates. Nature Communications 5:4122.
Wright DE, Zhou L, Kucera J, Snider WD (1997) Introduction of a neurotrophin-3 transgene into muscle selectively rescues proprioceptive neurons in mice lacking endogenous neurotrophin-3. Neuron 19:503-517.
Wu H, Williams J, Nathans J (2012) Morphologic diversity of cutaneous sensory afferents revealed by genetically directed sparse labeling. Elife 1:e00181.
Xu B, Zang K, Ruff NL, Zhang YA, McConnell SK, Stryker MP, Reichardt LF (2000) Cortical degeneration in the absence of neurotrophin signaling: dendritic retraction and neuronal loss after removal of the receptor TrkB. Neuron 26:233-245.
Yu XH, Ribeiro-da-Silva A, De Koninck Y (2005) Morphology and neurokinin 1 receptor expression of spinothalamic lamina I neurons in the rat spinal cord. J Comp Neurol 491:56-68.
Zhang J, Cavanaugh DJ, Nemenov MI, Basbaum AI (2013) The modality-specific contribution of peptidergic and non-peptidergic nociceptors is manifest at the level of dorsal horn nociresponsive neurons. J Physiol 591:1097-1110.
Zylka MJ, Rice FL, Anderson DJ (2005) Topographically distinct epidermal nociceptive circuits revealed by axonal tracers targeted to Mrgprd. Neuron 45:17-25.
Zylka MJ, Dong X, Southwell AL, Anderson DJ (2003) Atypical expansion in mice of the sensory neuron-specific Mrg G protein-coupled receptor family. Proc Natl Acad Sci U S A 100:10043-10048.

Zylka MJ, Sowa NA, Taylor-Blake B, Twomey MA, Herrala A, Voikar V, Vihko P (2008) Prostatic acid phosphatase is an ectonucleotidase and suppresses pain by generating adenosine. Neuron 60:111-122.